

Asymmetric Fused Fiber Couplers for Wavelength- and Space-Division Multiplexing

Von der Fakultät für Mathematik und Physik
der Gottfried Wilhelm Leibniz Universität Hannover
zur Erlangung des Grades

DOKTOR DER NATURWISSENSCHAFTEN
-Dr. rer. nat.-

genehmigte Dissertation von

Dipl.-Phys. Gabriel Pelegrina Bonilla
geboren am 02.12.1985 in Münster

2015

Referent: Prof. Dr. Uwe Morgner

Korreferent: Prof. Dr. Detlev Ristau

Tag der Promotion: 09.07.2015

Kurzfassung

Gabriel Pelegrina Bonilla

Asymmetrische Faserschmelzkoppler für das optische Wellenlängen- und Räummultiplexverfahren

Faseroptische Komponenten aus unterschiedlichen Glasfasern werden für das optische Wellenlängen- und Räummultiplexverfahren eingesetzt, um neue Funktionalitäten zu ermöglichen. Dazu gehören Faserschmelzkoppler aus mehreren Fasern, die verschmolzen und anschließend verjüngt werden, um Licht aus einer oder mehreren Eingangsfasern zu einer oder mehreren Ausgangsfasern zu koppeln. Das Ziel dieser Arbeit ist es asymmetrische 2×2 Faserschmelzkoppler bestehend aus unterschiedlichen Fasern universell zu beschreiben. Dabei wurden sowohl Eigenschaften der Faserkoppler angepasst als auch die Kopplungsmechanismen unter Berücksichtigung der Eigenmoden untersucht.

Asymmetrische Faserschmelzkoppler wurden experimentell durch das systematische Vorverjüngen einer der beiden Fasern realisiert, um den maximalen Leistungstransfer von der Quellfaser zur Zielfaser zu erhöhen. Damit war es unter anderem möglich zwei weit auseinander liegende Wellenlängen in dem Bereich von 795 nm und 1980 nm mit einer Transmission von 90 % für z. B. Anwendungen in einem Thulium-dotierten Faserverstärker zu kombinieren. Durch definiertes Einstellen der Kopplergeometrie mittels Vorverjüngung, Reduzierung des Faserdurchmessers und entsprechender Wahl des Verschmelzungsgrades wurde das Potential weiter ausgeschöpft. Ein modenselektiver Faserschmelzkoppler wurde erfolgreich demonstriert, um selektiv die LP_{11} Mode mit einer Transmission von 80 % bei einer Wellenlänge von 905 nm anzuregen.

Die Faserschmelzkoppler wurden numerisch modelliert, um Herstellungsparameter abzuschätzen und um einen Einblick in den zugrundeliegenden Kopplungsmechanismus zu erhalten. Deshalb wurde ein numerisches Model zur Beschreibung des Brechungsindexprofils erarbeitet. Eine allgemeingültige Analyse wurde durchgeführt, um den Einfluss von Veränderungen der Kopplergeometrie auf die Eigenmoden und deren modale Gewichtung zu untersuchen. Es konnte gezeigt werden, dass Modenkonzersion in asymmetrischen Faserkopplern stattfindet und dass die modale Zusammensetzung so eingestellt werden kann, dass die relevanten Eigenmoden gleich angeregt sind, was einen kompletten Leistungstransfer in die entsprechende Mode ermöglicht.

Schlagwörter: Faseroptische Komponenten, Asymmetrische Faserschmelzkoppler, Wellenlängenmultiplexverfahren, Räummultiplexverfahren

Abstract

Gabriel Pelegrina Bonilla

Asymmetric Fused Fiber Couplers for Wavelength- and Space-Division Multiplexing

Fiber optic components consisting of different glass fibers are employed for wavelength- and space-division multiplexing in order to achieve new functionalities. This includes fused fiber couplers (FFCs) consisting of several fibers which are fused and tapered and which allow for coupling light from one or several input fibers to one or several output fibers. The aim of this work is to generally analyze asymmetric 2×2 FFCs consisting of different fibers including the experimental tuning of the coupler characteristics by changing the degree of dissimilarity between the fibers and the numerical modeling of the coupling mechanisms in terms of eigenmodes.

Asymmetric FFCs were experimentally realized by systematically pretapering one of the fibers in order to efficiently increase the maximum coupled power from the original fiber to the target fiber. Therefore, it was possible to combine two widely separated wavelengths in the range of 795 nm and 1980 nm in a thulium-doped fiber amplifier with a transmission of 90 % for both wavelengths in the signal fiber. By defined tuning of the coupler geometry not only in terms of pretapering but also in terms of cladding diameter reduction and proper adjustment of the degree of fusion the capabilities of asymmetric FFCs were consecutively exploited. A fused-type mode-selective fiber coupler was successfully demonstrated which showed a selective excitation of the LP_{11} mode with a transmission of 80 % at a wavelength of 905 nm.

The FFCs were numerically modeled to estimate fabrication parameters and to gain insight into the underlying coupling mechanism. Therefore, a numerical model capable to describe the refractive index profile was elaborated. A universal analysis in terms of eigenmodes was conducted and revealed the influence of changes in the coupler geometry on the eigenmodes and their modal weighting. It was shown that mode conversion in asymmetric FFCs takes place and that the modal composition can be tuned in a way that the relevant eigenmodes are equally excited which enables a complete power transfer into the respective mode.

Key words: fiber optic components, asymmetric fused fiber couplers, wavelength-division multiplexing, space-division multiplexing

Contents

1	Introduction	1
2	Fundamentals of Fiber Optic Components	5
2.1	General Properties of Optical Fibers	5
2.2	Fiber Modes	7
2.3	Fiber Couplers	10
2.3.1	Coupling Mechanisms	11
2.3.2	Fiber Optic Components	17
2.4	Simulation Methods	19
3	Symmetric Fused Fiber Couplers	21
3.1	Fabrication and Characterization	21
3.2	Modeling the Refractive Index Profile of Fused Fiber Couplers	24
3.2.1	Determination of the Hot Zone and the Diameter in the Taper Waist	25
3.2.2	Parabolic Taper Shape	27
3.2.3	Transversal Position of the Fibers and Implementation of the Degree of Fusion	28
3.2.4	Modeled 3D Refractive Index Profile	28
3.2.5	Inverse Taper Ratio	29
3.2.6	Simplifications and Limitations of the Refractive Index Profile Model	30
3.3	Numerical Characterization	33
3.4	Modal Analysis	35
3.4.1	Implementation	36
3.4.2	Calculation of Super-Modes	38
3.4.3	Evolution of the Super-Modes and their Effective Refractive Index	39
3.4.4	Modal Decomposition	41
3.5	Conclusion	43
4	Asymmetric Fused Fiber Couplers for Wavelength-Division Multiplexing	45
4.1	Fabrication and Characterization	46
4.1.1	Pulling Signatures at Different Pretaper Lengths	46
4.1.2	Degree of Fusion	49
4.1.3	Output Beam Profile	50

4.2	Numerical Characterization	51
4.3	Modal Analysis	54
4.3.1	General Considerations of Guiding Properties at Different Wavelengths	55
4.3.2	Calculation of Super-Modes	56
4.3.3	Evolution of the Super-Modes and their Effective Refractive Index . .	57
4.3.4	Modal Decomposition	61
4.4	Fused Fiber Couplers for Core Pumping Thulium-Doped Fibers at 795 nm .	66
4.5	Conclusion	67
5	Asymmetric Mode-Selective Fiber Couplers for Space-Division Multiplexing	71
5.1	Fabrication	72
5.2	Experimental Characterization	75
5.2.1	Impact of the Cladding Diameter and the Pretaper Length	75
5.2.2	Discussion of the Loss Mechanisms	79
5.2.3	Impact of the Degree of Fusion	79
5.3	Numerical Characterization	81
5.4	Modal Analysis	83
5.4.1	Calculation of Super-Modes	84
5.4.2	Evolution of the Super-Modes and their Effective Refractive Index . .	85
5.4.3	Modal Decomposition	89
5.5	Conclusion	93
6	Summary and Outlook	95
	Bibliography	99
	Appendix	111
A	Fiber Specifications and Fused Fiber Coupler Fabrication	111
A.1	Fiber Parameters and Refractive Index Profiles	111
A.2	Wavelength-Dependent Numerical Aperture	112
A.3	Reproducibility of the Fused Fiber Coupler Fabrication	112
B	Listings	113
B.1	Calculation of the Refractive Index Profile	113
B.1.1	Parabolic Taper Shape	113
B.1.2	Position of the Fiber Cores	113
B.1.3	Derivation of the Separation of the Fiber Cores	113
	Publications	115
	Curriculum Vitae	119

Acronyms

Notation	Description
3D	three-dimensional
BPM	beam propagation method
DOF	degree of fusion
$\text{DOF}_{\text{Lacroix}}$	degree of fusion according to the definition given by [Lac94]
FFC	fused fiber coupler
FMF	few-mode fiber
HOM	higher-order mode
MMF	multi-mode fiber
MSFC	mode-selective fiber coupler
NA	numerical aperture
PL	pretaper length
PLAN	photonic lantern
SDM	space-division multiplexing
SM	super-mode
SMF	single-mode fiber
WDM	wavelength-division multiplexing

List of Symbols

Notation	Description
D_f	final diameter in the taper waist of a fiber
D_i	initial diameter at the beginning of the taper of a fiber

Notation	Description
E	electric field
L	length of the tapered region
V_{cc}	critical V parameter
V	V parameter
X	diameter of one fiber in the taper waist
Y	diameter of one fiber in the taper waist
Z	width of the cross section in the taper waist
ω	angular frequency
z_B	beat length
β	propagation constant
Δz	width of the hot zone
d	separation of the fiber cores
Δ	fractional refractive index change
κ	coupling coefficient
λ_c	cut-off wavelength
λ	wavelength
l	extension or pull length
Θ_{max}	maximum angle of acceptance to the optical path
n_{cl}	fiber cladding refractive index
n_{co}	fiber core refractive index
n_{eff}	effective refractive index

Notation	Description
n	refractive index
v_{ph}	phase velocity
r_{cl}	(unfused) fiber cladding radius
r_{co}	(unfused) fiber core radius
w_{ol}	width of overlapped region
k	wavenumber

CHAPTER 1

Introduction

Optical fibers consist of flexible and transparent extremely thin rods made of glass which enable the transmission of light between the two ends of the fiber. Since the 1960s the field of fiber optics has become indispensable in most photonic technologies. At the beginning researchers dealt with the problem of high attenuation in the order of 20 dB/km caused by material impurities [Kao66]. The use of high-purity silica glass allowed for the reduction of the attenuation to 4 dB/km which denotes the beginning of the optical fiber telecommunication era [Kec73]. The modern world-wide communication system relies on an extensive network of optical fibers whose potential is unlocked by the use of branching devices to route optical signals and to increase the bandwidth of the system [Tom08]. Regarding this, fiber couplers are essential components since they enable the coupling of light from one or several input fibers to one or several output fibers. The application of fiber couplers and optical fibers in general is not limited to telecommunication networks and extends also in the field of fiber lasers and amplifiers. Since the emergence of lasers in the 1960s [Mai60] researchers have build lasers made of fibers [Koe64; Sni61] for optical amplification of several decibels per milliwatt of absorbed pump power. This was of significant impact for the telecommunication as known today, because no solution for amplifying signals in optical fibers existed at that time [Ric10]. With the continuous development of fiber lasers and fiber based telecommunication systems the need for fused fiber components increased significantly. Nowadays, a huge variety of fiber components exist which satisfies specific demands of the respective system, for example for combining the pump and signal radiation in a fiber laser or for increasing the bandwidth of telecommunication systems.

According to a forecast [Cis14] the global Internet traffic will increase from 62 EB/month in 2014 to 132 EB/month in 2018. Up to now, the increasing demand for data-carrying capacity has been satisfied by the use of several techniques in current commercial systems

exploring and optimizing multiplexing in time, wavelength and polarization [Ric13]. Especially to be emphasized is wavelength-division multiplexing (WDM) which is based on the undisturbed propagation of electromagnetic radiation of different wavelengths in an optical fiber. The use of clearly separated wavelength bands allows for the transport of information in different data channels, each of them increasing the bandwidth of the system. In the 1990s this technique together with the availability of optical fiber amplifiers resulted in an increase of the system capacity by a factor of 1000 in just 10 years [Ess12]. However, the combination of current techniques is exploited to a high degree [Qia12] and new concepts are required to satisfy the world-wide growing demand for digital data-carrying capacity. The currently most promising approach is the exploitation of the spatial dimension as additional degree of freedom, commonly referred to as space-division multiplexing (SDM) [Win14].

In order to successfully implement SDM in future optical networks, further optical components are required to realize spatial mode multiplexers and demultiplexers and optical amplification devices. Currently, a high variety of different mode multiplexers already exists [Iga15] including fiber- and waveguide-based adiabatic tapers and couplers. All of these devices have in common that their function principle relies on an asymmetric refractive index profile formed of two different in- and output waveguides. Since the emergence of fused fiber couplers (FFCs) for WDM and fiber lasers in the 1980s, researchers have drawn their attention to devices consisting of different fibers [Bir88b; Mor85; Sor86] in order to exploit new functionalities.

In general, modeling of FFCs has always been a challenge. Intuitively, fiber couplers have often been described by the coupled mode theory assuming two independent and weakly interacting waveguides [Sny72]. However, it was found that common FFCs are tapered to such an extent that the light is not guided by isolated waveguides anymore but by the whole glass structure [Bur83]. Therefore, the cross section and the longitudinal profile of the coupler need to be considered. Researchers have assumed different approximations of the transverse and longitudinal geometry in order to enable the calculation of the eigenmodes which are commonly also referred to as super-modes. A complete analysis in terms of super-modes of symmetric 2×2 FFCs using an accurately modeled refractive index profile was made by Lacroix et al. [Lac94], but only for the case of two identical fibers. However, asymmetric FFCs have not been extensively modeled in terms of super-modes so far, worth mentioning here [Oka90]. However, previous studies were performed under the assumption of independent waveguides using the coupled mode theory [Ism14; Son02; Son03] whose results need to be interpreted carefully, as they lack general validity and fail to describe FFCs exhibiting a high degree of fusion for which independent waveguides cannot be assumed anymore.

The aim of this work is to perform a general analysis of arbitrarily fused asymmetric 2×2 FFCs consisting of different fibers. This includes on the one hand the experimental tuning of coupler characteristics by changing the degree of dissimilarity between fibers and on the other hand the universal description of the coupling mechanism in terms of super-modes. Asymmetric FFCs are evaluated for applications in wavelength- as well as space-division multiplexing.

This work is organized as follows: Chapter 2 gives a brief overview about the essential fundamentals of optical fibers as well as their light guiding properties. The mechanism of coupling in fiber couplers is extensively discussed based on both the coupled mode theory and in terms of super-modes. In Chapter 3 the fused biconical taper technique is presented which is commonly used for the fabrication of FFCs. For this purpose symmetric FFCs are fabricated and characterized. In order to numerically investigate the FFCs in terms of super-modes a numerical model for the calculation of the refractive index profile in three dimensions was elaborated. This model is used to conduct an in-depth analysis of the modal evolution throughout a symmetric FFC. In Chapter 4 and 5 asymmetric FFCs are presented and numerically analyzed in terms of super-modes including the numerical routines which are established and verified for the case of symmetric FFCs. Chapter 4 focuses on asymmetric FFCs which can be used to increase the range of combinable wavelengths for WDM applications. The power-splitting ratio is tuned by pretapering one fiber in order to achieve coupling from the fundamental mode of one fiber to the fundamental mode of the second fiber. A profound analysis of the coupling mechanism is presented discussing the impact of pretapering on the evolution of the super-modes. The concrete application of an asymmetric FFC for the combination of two widely separated wavelengths is demonstrated in a core pumped thulium-doped fiber amplifier at a wavelength of 795 nm. In Chapter 5 the capabilities of asymmetric FFCs are exploited for selective coupling from the fundamental mode of a single-mode fiber to the LP_{11} mode of a few-mode fiber. These fused-type mode-selective fiber couplers are potential candidates for SDM and are experimentally fabricated and numerically analyzed. The impact of tuning the coupler geometry by cladding diameter reduction, pretapering and fusion with respect to the transmission and the higher-order mode excitation are discussed. The modal evolution of the super-modes in arbitrarily fused mode-selective fiber couplers is analyzed enabling a profound understanding of the coupling mechanism. Finally, in Chapter 6 an overall conclusion is drawn and an outlook is given.

CHAPTER 2

Fundamentals of Fiber Optic Components

This chapter gives an overview about the theoretical background related to the present work. It provides a compact description of the most relevant fundamentals. More detailed information can be obtained from [Bur09] and common textbooks [Mit05; Oka06; Pas08; Rei97; Sal07]. First, the general properties of optical fibers are introduced and their light guiding characteristics in terms of modes are discussed. On this basis, the combination of independent fibers forming a fiber coupler is presented and the coupling of light from one fiber to the other is interpreted according to two approaches. The use of these fiber optic components in current applications is outlined and finally simulation methods are shown which allow for a numerical characterization of these components.

2.1 General Properties of Optical Fibers

Optical fibers are cylindrical symmetric dielectric waveguides made from transparent material such as fused silica glass. They enable low-loss transmission of light with typical losses in the order of 0.15 dB km^{-1} . They consist of a core, with radius of r_{co} and a refractive index of n_{co} , surrounded by a cladding with radius of r_{cl} and slightly lower refractive index n_{cl} . Typically, the fiber core is doped with low concentrations of materials such as germanium oxide to slightly increase the refractive index. For mechanical stability against external influences the cladding is usually coated with a polymer material which is called coating. For typical processing of the fibers the coating has to be removed making the air the surrounding medium. The cross section and the one-dimensional refractive index profile of a step-index fiber is depicted in Fig. 2.1. In this work, single-mode fibers (SMFs) or few-mode fibers (FMFs) are used with typical dimension of the fiber core diameter in the order of $5 \mu\text{m}$ to $10 \mu\text{m}$ which is slightly larger than the used wavelength. Multi-mode fibers (MMFs) have typically fiber cores which are much larger than the wavelength. Common fiber cladding radii are for example $125 \mu\text{m}$.

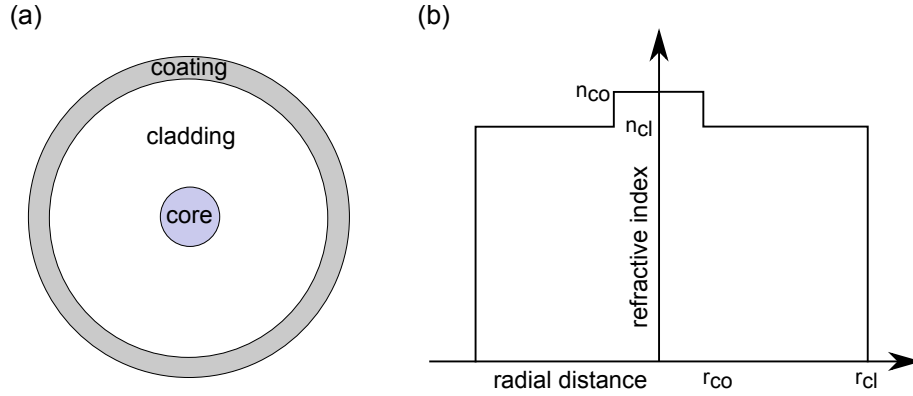


Figure 2.1: Sketch of (a) the cross section and (b) the corresponding one-dimensional refractive index profile of a step-index fiber. r_{co} and n_{co} denote the radius and the refractive index of the core, while r_{cl} and n_{cl} represent the respective values of the cladding. The sketch is not drawn to scale.

Light transmitted in an optical fiber is guided in the core whereby the light guidance can be interpreted in terms of either geometric optics or wave optics. In the case of geometric optics light is guided due to total internal reflection of rays at the core-cladding boundary since the cladding is the optical thinner medium. The maximum angle of acceptance Θ_{max} to the optical path is defined by the numerical aperture (NA) and the refractive index difference between core and cladding:

$$NA = \sin \Theta_{max} = \sqrt{n_{co}^2 - n_{cl}^2}. \quad (2.1)$$

The refractive index of the core and the cladding differs only slightly which means that the fractional refractive index change is small:

$$\Delta \equiv \frac{n_{co}^2 - n_{cl}^2}{2n_{co}^2} \approx \frac{n_{co} - n_{cl}}{n_{co}} \ll 1. \quad (2.2)$$

The refractive index of the cladding ranges from 1.44 to 1.46, depending on the wavelength so that Δ is in the order of 0.01. In MMFs a high number of rays can be guided covering a continuum of possible angles. However, in SMF or FMF the light guidance is described by modes instead of rays and the angles have discrete values.

2.2 Fiber Modes

In the wave optical description light guided in optical fibers is represented as a linear superposition¹ of N discrete eigenmodes, each having different propagation constants β_k , a unique and self-consistent transversal electric field profiles $E_k(x,y)$ and two independent polarization states. The amplitude and phase varies along the propagation direction z with

$$E(x,y,z) = \sum_{k=1}^N E_k(x,y,z=0) \cdot \exp(-i\beta_k z), \quad (2.3)$$

where the explicit time dependence $\exp(i\omega t)$ is omitted. The number of eigenmodes is defined by the wavelength and the geometry of the optical fiber, whereby in the case of an SMF $N=1$. For several superimposing eigenmodes, the resulting electric field profile changes along the propagation due to different propagation constants of the eigenmodes and results in an interference pattern.

The propagation constant is defined as phase change per unit length for light propagating in a medium or waveguide². It relates to the wavenumber k , the phase velocity v_{ph} and the angular frequency ω by

$$\beta = n_{\text{eff}} \cdot k = n_{\text{eff}} \cdot \frac{2\pi}{\lambda} = \frac{\omega}{v_{\text{ph}}}, \quad (2.4)$$

where n_{eff} is the effective refractive index. In general, the refractive index $n = \frac{c}{v_{\text{ph}}}$ quantifies the factor by which the phase velocity v_{ph} is decreased in a transparent optical medium relative to the velocity of light in vacuum c . The effective refractive index n_{eff} corresponds to the refractive index of an eigenmode in a guided medium or waveguide. The propagation constant β and the effective refractive index n_{eff} are equivalent up to the constant factor of the wavenumber k . Both terms are used equivalently in this work and have the same meaning.

The value of the effective refractive index (or analogous the propagation constant) of an eigenmode guided by the core ranges from the refractive index of the cladding to the

¹ Mathematically, the eigenmodes form a basis in a complete orthogonal system.

² It should be mentioned that different definitions exist in literature. Sometimes the propagation constant is denoted with the symbol γ and is a complex quantity which is written as $\gamma = \alpha + i\beta$, where the real part α is the attenuation constant and the imaginary part β the phase constant. In lossless media with $\alpha = 0$ γ is purely imaginary and equals $i\beta$ which is the reason why β is often called the propagation constant.

refractive index of the core

$$n_{cl} < n_{\text{eff}} < n_{co} \quad (2.5)$$

and is determined by the waveguide design and the order of the eigenmode. Therefore, the phase velocity v_{ph} is different for each eigenmode, whereby the fundamental mode has the highest n_{eff} and the highest-order mode has the lowest n_{eff} . The numerical value of the n_{eff} can be obtained by mode calculations as shown in Sec. 2.4.

Mathematically, the set of guided modes is obtained by solving the Helmholtz equation for electromagnetic waves in cylindrical coordinates

$$\frac{\partial^2 U}{\partial r^2} + \frac{1}{r} \frac{\partial U}{\partial r} + \frac{1}{r^2} \frac{\partial^2 U}{\partial \varphi^2} + \frac{\partial^2 U}{\partial z^2} + n^2 k^2 U = 0, \quad (2.6)$$

where $U(r, \varphi, z)$ is a wave function of either the electric or the magnetic field. The ansatz

$$U(r, \varphi, z) = R(r) \Phi(\varphi) \exp(-i\beta z) \quad (2.7)$$

is chosen in order to separate Eq. (2.6) into differential equations for the radial field amplitude $R(r)$ and the azimuthal field amplitude $\Phi(\varphi)$. The solution of these equations yields for the core region a sine or cosine function with a radially decaying amplitude which is mathematically described by a Bessel-function $J_l(u)$ of the first kind and order l . In the cladding region the solution is a modified Bessel-function $K_l(w)$ of the second kind and order l which corresponds to an exponential decrease of the amplitude. The normalized constants u and w determine the rate of change of the amplitude in the core and cladding, respectively. A large value of u means more oscillation of the amplitude in the core and a large value of w means a more rapidly decaying amplitude in the cladding. Both constants are given as:

$$u := r_{co} \sqrt{n_{co}^2 k^2 - \beta^2} \quad \text{and} \quad w := r_{co} \sqrt{\beta^2 - n_{cl}^2 k^2}. \quad (2.8)$$

The sum of the squares $u^2 + w^2 = k^2(n_{co}^2 - n_{cl}^2)r^2 = V^2$ is a constant and

$$V = r_{co} \frac{2\pi}{\lambda} \text{NA} \quad (2.9)$$

is the V parameter which describes the number of guided modes in dependency of the fiber core radius r_{co} , the wavelength λ and the numerical aperture NA.

Most fibers are weakly guiding ($\Delta \ll 1$; Eq. (2.2)) which means that the light is guided approximately parallel to the fiber axis. Therefore, the longitudinal components of the electric and magnetic fields are weaker than the transversal components so that the guided waves are approximately transverse electromagnetic (TEM).

So far, different solutions for Eq. (2.6) in form of Bessel-functions were assumed for the core and cladding region, respectively. Both solutions must be continuous and have a continuous derivative at the core-cladding boundary. These two conditions are satisfied in the weakly-guiding approximation and lead to the characteristic equation

$$u \frac{J_{l\pm 1}(u)}{J_l(u)} = \pm w \frac{K_{l\pm 1}(w)}{K_l(w)}. \quad (2.10)$$

Equation (2.10) can be solved graphically by plotting the left and right side of the equation against u (refer to [Sal07] for the graphical solution). The left side has multiple branches and the right side decreases monotonically with increasing u and vanishes when $u = V$ which leads to a cut-off of higher-order modes (HOMs). The number of intersections determines the number of guided modes for a given V parameter and azimuthal number l . Each intersection m corresponds to a propagation constant $\beta^{(lm)}$ with its corresponding transversal electromagnetic field profile according to Eq. (2.7). Each eigenmode is described by the indices l and m , whereby for $l \geq 1$ each mode set consists of two rotated versions with identical propagation constant. In addition, each eigenmode can be in two orthogonal polarization states which have in the case of the weakly-guiding approximation identical propagation constants so that they are classified as one eigenmode. The solutions are called linearly polarized LP_{lm} modes. Some LP_{lm} modes are depicted in Fig. 2.2. Physically, m corresponds to the number of transverse intensity maxima in the radial direction and l to the number of azimuthal nodes.

The number of intersections in the graphical solution of Eq. (2.10) increases with increasing V parameter. For $V < 2.405$ only the fundamental LP_{01} mode is guided and the fiber operates in the single-mode regime. For a given fiber geometry $V = 2.405$ determines the cut-off wavelength λ_c which means that for larger wavelengths the fiber is single-mode and that for lower wavelengths the next HOM can be guided.

For an increasing V parameter the number of guided modes is proportional to V^2 and it is possible to guide an arbitrary number of modes. However, in most textbooks it remains unmentioned that there is a non-zero lower limit for the V parameter for which light is guided in the core. According to Black and Bourbonnais [Bla86] this corresponds to a

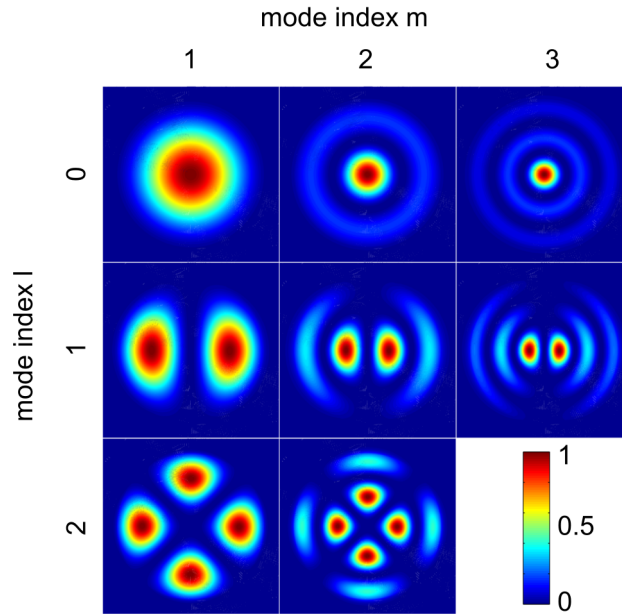


Figure 2.2: Intensity profiles for different LP_{lm} modes in a step-index fiber.

critical V parameter given by

$$V_{cc} \approx \sqrt{\frac{2}{\ln S}} \quad \text{with} \quad S = \frac{r_{cl}}{r_{co}}. \quad (2.11)$$

Below this critical V parameter V_{cc} even the fundamental LP_{01} is not guided in the core. This means that if the core is consecutively reduced in diameter to such an extent that the light breaks out of the core the light is guided by the cladding instead¹. At this transition a former LP_{lm} core mode becomes a cladding mode which due to the strong refractive index difference between cladding and air is not an LP_{lm} mode anymore. In addition, it should be mentioned that the V_{cc} depends on the dimensionality. In two dimensions the V_{cc} is lower than in three dimensions which means that simulations must be performed in 3D in order to obtain reliable results.

2.3 Fiber Couplers

Fiber couplers² are basic fiber optic devices which are used for coupling light from one or several input fibers to one or several output fibers. Such $N \times N$ fiber couplers can be fabricated in different ways. One method is performed by thermally tapering and fusing

¹ It is assumed that the fiber has no coating. Otherwise the cladding light would be absorbed by the coating.

² The term is also used for devices for coupling or launching light from free space into a fiber.

two fibers together. Other methods comprise side-polished or etched fibers in order to gain access to the fiber cores. In all of these methods, the fiber cores are brought in near proximity to each other which allows for coupling light from one core to the other. There are also optical couplers based on planar lightwave circuits where waveguides are brought into substrates by etching or light inscription.

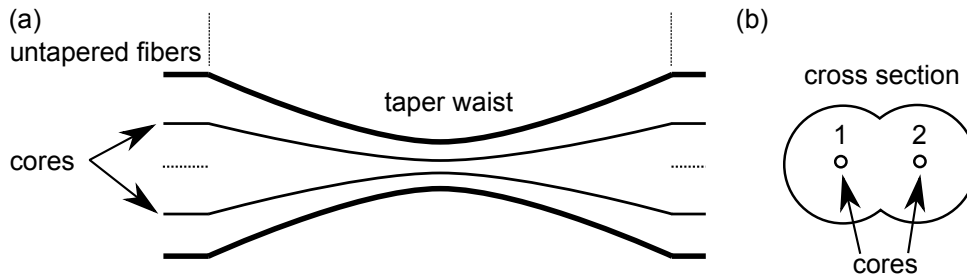


Figure 2.3: Schematic of a 2×2 FFC in topview (a) and in cross section (b).

The main focus of this work are 2×2 fused fiber couplers (FFCs), as depicted in Fig. 2.3 which are fabricated by tapering and fusing two fibers. By tapering it is meant that the fibers are heated and permanently pulled to narrow them down in a defined region. This type of FFCs is for example used for the division of power or for the separation and combination of wavelengths. In the first case, the initial power in fiber 1 is divided into arbitrary power-splitting ratios (coupling ratios) of the power at the output of fiber 1 and 2. In the second case, two different wavelengths launched into fiber 1 are separated according to their wavelength to fiber 1 and fiber 2, respectively. Note, that this can also be used reversely for combining two wavelengths. Both of these applications are widely used in the telecommunication sector for performing WDM or in fiber laser and amplifiers for combining light with different wavelengths.

For these applications typically identical fibers are used and the respective couplers are called symmetric FFCs due to the symmetric refractive index profile¹. However, a symmetric FFC is only a special case of an FFCs consisting of arbitrary fibers. These FFCs are called asymmetric FFCs due to the asymmetric refractive index profile and are the main focus of this work.

2.3.1 Coupling Mechanisms

The origin of the coupling in FFCs is typically explained by two approaches. The first is named evanescent field coupling which describes the energy transfer between the core

¹ The refractive index profile is the distribution of refractive indices of materials. In the frame of this work the refractive index profile $n(x,y,z)$ corresponds to the 3D geometry of the coupler structure that varies with x , y and z .

modes of the individual guides due to the overlap of their evanescent part. In this case the light has to be confined in each core so that both can be considered independently. The second mechanism considers the modes of the entire coupler and the beating between them. This approach is valid no matter if independent cores can be assumed or not. In general, taking the complete coupler into account is superior to the assumption of independent cores. The eigenmodes of the complete coupler include the eigenmodes of the independent cores, but not vice versa. The eigenmodes of the entire coupler are called super-modes (SMs) and the coupling mechanism is referred to as super-mode coupling. In this section both coupling approaches are presented and their application in typical FFCs is discussed.

Evanescence Field Coupling

In case of evanescent field coupling the overlap integral between the core modes of fibers 1 and 2 is non-zero. Therefore, light launched into fiber 1 couples into fiber 2 and the power in fiber 2 continuously increases up to a complete power transfer. With continuous propagation the light couples back and forth between both fibers. The final power ratio at the end of the coupler depends on the strength of the coupling and the length of the coupler.

Mathematically, this can be described by the coupled mode theory¹ [Sny72]. The field amplitudes in both fibers A_1 and A_2 are described as differential equations

$$\frac{dA_1}{dz} = -i\kappa A_2 \exp(-i\Delta\beta z) \quad \text{and} \quad \frac{dA_2}{dz} = -i\kappa A_1 \exp(i\Delta\beta z), \quad (2.12)$$

where $\kappa(V,d)$ is the coupling coefficient and $\Delta\beta = \beta_1 - \beta_2$. Strictly speaking $\kappa(V,d)$ is in general different for each core ($\kappa_{12} \neq \kappa_{21}$), however under the assumption of identical cores κ is equal for both of them. In addition, $\kappa(V,d)$ depends on the separation of the cores $d(z)$ which in general changes in FFCs along the longitudinal position in the coupler due to the tapered profile. Also $\kappa(V(r,\lambda,NA),d)$ changes with wavelength. If two unequal wavelengths are launched into one fiber of the coupler and the length is chosen appropriately both wavelengths can be separated due to the differing coupling coefficients. In order to calculate $\kappa(V,d)$ analytical approximations exist in literature, as for example given in [Tew86]. Therefore, the evanescent field coupling approach allows for the analytical description of the coupling.

¹ The exact analysis of a coupler comprises solving the Maxwell equations using the boundary conditions for different regions to determine the modes of the overall coupler. These modes are different from those of independent waveguides. Under the weakly-guiding approximation it is possible to consider the waveguides independently as if the other waveguide is absent. Coupling between waveguides is then considered as small perturbation.

According to the coupled mode equations the optical power in waveguide 1 and 2 is given in general by

$$\frac{P_1(z)}{P_1(0)} = 1 - \frac{\kappa^2}{\gamma^2} \sin^2(\gamma z) \quad \text{and} \quad \frac{P_2(z)}{P_1(0)} = \frac{\kappa^2}{\gamma^2} \sin^2(\gamma z), \quad (2.13)$$

where $\gamma^2 = \kappa^2 + \frac{\Delta\beta^2}{4}$. For two identical parallel cores with phase matched propagation constants $\Delta\beta = 0$ a periodic complete power transfer between both cores is achieved, as depicted in Fig. 2.4(a) (a realistic value for the coupling coefficient is assumed $\kappa = 0.5 \times 10^3 \text{ m}^{-1}$). At a normalized taper position of 1 the first coupling cycle is complete and its coupling maximum is located at a taper position of 0.5. At the end of the coupler at a taper position of 1.5 the power is completely coupled to the other core. In case that both cores are different a phase mismatch is present $\Delta\beta \neq 0$ and the power transfer is not complete anymore, as depicted in Fig. 2.4(b). Here, the maximum coupled power is limited to 25%.

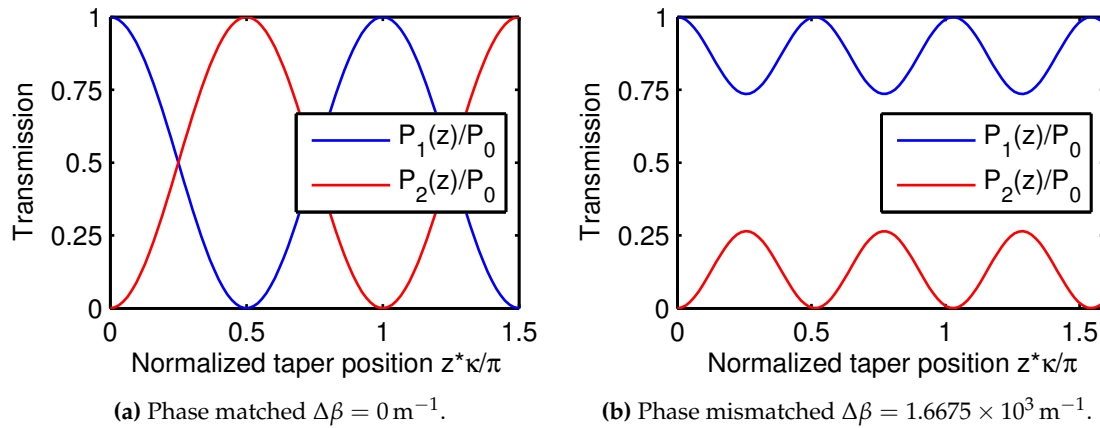


Figure 2.4: Power transfer between two parallel waveguides with $\kappa = 0.5 \times 10^3 \text{ m}^{-1}$.

In conclusion, the power transfer or beating in the evanescent field coupling approach both in the matched and mismatched case is due to a non-zero value of the coupling coefficient. The difference in the propagation constants of both modes defines the maximum coupled power. In contrast to the evanescent field coupling approach where both waveguides are considered independently, in the super-mode coupling approach the complete coupler is taken into account.

Super-Mode Coupling

In general, in $N \times N$ couplers as fabricated by Mortimore et al. [Mor90a; Mor90b] the number of eigenmodes which have non-zero intensity in the cores corresponds to the

number of SMs. All further eigenmodes are referred to as cladding modes and are not guided by the cores. In case of a 2×2 FFC with SMFs two SMs exist, which are referred to as symmetric and antisymmetric SM. The SMs result from a sum (cf. Fig. 2.5(a)) and difference (cf. Fig. 2.5(b)) combination of the core modes of each fiber.

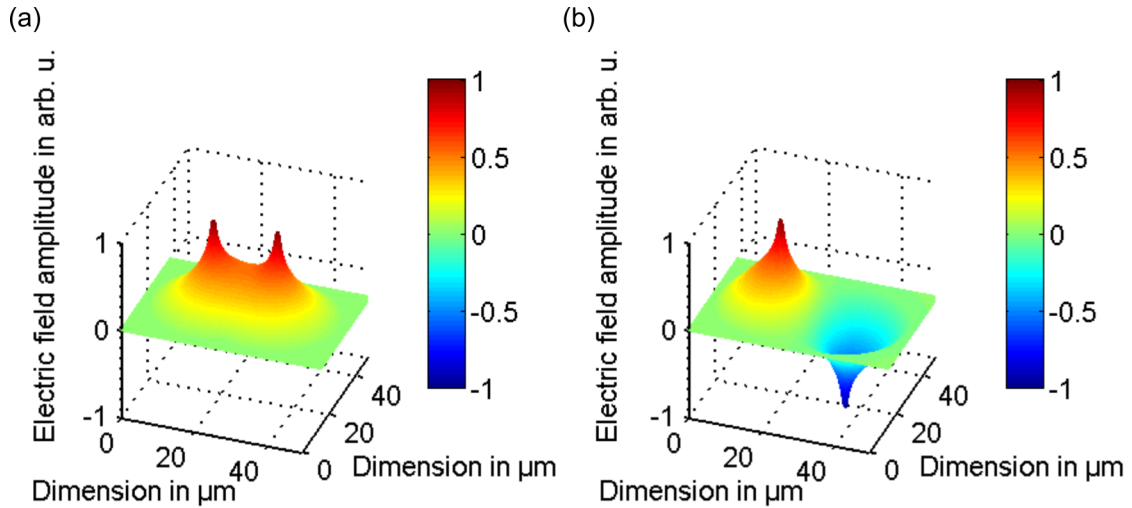


Figure 2.5: Electric field profile of the symmetric (a) and antisymmetric (b) SM in a 2×2 FFC.

If the 2×2 FFC is symmetric the launched field is superimposed as equal addition of the symmetric and antisymmetric SM. The number of SMs equals the number of cores. However, if the coupler is asymmetric both SMs are excited in general unequally and only the SM is excited which corresponds to the fundamental mode of the core where the light is launched.

The symmetric SM (which can also be referred to as first SM) has the highest propagation constant β_s and the antisymmetric SM (also referred as second SM) has the next lower propagation constant $\beta_a < \beta_s$. In general, both SMs propagate at different phase velocities and they accumulate phase difference which leads to beating oscillations and therefore results in a power exchange between both fibers. The power transfer is analogous to the one shown in Fig. 2.4 for the evanescent field coupling approach. The length of a complete coupling cycle is given by the beat length

$$z_B(z) = \frac{2\pi}{\beta_s(z) - \beta_a(z)}. \quad (2.14)$$

The beat length explicitly depends on the taper position z , because $\Delta\beta(z)$ changes along a tapered coupler. At the beginning of the taper both SMs have quasi identical propagation

constants so that no beating occurs, whereas in the taper waist $\Delta\beta(z)$ is maximal and the SMs beat rapidly. Therefore, in the super-mode coupling approach the power transfer is due to different propagation constants of both SMs and the maximum coupled power is given by the excitation ratio of both SMs. This means that in case of equal excitation a complete power transfer can be achieved, otherwise in case of an unequal excitation the coupling is incomplete.

Considering the case of a symmetric 2×2 FFC both SMs at the beginning of the coupler remain equally excited along the complete coupler if the taper is adiabatic [Oka90]. This means that the taper is smooth enough and the cross section changes only slightly in z direction so that the propagating light can adapt to the local set of SMs. Otherwise, if the taper is too strong the propagating light cannot adapt to the local set of SMs and coupling to lossy higher-order cladding modes occurs which results in increased insertion loss. A mathematical description of the adiabaticity criterion is given in [Lov91].

In conclusion, the evanescent field and SM coupling approaches both explain the periodic power transfer in fiber couplers. However, the evanescent field coupling approach is limited to the case that independent waveguides can be assumed. In this case it offers an analytic method to calculate the coupling. If the waveguides cannot be considered independently the coupling has to be calculated according to the super-mode coupling approach which implies the numerical calculation of the propagation constants.

Light Propagation

FFCs are normally fabricated by fusing and tapering two independent fibers creating a unique 3D distribution of the refractive indices. The resulting refractive index profile is depicted schematically in Fig. 2.6. Light launched into one fiber is guided in the core up

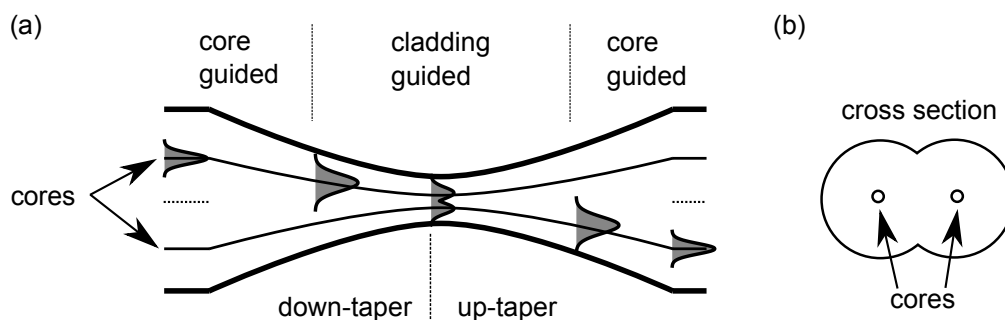


Figure 2.6: Schematic of the refractive index profile of a 2×2 FFC in topview (a) illustrating the coupling along the longitudinal profile and in cross section (b).

to a position in the down-taper where the core radius is reduced to such an extent that the light is not guided by the core anymore. This is the case for the most common FFCs

and was first reported in [Bur83]. At this core-cladding transition the V parameter equals V_{cc} and the light is guided by the cladding-air boundary. In fact the entire fiber becomes the core with the air as the cladding and the original core is only a small but significant perturbation. In addition, the n_{eff} of the SM equals n_{cl} at this position.

According to the aforementioned approaches for describing the coupling this means that in the cladding guided region the application of the evanescent field coupling approach fails, because no independent waveguides exist anymore¹. Then, the coupling must be described by the super-mode coupling approach where the whole arbitrarily fused coupler structure is considered.

In the core guided region the coupling can be described by both approaches, although in this region nearly no coupling occurs. This is due to the fact that in common FFCs, mostly fabricated with 125 μm cladding fibers, the core separation is too large to observe significant coupling no matter how strong the fusion is. In the evanescent field coupling approach this means that the coupling coefficient is zero and in the super-mode coupling approach this means that the propagation constant difference is zero. Theoretically, coupling could also occur in the core-guided region by using for example fibers with a reduced cladding diameter. However, with increased extension the coupling is gradually overtaken by coupling in the cladding-guided region [Pal03].

The power transfer between both fibers starts when the SMs begin to propagate with different velocities and to accumulate phase difference in the down-taper which becomes visible as characteristic mode beating. This occurs at the transition between the core guided and the cladding guided region. The beat length defines by which fiber the light is recaptured in the up-taper region when the cores become large enough to guide the light again. Due to the fact that the taper is adiabatic, the transitions between core-cladding and cladding-core guidance are loss-less.

In conclusion, it is the most powerful way to describe the coupling in FFCs by the super-mode coupling approach. It allows for the theoretical consideration of arbitrarily fused FFCs over the complete length. However, this implies an accurate refractive index profile model of the FFC in order to numerically calculate the propagation constants and the shape of the SMs. In the frame of this work such a refractive index profile model was elaborated and is presented in Sec. 3.2.

¹ In the case that both fibers are only weakly-fused the light is guided in the cladding of the fiber where it was initially launched. In this particular case the coupling could be treated according to the evanescent field coupling approach and an approximation for κ was derived [Pay85b]. Also the strongly-fused case has been approximated by the use of a rectangular waveguide structure and an approximation for κ exists [Pay85a].

2.3.2 Fiber Optic Components

Fiber optic components have become relevant in all fields of application where optical fibers are employed. In fiber lasers and amplifiers they allow for combining the pump and signal radiation in one fiber which enables pumping directly into the core of the fiber. By specially designed components it becomes possible to combine wavelengths with a separation in the order of $1\ \mu\text{m}$ [Pel12] which can handle power levels in the order of 200 W [Ott15]. The large variety of fiber components also includes for example pump and signal combiners for pumping double-clad fibers [The12].

In addition to the use in fiber lasers and amplifiers, fiber optic components are nowadays extensively used in optical communication systems for both long-haul optical data transmission and high-speed local area networks. Fiber-optic links consist of a data transmitter, an optical fiber (possibly with built-in fiber amplifier) and a receiver. Standard wavelengths used for telecommunication are $1.3\ \mu\text{m}$ and $1.5\ \mu\text{m}$, because they show low absorption in silica. The data rate can be increased by multiplexing several data channels which are transmitted through the fiber and afterwards separated for detection.

Optical data can be transmitted by the use of several techniques which exploit all possible physical dimensions, as time, frequency, polarization and space [Win14]. The most common technique is known as WDM which relies on the transmission of several densely packed wavelengths each of them assigned to a different data channel. For example, up to 160 data channels with a spectral width in the order of nanometer are used. Another technique is time-division multiplexing, where several data channels are transmitted in a sequence of time frames. In case of polarization-division multiplexing (PDM), several data channels are transmitted by exploiting the polarization dimension. These methods are currently well established and already highly developed [Qia12].

For future developments the use of the spatial dimension is required, since it is the only remaining degree of freedom which offers the potential to scale the capacity by multiple orders of magnitude [Li14; Ric13]. A concrete implementation of SDM is based for example on the transmission of HOMs in optical fibers. Currently, research focuses on the implementation of SDM in existing multiplexing systems based on WDM and PDM [Cha14; Cha15].

Photonic Lanterns

Especially interesting fiber-based mode-selective devices for SDM are so called photonic lanterns (PLANs) whose operation principle is based on the adiabatic propagation of light [Bir15]. PLANs consist of N isolated SMFs that are packed into a capillary which has a lower refractive index than the fiber cladding (cf. Fig. 2.7, image taken from [Hua15a]).

The complete structure is then adiabatically tapered. In the taper waist the initial fiber cores are reduced to such an extent that they do not guide the light which is instead guided by the core generated by the fiber cladding. The low-index capillary is the new cladding forming a multi-mode fiber section. Depending on the application, PLANs are cleaved in the taper waist so that one side consists of SMFs and the other side out of the MMF section.

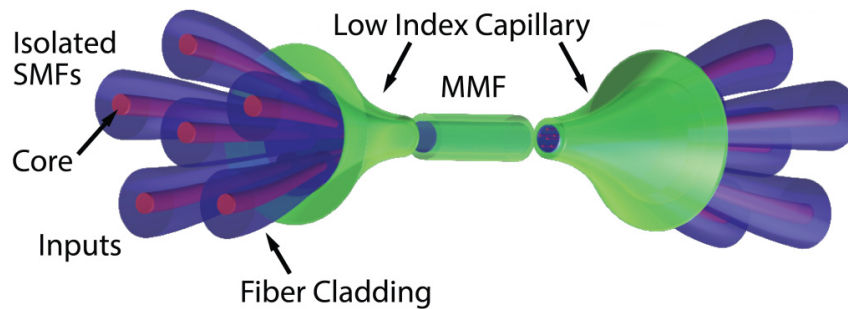


Figure 2.7: Schematic of a photonic lantern (image taken from [Hua15a]).

The number of excited SMs corresponds to the number of the SMF cores [Bir12]. If for symmetric PLANs consisting of N cores, light is launched into one fiber core all SMs get excited. Those devices were initially developed for astrophysical applications [Bla09], because reversely operated the N lowest order modes coupled into the MMF section evolve into the fundamental modes of the N SMFs due to the adiabatic transition. In other words, this allows for single-mode behaviour within an MMF. Any mode of a higher order excited in the multi-mode section does not evolve into the SMF cores, because this would be a violation of the conservation of entropy [Fon12].

Within the framework of SDM asymmetric PLANs made out of dissimilar fibers are of major interest. Light launched into one fiber of an asymmetric PLAN excites only one SM at the beginning of the taper. Light can be launched into each SMF which excites a different SM, respectively. Due to the adiabatically tapered structure, the order of the initially excited SM is preserved so that the initially excited n -th SM evolves into the corresponding n -th mode in the multi-mode fiber section. Therefore, it is possible to selectively excite for example the LP_{11} mode in the multi-mode fiber section simply by choosing the input SMF with the corresponding propagation constant [Leo14; Yer14].

In conclusion, the principle of function of (mode-selective) PLANs relies on the adiabatic propagation of light. This enables the selective excitation of HOMs without the need to rely on mode matching conditions. A 2×2 FFC, as treated in this work, is basically a PLAN consisting of two fibers and without the low-index capillary. With respect to the propagation of light both devices are very similar.

2.4 Simulation Methods

FFCs exhibit an axial varying waveguiding structure with a complex geometry which consists of cores, cladding and the surrounding medium. A rigorous mathematical description of such structures is challenging and has been approximated for example by the coupled mode theory [Sny72]. As discussed in Sec. 2.3.1, the coupled mode theory is limited to the assumption of isolated waveguides. The super-mode coupling approach allows for the description of arbitrarily fused structures. However, in this case numerical calculations are required to obtain the propagation constants and shapes of the SMs. In literature different methods exist as for example beam propagation [Kac87], effective index [Chi86], finite element [Zhe86] and others [Pal03].

In the frame of this work, the commercial software tool BeamPROP [RSo10] was used which is based on the beam propagation method (BPM) [Sca00]. BPM is widely used to investigate linear and nonlinear lightwave propagation phenomena in axially varying waveguides [Oka06]. Basically, it is a method which approximates the Helmholtz equation (cf. Eq. (2.6)) and solves it numerically. One of the approximations is the paraxial approximation ($\frac{\partial^2}{\partial z^2} = 0$) which can be assumed, since the electromagnetic field changes only slightly in z direction. For the computation this means that only structures can be calculated in which the electromagnetic field propagates mainly along the z axis, however the computation speed is dramatically increased due to the fact that only the first order derivative in z is involved. In addition to the paraxial approximation BPM exhibits also simplification for scalar fields and unidirectional propagation. However, current simulation tools as BeamPROP include the possibility to handle vectorial fields, bi-directional propagation and the paraxial limitation. Standard numerical techniques are then used to calculate the propagation in z direction. Typically, these are either the split-step Fourier method or the ADI¹ method.

The simulation tasks in this work consist on the one hand of calculating the local propagation constants and shapes of the SMs and on the other hand of calculating the light propagation along the longitudinal varying profiles. The eigenmode calculation was performed with BeamPROP, using the build-in mode solver utility based on the ADI method. The light propagation was simulated with a self-implemented simulation tool [Tün13]. It uses a BPM algorithm based on the split-step Fourier method and was accelerated on a

¹ The alternating direction implicit (ADI) method is a finite difference method for solving partial differential equations which is based on the Crank-Nicholson scheme.

graphics processing unit using the CUDA¹ architecture [NVI12]. Depending on the length of the simulated FFC the calculation time² was about less than 4 min. In comparison to that, a simulation run with the same parameters executed in BeamPROP takes by a factor of more than ten computation time. Therefore, the tool [Tün13] is significantly faster than BeamPROP due to the execution on a graphics processing unit instead of the execution on a single thread of a central processing unit. The simulation results of both simulation tools are in good agreement with the experimental results and are further discussed in the following Chapter 3.

1 CUDA (also known as Compute Unified Device Architecture) is a parallel computing platform and programming model describing NVIDIA graphics processors.

2 The simulation was executed on an NVIDIA GeForce GTX 680.

CHAPTER 3

Symmetric Fused Fiber Couplers

In this chapter basic symmetric fused fiber couplers are introduced and analyzed both experimentally and numerically. A method for the fabrication of FFCs and their characterization is described and a numerical model for the calculation of the refractive index profile in three dimensions is presented which is used to numerically characterize the fabricated FFCs. A modal analysis is performed to describe the coupling mechanism according to the SM coupling approach throughout the taper.

3.1 Fabrication and Characterization

Fused Biconical Taper Technique

In this work, FFCs were fabricated by the well-developed fused biconical taper technique [Bri84; Kaw81]. The presented experiments were performed with a commercial single-mode tapering rig (SIFAM Fiber Optics) which is schematically depicted in Fig. 3.1. For the FFC fabrication process the fibers are fixed at the stepper motors with fiber clamps. Both fibers are put into a ceramic crucible, which homogeneously distributes the heat, and are twisted by rotating the right fiber clamp for 720° . A hydrogen burner is used to warm up the crucible up to the softening temperature of fused silica¹ (approx. 1600°C). The burner consists of two torches which can be varied in height in order to adjust the resulting temperature in the crucible.

The fabrication process is conducted in two consecutive steps (cf. Fig. 3.2): First the fibers are pulled by applying axial tension for a certain pull length at a high temperature in order to achieve the fusion of both fibers. The resulting degree of fusion (DOF) of both fibers is mainly determined in this phase of the manufacturing process by the applied

¹ Amorphous silicon dioxide.

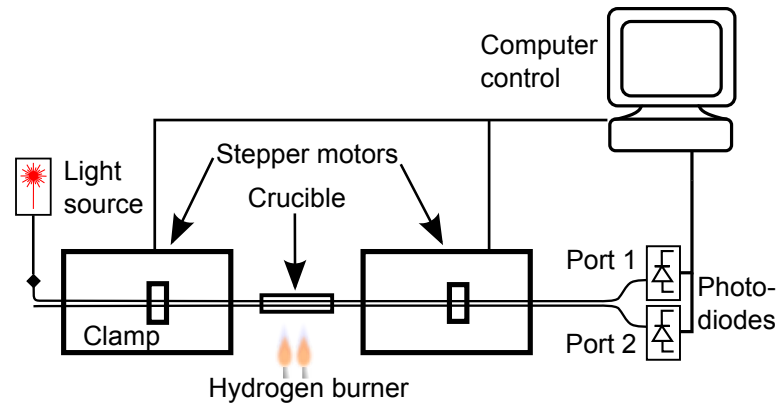


Figure 3.1: Schematic setup of the single-mode tapering rig for the fused biconical taper technique.

extension (also called fuse extension) and the temperature in the crucible. In the second step the FFC is continuously pulled at lower temperatures which is achieved by lowering the burner height position. In this phase the taper waist is consecutively reduced in diameter whereby the DOF is nearly maintained. During the whole pulling procedure light is injected into one fiber while the transmission is monitored at the fiber outputs in real-time by using photodiodes. With the help of computer assisted measurement and control electronics the manufacturing process can be conducted fully automated.

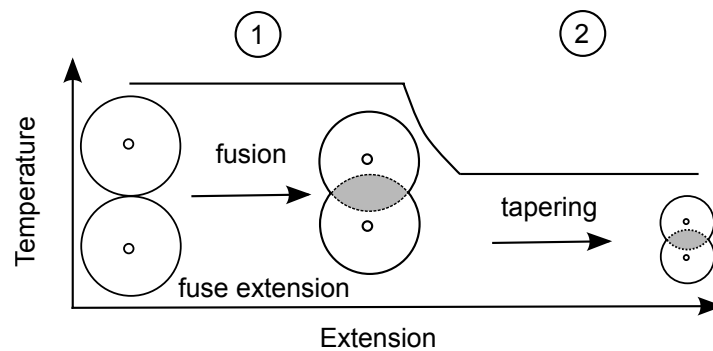


Figure 3.2: Scheme of the FFC fabrication process conducted in two steps: First fusion of the fibers and then tapering.

Pulling Signatures

Two types of symmetric FFCs were fabricated using the SMFs 780-HP and SM2000 (cf. Sec. A.1 for fiber parameters). Light sources at wavelengths of 795 nm and 1980 nm were employed which showed single-mode guidance in the fibers, respectively. In Fig. 3.3 the measured characteristic pulling signature of an FFC made from 780-HP at a wavelength of 795 nm is depicted showing the transmission at both fiber output ports during the

fabrication process. The FFCs were pulled up to their destruction which leads to an unusual coupling behaviour at the end of the pulling signature. At an extension of (13.5 ± 0.5) mm the light starts to couple from port 1 to port 2. The first coupling maximum is located at an extension of about 18 mm and further maxima can be observed at approx. 21 mm and 22.5 mm. The distance of the maxima decreases with increasing extension which means that the periodicity of the coupling cycles changes during the pulling process. This is due to the fact that the taper waist becomes thinner with consecutive pulling and therefore the difference in the propagation constants between the symmetric and antisymmetric SM increases resulting in a larger accumulated phase difference and shorter beat length.

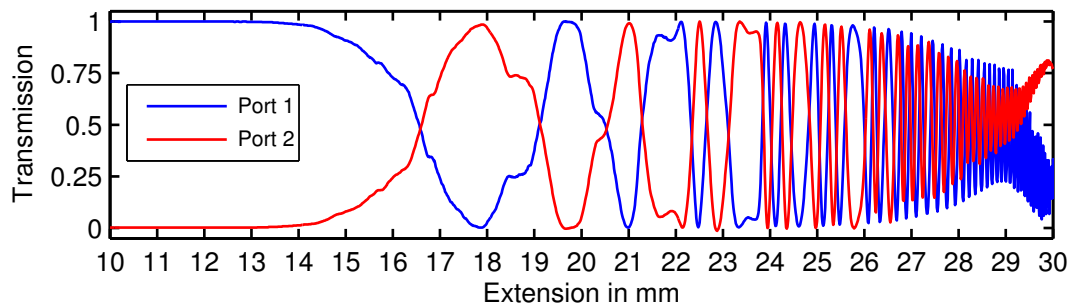


Figure 3.3: Measured pulling signature in a symmetric FFC made from 780-HP at a wavelength of 795 nm.

In Fig. 3.4 the pulling signature of an FFC consisting of two SM2000 fibers using a light source at a wavelength of 1980 nm is depicted. In this case the coupling starts at an extension of (9.5 ± 0.5) mm and the first coupling maximum is located at an extension of about 13.3 mm. For higher values of the extension a modulation of the envelope is visible which is due to the fact that FFCs with many coupling cycles or very thin tapered fibers are birefringent [Bil88; Lov85]. This is due to the splitting of the propagation constant for each SM into two, respectively for each polarization, so that in total four SMs are involved [Bri85; Pay85b]. Weakly-fused couplers do not possess circular symmetry which means that each SM splits into two SMs with a respectively different propagation constant for each polarization axis. However, in strongly-fused couplers the cross section is less asymmetric and the polarization induced splitting of the propagation constants is less pronounced. Linear polarized light injected into the FFC with a slight offset angle from the principal axes results therefore in a superimposed modulation in the pulling signature.

Since both FFCs were pulled up to their destruction, it was not possible to measure the DOF in the taper waist. According to the DOF measurement of FFCs which were

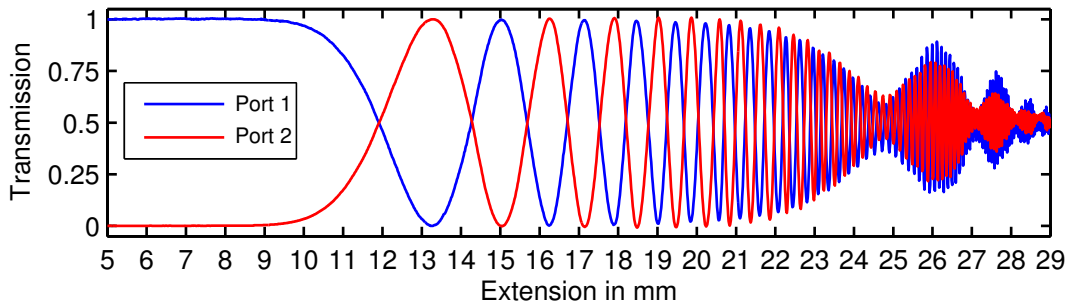


Figure 3.4: Measured pulling signature in a symmetric FFC made from SM2000 at a wavelength of 1980 nm.

fabricated with similar parameters, both fibers are strongly fused¹. The reproducibility of the fabrication process was verified by pulling two FFCs made from SM2000 at a wavelength of 1980 nm with identical fabrication parameters and measuring the pulling signatures of both FFCs at the same fiber port (cf. Fig. A.3).

In conclusion, these results demonstrate that the fused biconical taper technique can be used to fabricate fused fiber components for common used wavelengths around 800 nm and also for wavelengths in the innovative spectral region of 2 μm [Pis13].

3.2 Modeling the Refractive Index Profile of Fused Fiber Couplers

In order to numerically characterize the fabricated FFCs shown in the last section a numerical model for the calculation of the refractive index profile of tapered fiber couplers is required. In literature the shape of single fiber tapers has been extensively investigated by assuming different taper profiles [Bir92]. Also the refractive index profile of tapered fiber couplers has been described by the use of a sophisticated model solving the diffusion-convection equation [Pon04a; Pon04b]. In this work, a more basic numerical model for the calculation of the refractive index profile is elaborated.

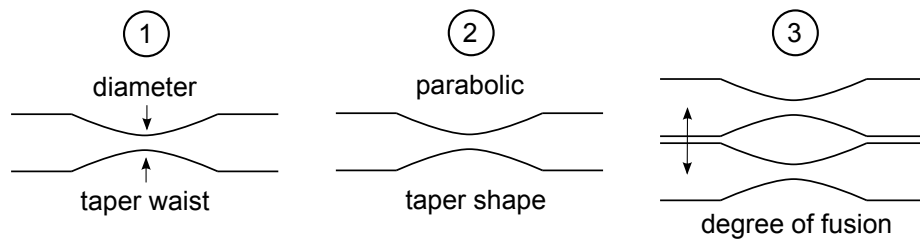


Figure 3.5: Route for the refractive index profile calculation.

¹ The specific value of the DOF of the fabricated FFCs should be in the order of 1.3 ± 0.1 which is strongly fused.

The route, as illustrated in Fig. 3.5, is to first calculate the final diameter in the taper waist D_f of a single fiber for a certain pull length or extension l . In the next step a parabolic taper shape is used to calculate the diameter of a single fiber for the transition between the taper waist and the beginning of the taper. In the final step the transversal position of the fibers to each other is calculated considering the overlap of both fibers by applying a certain DOF. Since the presented model should consider the core-cladding and the cladding-air boundary, the same calculations need to be performed for the fiber core, as well. Chiang [Chi87] demonstrated that the effect of the fiber core on the FFC characteristics, e.g. the SM profile, is not negligible. Figure 3.6 depicts a schematic of the refractive index profile in the untapered and tapered case and also the cross section in the taper waist when both fibers overlap to a certain degree.

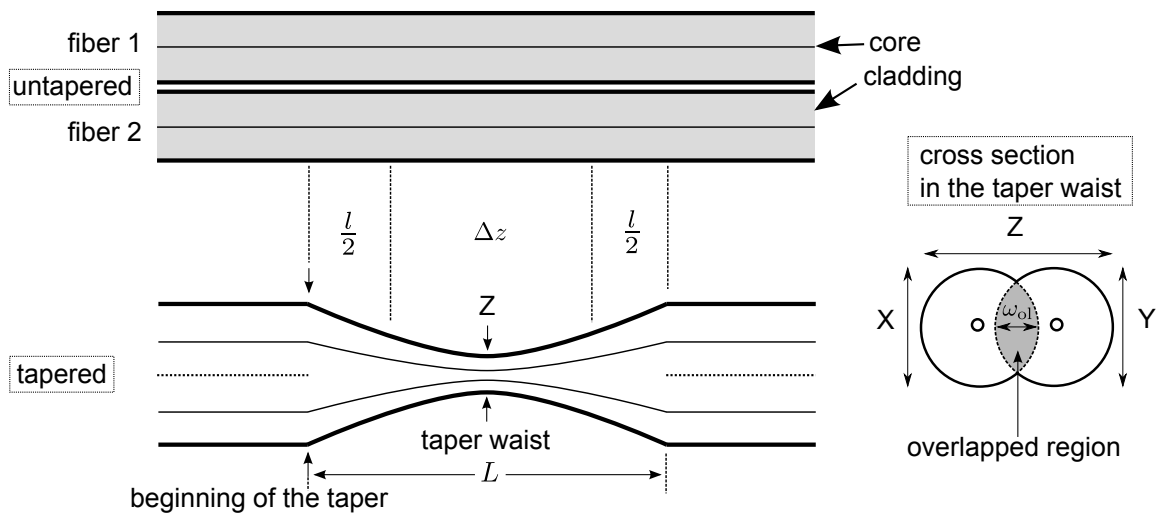


Figure 3.6: Schematic of the refractive index profile of an FFC in the untapered and tapered case. l is the extension, Δz the width of the hot zone, L the length of the taper, X and Y the diameters of fiber 1 and 2 in the taper waist, Z the width of the cross section in the taper waist and w_{ol} the width of the overlapped region in the taper waist.

3.2.1 Determination of the Hot Zone and the Diameter in the Taper Waist

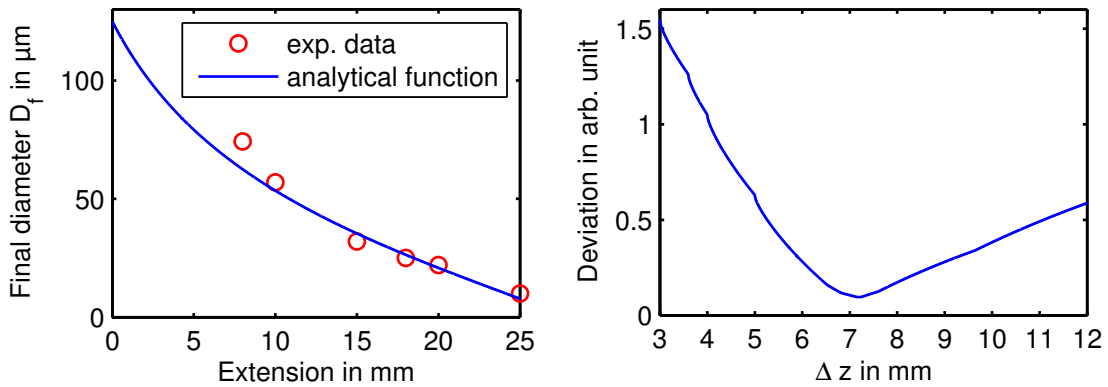
During the heating process a certain cylindrical region of the glass volume is softened which corresponds to the hot zone [Bur85]. The width of the hot zone Δz , the region from which the material is taken during the tapering, cannot be simply assumed as the breadth of the heater flame, since it depends on the heat distribution in the crucible. The heat distribution itself depends on parameters as the pressure and composition of the hydrogen gas, the distance of the torches and the height of the burner. The hot zone is therefore a characteristic parameter of the single-mode tapering rig. During the tapering the width of

the hot zone Δz remains constant whereas the volume from which the material is taken is consecutively reduced. The glass volume which is removed from the hot zone solidifies.

In order to determine Δz , various FFCs were pulled by applying axial tension with different extensions. This results in a tapered region with the length of $L = \Delta z + l$. The FFCs were cleaved in the taper waist and the final diameter D_f of one fiber was measured with the help of an optical microscope. The experimental data is shown in Fig. 3.7(a). Burns et al. [Bur85] formulated an analytical equation, assuming the conservation of the glass volume, to calculate the final diameter in the taper waist D_f of a single fiber in dependency of the initial diameter at the beginning of the taper D_i , the extension l and the width of the hot zone Δz :

$$D_f(D_i, l, \Delta z) = \frac{\frac{3}{2} \left(4 - \frac{l}{\Delta z}\right)}{\left(1 + \frac{l}{\Delta z}\right) + 5\sqrt{\left[\left(1 + \frac{l}{\Delta z}\right) \left(1 - \frac{l}{5\Delta z}\right)\right]}} \cdot D_i. \quad (3.1)$$

The analytical expression was fitted on the experimental data by calculating the minimum deviation (method of least squares) of both data sets by varying the Δz parameter. The minimum of the result shown in Fig. 3.7(b) indicates that the best fit corresponds to a value of approx. 7 mm. The corresponding curve for the analytical function is plotted in Fig. 3.7(a). The determination of the characteristic hot zone of the used equipment enables the calculation of the diameter in the taper waist for arbitrary extensions.



(a) Final diameter in the taper waist D_f vs. the applied extension. The analytical function is for $\Delta z = 7$ mm.

(b) Deviation of the analytical function to the experimental data by varying Δz . The best fit parameter is $\Delta z \approx 7$ mm.

Figure 3.7: Determination of the width of the hot zone Δz .

3.2.2 Parabolic Taper Shape

Based on the calculation of the diameter in the taper waist D_f it is possible to model the transition between the beginning of the taper and the taper waist and therefore to calculate the diameter at each taper position. In literature different taper profiles have been used, as for example sinusoidal [Lov86] or parabolic [Bur83; Bur87] taper profiles. In the present model a parabolic taper shape is chosen based on the measurement of the diameter along different fiber tapers. In Fig. 3.8 longitudinal taper profiles at extensions of 10, 15 and 20 mm are shown (circles) which were measured with an optical microscope. It should be mentioned that for each taper the length L is approximately the applied extension l plus the width of the hot zone Δz which confirms the determined value of $\Delta z = 7$ mm from Fig. 3.7.

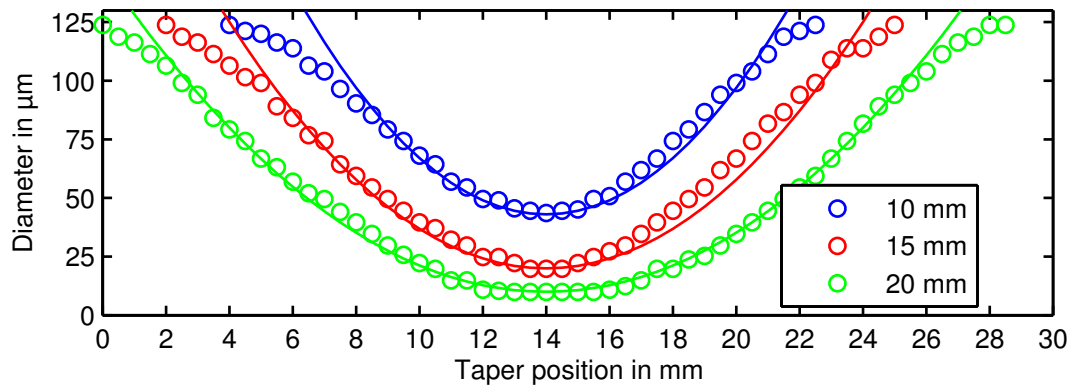


Figure 3.8: Experimental measurement of the longitudinal taper profile for l of 10, 15 and 20 mm (circles). The solid lines are parabolic curves of the general form $y = a(x - x_0)^2 + y_0$.

The respective parabolic curves of the general form $y = a(x - x_0)^2 + y_0$ in Fig. 3.8 (solid lines) indicate the parabolic shape of the tapers. In the central part of the taper the measured profile corresponds to a high degree to a parabolic function. But at the outer taper positions at the transition to the non-tapered region the profile deviates from the parabolic form. This means for the modeling that the real smooth transition between the tapered and non-tapered region is implemented as abrupt transition. However, the impact of the deviations from the parabolic form at the outer taper positions is of minor interest, because the light is guided in the cores and the exact shape of the cladding at these taper positions is nearly irrelevant. The concrete implementation for the calculation of the diameter at each taper position is shown in Sec. B.1 of the appendix.

3.2.3 Transversal Position of the Fibers and Implementation of the Degree of Fusion

Finally, the transversal position of both fibers to each other has to be calculated. According to the parabolic taper shape of the fibers, the center position of the fiber or respectively the position of the core in the 3D space is assumed to be a parabolic function in dependency of the taper position, too (cf. Sec. B.1 for the implementation). In addition, the overlap of both fibers due to the fusion during the fabrication process has to be considered as well. According to the single-mode tapering rig supplier's manual [Opt08], the DOF is defined as

$$\text{DOF} = \frac{2 \cdot Z}{X + Y} \quad (3.2)$$

whereby Z is the width of the cross section in the taper waist, X the diameter of one fiber and Y the diameter of the other fiber in the taper waist (cf. cross section in Fig. 3.6). In this definition a DOF of 2 means no fusion (tangent fibers) and a DOF of 1 complete fusion (circular cross section). The separation of the fiber cores d is given by

$$d = \frac{(X + Y)}{2} (\text{DOF} - 1) \quad (3.3)$$

(cf. Sec. B.1 for the derivation) and the width of the overlapped region w_{ol} (cf. Fig. 3.6) is

$$w_{\text{ol}} = (X + Y) \left(1 - \frac{\text{DOF}}{2}\right). \quad (3.4)$$

It is important to note that the width of the overlapped region w_{ol} is calculated in the taper waist. The width of the overlapped region is then constant along the whole length of the FFC. This results in a non-constant DOF throughout the FFC which is reasonable, because the real DOF of fabricated FFCs changes from no fusion in the untapered region to a certain DOF in the fused region.

3.2.4 Modeled 3D Refractive Index Profile

In addition to the position and diameter of the fiber cladding, also the parameters of the fiber core itself are implemented in order to consider the core-cladding boundary. It is assumed that the position of the core corresponds to the center position of the fiber and that the ratio between the core and cladding diameter of the untapered fiber is kept constant throughout the taper [Lov91].

In Fig. 3.9 an example of a calculated 3D refractive index profile is depicted for an extension of 15 mm and a DOF of 1.5. The cladding-air boundary is shown in blue and the

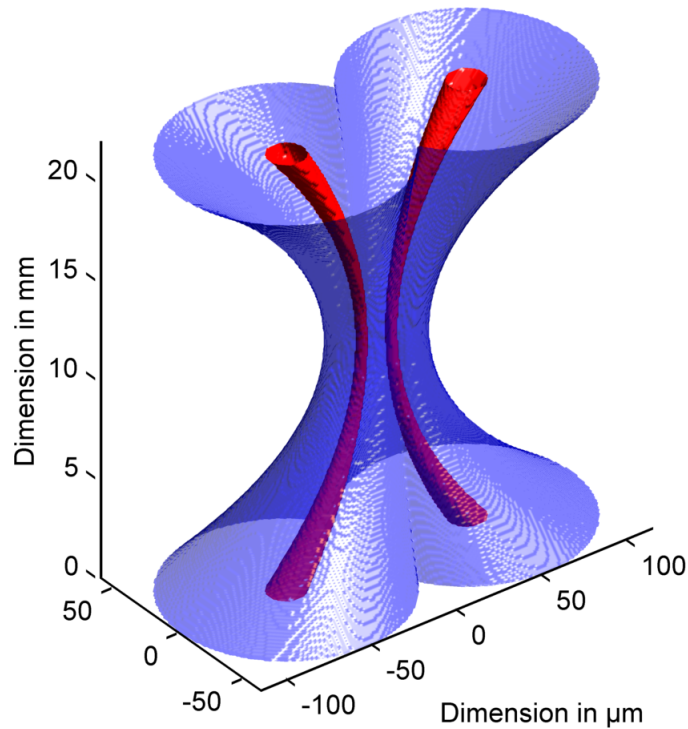


Figure 3.9: Modeled 3D refractive index profile of an FFC with an extension of 15 mm and a DOF of 1.5. The cladding-air boundary is shown in blue and the core-cladding boundary in red, whereby for illustration purposes the cores are not drawn to scale (enlarged by a factor of 5).

core-cladding boundary in red, whereby for illustrative purposes the cores are not drawn to scale (enlarged by a factor of 5). Therefore, the refractive index profile model calculates the distribution of the refractive indices $n(x,y,z)$ in all three spatial dimensions.

3.2.5 Inverse Taper Ratio

In the model the longitudinal taper profile is fully defined by the hot zone and the extension. However, the hot zone is fixed at the beginning of an experiment, whereby the extension is consequently increased during the pulling procedure. The permanent measurement of the transmitted power provides the characteristic pulling signature of the FFC, as shown in Fig. 3.3 and 3.4. The presentation of the pulling signature plotted against the extension is very intuitive, but not universal and complicates the comparison with experiments where different setups are used. Therefore, the use of a normalized dimension of the cross section, for example the inverse taper ratio $\left(\frac{x}{D_i}\right)$, would be more general. However, in the framework of this work it is desirable to maintain the intuitive presentation using the extension in order to facilitate the interpretation of the results.

Nevertheless, the inverse taper ratio allows for the comparison with other experimental data in literature and is depicted in Fig. 3.10 for the used refractive index profile model.

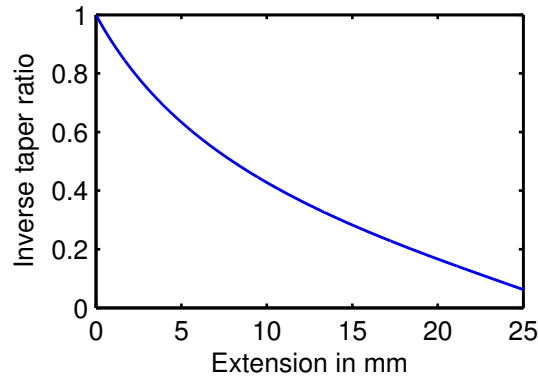


Figure 3.10: Relation between the inverse taper ratio and the applied extension.

3.2.6 Simplifications and Limitations of the Refractive Index Profile Model

Although the presented numerical refractive index profile model should be in relative good agreement with the real refractive index profile there are several simplifications and limitations which are discussed in the following.

Twisting

In comparison to the FFC fabrication process the twisting of the fibers is completely ignored in the modeling. Experimentally, the twisting is important to ensure the fusion during the application of the axial tension. Numerically, this fact is irrelevant, since the DOF can simply be adjusted. In addition, the twisting can also influence the polarization properties especially in FFCs with many coupling cycles, due to the propagation constant splitting of the SMs. Post-fabrication axial twisting can also be used to tune the power-splitting ratio of the FFC [Bir88a; Bir89]. Twisting influences the characteristics of the FFC mainly because of the polarization which means that by not considering the twisting polarization effects are neglected in the simulations. However, the self-implemented simulation tool [Tün13] uses a scalar algorithm and therefore polarization effects are not implemented. As discussed in the following section, experiment and simulation are in relative good agreement and essential features are covered by them.

Degree of Fusion

A further simplification concerns the implementation of the DOF. The critical aspect is that the position of the fiber cores is assumed to correspond to the middle of the respective fiber. For the application of the DOF both fibers are moved into each other which leads to

completely overlapping cores at a DOF of 1 (cf. Eq. (3.3)). This is due to the fact that the material conservation is ignored in this model, but the core separation in the experiments is non-zero even at the maximum DOF.

An alternative DOF definition, which considers material conservation, is given by Lacroix et al. [Lac94]:

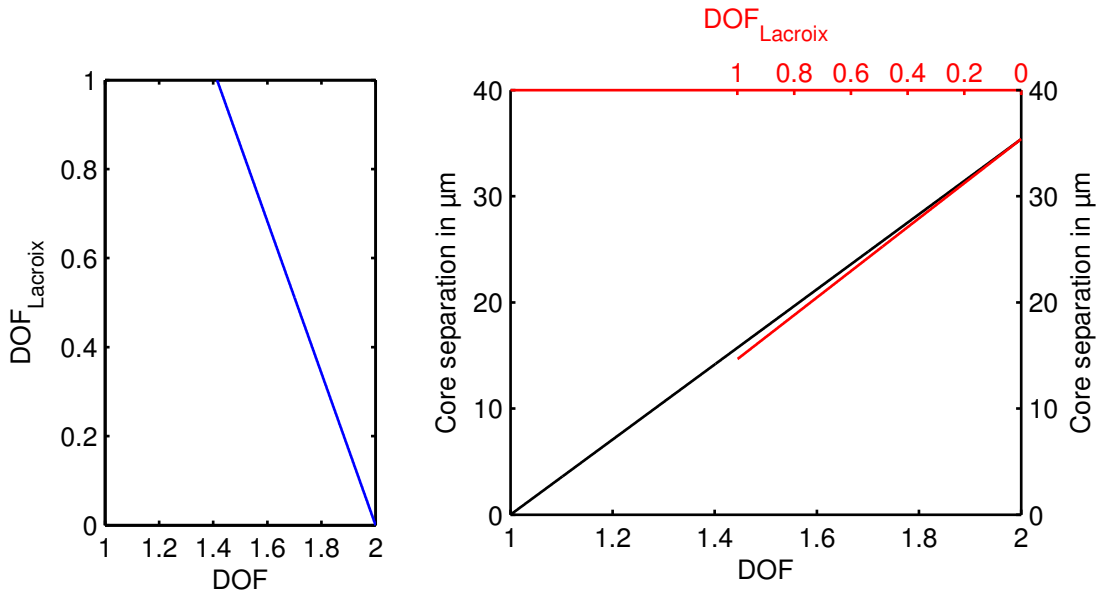
$$\text{DOF}_{\text{Lacroix}} = \frac{2r_{cl} - d_{\text{Lacroix}}}{2(2 - \sqrt{2})r_{cl}} \quad \text{with} \quad d_{\text{Lacroix}} = 2(\sqrt{2} - 1)r_{cl} \quad (3.5)$$

for the fiber-center separation, whereby r_{cl} is the unfused fiber-cladding radius. In this definition $\text{DOF}_{\text{Lacroix}} = 0$ is for tangent fibers and $\text{DOF}_{\text{Lacroix}} = 1$ for a circular cross section. In addition, the position of the fiber cores is not assumed to be in the middle of the respective fiber in this $\text{DOF}_{\text{Lacroix}}$ definition and is calculated by Eq. (3.5).

Both definitions given in Eq. (3.2) and Eq. (3.5) are different and correspond to each other according to Fig. 3.11(a) for a symmetric FFC¹. In the definition of $\text{DOF}_{\text{Lacroix}}$ the lower limit of the width of the cross section in the taper waist Z is higher than the diameter of one fiber, because the material conservation is considered. A DOF of 1.4 corresponds to a $\text{DOF}_{\text{Lacroix}}$ of 1 in terms of core separation and is the experimentally lowest value for the DOF where the core separation is considered correctly in the present modeling. This means for the model used in this work that a value of the DOF below approx. 1.4 would lead to FFCs with core separations lower than experimentally possible and it is therefore not recommendable to use.

The respective core separations for both definitions of the DOF are shown in Fig. 3.11(b). The maximal difference between both definitions with respect to the core separation is in the order of 1 μm as long as the DOF is above 1.4. For a DOF below 1.4 the fiber cores approach more, because the core position is assumed to be the center position of the respective fiber. Although, in reality the fiber cores do not approach more due to material conservation.

¹ This is calculated by varying the width Z of the cross section (cf. Fig. 3.6) from the diameter of one fiber X up to the diameter of both fibers $X + Y$.



(a) Relation of the DOF used in this work and $DOF_{Lacroix}$.

(b) Core separation.

Figure 3.11: Comparison of the definitions of the DOF used in this work and the definition $DOF_{Lacroix}$ given in [Lac94] for a symmetric FFC.

In conclusion, the actual implementation of the DOF in the numerical refractive index profile model suffers from two problems. First, the separation of the cores is only reliable in a DOF range between 1.4 and 2. The corresponding deviation with respect to the core separation is negligible in this DOF range. Below a value of 1.4 the fiber cores would approach more than experimentally possible. This problem can be avoided by simulating FFCs with a DOF higher than 1.4 which should be an acceptable limitation¹. However, for symmetric and asymmetric FFCs with standard cladding diameter the exact value of the DOF normally has a low impact on the coupler characteristics as discussed later on in detail. Second, the calculated profiles are thinner than the real ones, because the material which corresponds to the overlapped region is neglected. This might result in an increased propagation constant separation and a shorter beat length.

Despite all these simplifications, it should be noted that it is nearly impossible to take all experimental parameters into account: for example, the DOF throughout the FFC defined by the heat distribution in the crucible during the pulling process, or the core dopant diffusion.

¹ If not stated otherwise the DOF definition given in Eq. (3.2) is used in this work.

3.3 Numerical Characterization

In the previous Sec. 3.2 a model for the calculation of the refractive index profile $n(x,y,z)$ was developed which is used in the following to simulate the properties of the fabricated FFCs from Sec. 3.1. The simulations were performed with help of the self-implemented simulation tool [Tün13] described in Sec. 2.4 based on the BPM algorithm.

Simulation Parameters

If not stated otherwise, the simulations in this work were executed with the parameters given in Tab. 3.1. The values for the grid dimensions and step sizes which were used for calculating the refractive index profile $n(x,y,z)$ represent lower limits, because rarely higher grid resolutions could have been used. However, the accuracy is high enough to guarantee the convergence of the results. The refractive index of the cladding n_{cl} corresponds to the refractive index of fused silica at a wavelength of 650 nm [Pol14]. According to the chromatic dispersion of fused silica, the refractive index of the cladding changes for different wavelengths. However, a constant n_{cl} was assumed in this work, which is reasonable, since the important parameter is the NA or respectively the refractive index difference between cladding and core. Strictly speaking also the NA is wavelength-dependent, since the dispersion of undoped fused silica is different from the dispersion of the germanium-doped fused silica (4 mol %) core. In the wavelength range between 800 nm and 2 μm the NA changes in the order of 0.001 [Men06] (cf. Fig. A.2) which is negligible for the typical SMF NA of 0.13. Therefore, the NA is nearly wavelength-independent and was assumed to be constant. According to the discussion in the previous Sec. 3.2 the refractive index profile model is inaccurate at a DOF below 1.4. Therefore, a DOF of 1.5 was assumed in the simulations (if not stated otherwise) to ensure a reasonable agreement between the real and the calculated refractive index profile. The input mode was the fundamental fiber mode LP_{01} .

Table 3.1: Parameters of the refractive index profile grid $n(x,y,z)$ for the BPM simulations using the self-implemented simulation tool [Tün13].

Parameter	Value
Grid dimension x, y	$[-100 \mu\text{m}, 100 \mu\text{m}]$
Step size (transverse) x, y	$0.2 \mu\text{m}$
Step size (propagation direction) z	$0.25 \mu\text{m}$
n_{cl}	1.4565 at 650 nm [Pol14]
DOF	1.5
Input mode	LP_{01}

Pulling Signatures

In Fig. 3.12 and 3.13 the experimental and simulated pulling signatures of symmetric FFCs made from SM2000 and 780-HP are depicted, respectively. Considering the capabilities of the presented refractive index profile model the simulations show a good agreement with the experimental data in both cases. The simulated coupling starts at nearly the same extension as the experimental does, whereby in the case of the simulated SM2000 FFC the starting point occurs at an extension of (9.5 ± 0.5) mm. In addition to the beginning of the coupling, also the further trend of the pulling signatures with respect to the coupling cycle position and periodicity agrees with the experimental data. In the case of the 780-HP FFC the agreement is not as good as for the case of the SM2000 FFC. The beginning of the coupling differs by 1 mm and the further coupling maxima are at slightly different extensions.

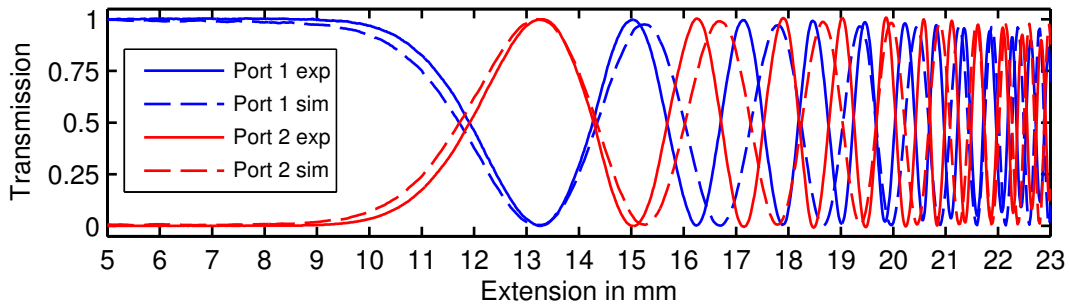


Figure 3.12: Experimental (exp) and simulated (sim) transmission in a symmetric FFC made from SM2000 at a wavelength of 1980 nm.

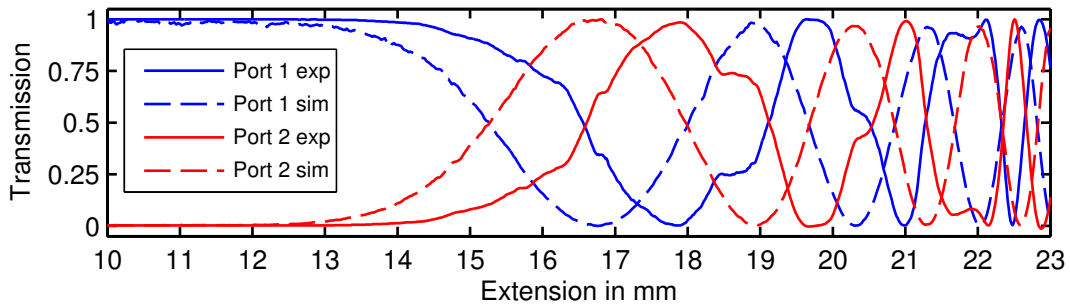


Figure 3.13: Experimental (exp) and simulated (sim) transmission in a symmetric FFC made from 780-HP at a wavelength of 795 nm.

In general, the agreement is strictly speaking not exact which is mainly due to the fact that the refractive index profile model suffers from certain limitations as discussed in Sec. 3.2.6 and it is nearly impossible to take all experimental parameters into account. In the presented experiments for example it was not possible to set the correct DOF in the

simulations, because the experimental value could not be measured. This is due to the fact that the FFC was pulled up to the destruction in order to record the complete pulling signature, impeding the measurement of the DOF. According to the assumption made in Sec. 3.1 concerning the experimental DOF of 1.3 ± 0.1 the refractive index profiles differs in any case. In addition, the simulations are only reliable for few-cycle FFCs which do not exhibit a superimposed modulation of the pulling signature due to polarization effects.

The agreement between experiment and simulation is meant in a more general way which means that essential features are covered by the simulations. The beginning of the coupling and the first coupling maximum are nearly at the same position within a deviation of 1 mm and the periodicity of the coupling cycles increases with consecutively pulling. With further progression the experimental and simulated curves differ which results in the fact that for example the n -th experimental coupling maximum coincides with the n -th minus one simulated coupling maximum. This is due to a slightly different periodicity of the coupling cycles which accumulates so that the maxima drift apart.

This behavior also occurs in the experiment, because of slightly different fabrication conditions, influenced for example by a slightly different heat distribution in the crucible. Therefore, two successively pulled FFCs with the same fabrication parameters do not have to exhibit exactly the same pulling signatures (cf. Fig. A.3). Experimentally this is not a big issue, since the output power is monitored during the pulling process and it can be stopped at the desired coupling ratio. The simulation cannot deliver the exact extension for the termination of the pulling process, but it offers the possibility to estimate the process parameters which is for example useful for the fabrication of FFCs with specific wavelength characteristics at which the respective light sources for the pulling process are not available.

In conclusion, the general agreement between experiments and simulations is good and confirms the suitability of both the simulation tool and the refractive index profile model to analyze FFCs. In the following it is used to perform a modal analysis in order to gain insight into the coupling mechanism.

3.4 Modal Analysis

As discussed in Sec. 2.3 the coupling in FFCs can be described by the evanescent field coupling and the SM coupling approach. According to Bures et al. [Bur83] the coupling in typical FFCs starts once the light breaks out of the core. Therefore, the analysis of the coupling mechanism requires the calculation of the SMs. In symmetric FFCs consisting of two identical fibers two SMs are present, the symmetric and antisymmetric SM which are equally excited along the whole longitudinal taper profile. As opposed to this, in

asymmetric FFCs the modal excitation is completely different and modal conversion can take place along the FFC [Oka90].

For the understanding of the coupling mechanisms in asymmetric FFCs it is essential to know the modal evolution along the propagation in the taper. Therefore, a modal analysis of symmetric FFCs is presented in this section in terms of effective refractive index considerations and modal decomposition. This facilitates the understanding of asymmetric FFCs having a more complex modal evolution. In this section, the implementation of the eigenmode calculation is explained and the SMs are calculated at the beginning of the taper and in the taper waist. Afterwards, it is investigated how the SMs evolve along the propagation in the taper in terms of their shape and n_{eff} . On this basis, the modal composition along the complete taper is determined.

3.4.1 Implementation

The light propagation was simulated by the self-implemented simulation tool [Tün13] and for the calculation of the eigenmodes the built-in mode solver utility of BeamPROP [RSo10] was employed (cf. Sec. 2.4). Technically, the eigenmode calculation is performed by launching a defined field into a straight waveguide section and determining the converging eigenmode solutions. The calculations have to be performed in a straight section, because in a permanently changing refractive index profile it is not possible to find converging solutions of the eigenmodes. Therefore, a straight waveguide with the same geometrical properties corresponding to the respective position in the taper was used. The position of the launched $5\ \mu\text{m}$ wide Gaussian field was in the center of the waveguide and the first ten eigenmodes¹ were calculated². Table 3.2 summarizes the minimal simulation parameters for the eigenmode calculation.

1 Due to unknown reasons BeamPROP does not calculate the eigenmodes according to their order which is determined by the n_{eff} . For this reason, the real second eigenmode is for example calculated on seventh position, although the corresponding n_{eff} classifies the eigenmode as the second. This circumstance makes it necessary to calculate more eigenmodes than actually necessary and to sort them afterwards according to the n_{eff} . In practice the calculation of ten eigenmodes has been shown to be sufficient, however this leads to a significantly increased computation time.

2 The iterative method of the mode solver utility was used and the convergence tolerance was 1×10^{-9} with respect to the normalized effective index.

Table 3.2: Parameters of the refractive index profile grid $n(x,y,z)$ for the eigenmode calculations.

Parameter	Value
Grid dimension x, y	$[-125 \mu\text{m}, 125 \mu\text{m}]$
Step size (transverse) x, y	$0.5 \mu\text{m}$
Step size (propagation direction) z	$0.5 \mu\text{m}$
n_{cl}	1.4565 at 650 nm [Pol14]
DOF	1.5
Input mode	Gaussian ($5 \mu\text{m} \frac{1}{e}$ width)

The simulated electric field E_{sim} (output from simulation tool) was decomposed on the calculated eigenmodes E_i (output from BeamPROP) by projecting the simulated field on the eigenmodes with the coefficients c_i given by [Pau12; Soh04]:

$$c_i = \frac{\iint E_{\text{sim}}(x,y) \cdot E_i^*(x,y) dx dy}{\sqrt{(\iint |E_{\text{sim}}(x,y)|^2 dx dy) \cdot (\iint |E_i(x,y)|^2 dx dy)}}. \quad (3.6)$$

These complex coefficients can be used to calculate the reconstructed electric field E_{rec} as weighted superposition of the calculated eigenmodes E_i with

$$E_{\text{rec}}(x,y) = \sum_{i=0}^N c_i \cdot E_i(x,y). \quad (3.7)$$

The modal weight of each eigenmode is then given by $|c_i|^2$. To evaluate the accuracy of the reconstruction the modal weights of the ten eigenmodes $\sum_{i=0}^9 |c_i|^2$ were summed, whereby the sum is ideally 1. A minimal sum of 0.75 was identified as acceptable accuracy and typically values between 0.8 and 0.95 were calculated. The difference to the ideal value is mainly due to numerical inaccuracies which are attributed to discrete grid parameters of both involved simulations. Lower values than 0.75 are assumed as an indication of miscalculation. The problematic aspect in this two-part calculation is the locally correct combination of both the simulated field and the corresponding eigenmodes at the exact same position along the complete longitudinal taper. If the calculated eigenmodes do not correspond to the eigenmodes at the taper position, the sum of the modal weights drastically decreases.

3.4.2 Calculation of Super-Modes

The SMs of a symmetric FFC consisting of two 780HP fibers were calculated at a wavelength of 795 nm and an extension of 20.3 mm which corresponds to the second coupling maximum shown in Fig. 3.13. Figure 3.14 shows the electric field of the symmetric and antisymmetric SM at the beginning of the taper, whereby the symmetric SM corresponds to the first eigenmode and the antisymmetric SM to the second eigenmode defined by the n_{eff} in descending order. The field is localized at the position of the fiber cores, respectively. The first two eigenmodes are therefore core modes, whereby each mode of a higher order is a cladding mode which expands into the whole cladding. In symmetric fiber devices, as FFCs and photonic lanterns, light launched into one fiber core excites all SMs or, in other words, the guided core mode is a superposition of all SMs. The number of the excited SMs equals the number of the fiber cores [Leo10].

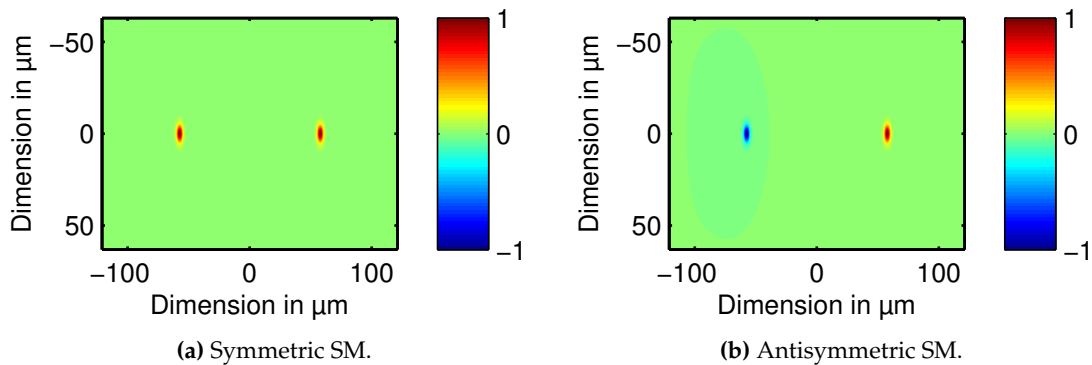


Figure 3.14: Electric field of the SMs at the beginning of the taper in a symmetric FFC consisting of 780HP fibers at a wavelength of 795 nm.

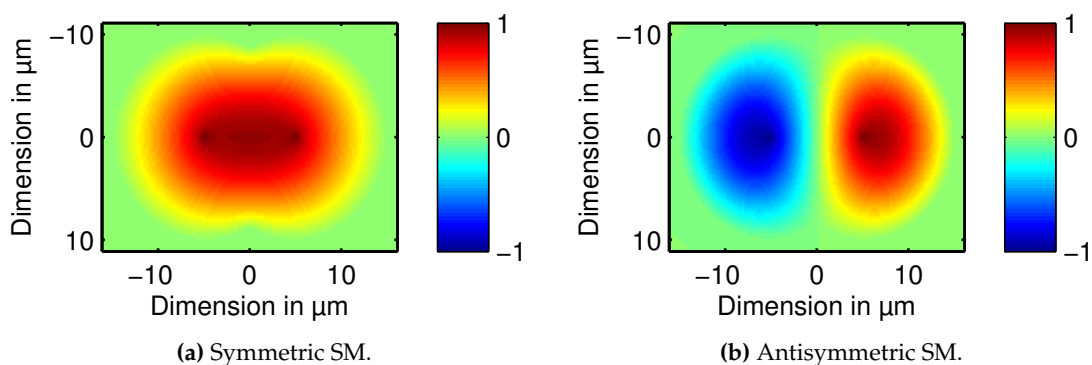


Figure 3.15: Electric field of the SMs in the taper waist of a symmetric FFC consisting of 780HP at a wavelength of 795 nm.

In Fig. 3.15 the electric fields of the SMs in the taper waist are depicted. At this taper position the cores do not guide the light anymore and the SMs fill out the complete

cladding. However, these cladding modes experience a residual influence of the cores which leads to a localization of the field at their position. Apart from that, the SMs are similar to the SMs at the beginning of the taper. The symmetric SMs are both line symmetric and the antisymmetric SMs are centrally symmetric, whereby if the electric fields' square of the absolute values is considered all SMs are line symmetric. In the following, the evolution of the SMs from the beginning of the taper to the taper waist is discussed.

3.4.3 Evolution of the Super-Modes and their Effective Refractive Index

Along the adiabatic taper transition from the beginning of the taper to the waist the core guided SMs consecutively evolve into SMs guided by the cladding. Accordingly, the n_{eff} decreases in the down-taper part as depicted in Fig. 3.16(a). At a taper position of approx. 8 mm the n_{eff} curves of the SMs cross the line of the refractive index of the cladding. This point corresponds to the transition from core guidance to cladding guidance. Up to this position the curves of both SMs have quasi identical n_{eff} , are propagating at the same phase velocity and are strongly localized at the position of the cores. In analogy to quantum mechanics both SMs are degenerated [Leo10]. Both SMs experience only the cladding refractive index and not the high refractive index difference to the surrounding medium.

After the core-cladding transition the curves become non-degenerated which results in different propagation constants β_s and β_a of the symmetric and antisymmetric SM. The splitting is due to the fact that both SMs notice the influence of the high refractive index difference of the surrounding medium, an effect that is pronounced due to the consecutively tapered thinner fibers. This splitting leads to the observed mode beating and enables the power transfer from one fiber to the other. It is therefore essential for the functionality of the FFC that the curves split up and accumulate phase difference, because otherwise no mode beating would occur. Consecutive pulling would result in a longer region with different propagation constants and therefore in more overall phase difference and more frequent mode beating. In addition, the curves of both SMs would split up even more since the cladding becomes thinner and the effect of the surrounding medium gets more pronounced. This is the reason why the periodicity of the coupling cycles increases with consecutive pulling (cf. Fig. 3.4).

In addition, Fig. 3.16(a) depicts the n_{eff} curves of the third to tenth eigenmode which correspond to the first eight HOMs. These are all guided in the cladding and have therefore n_{eff} values below the refractive index of the cladding. At the beginning of the taper all HOMs have identical values of the n_{eff} , analogous to the curves of both SMs

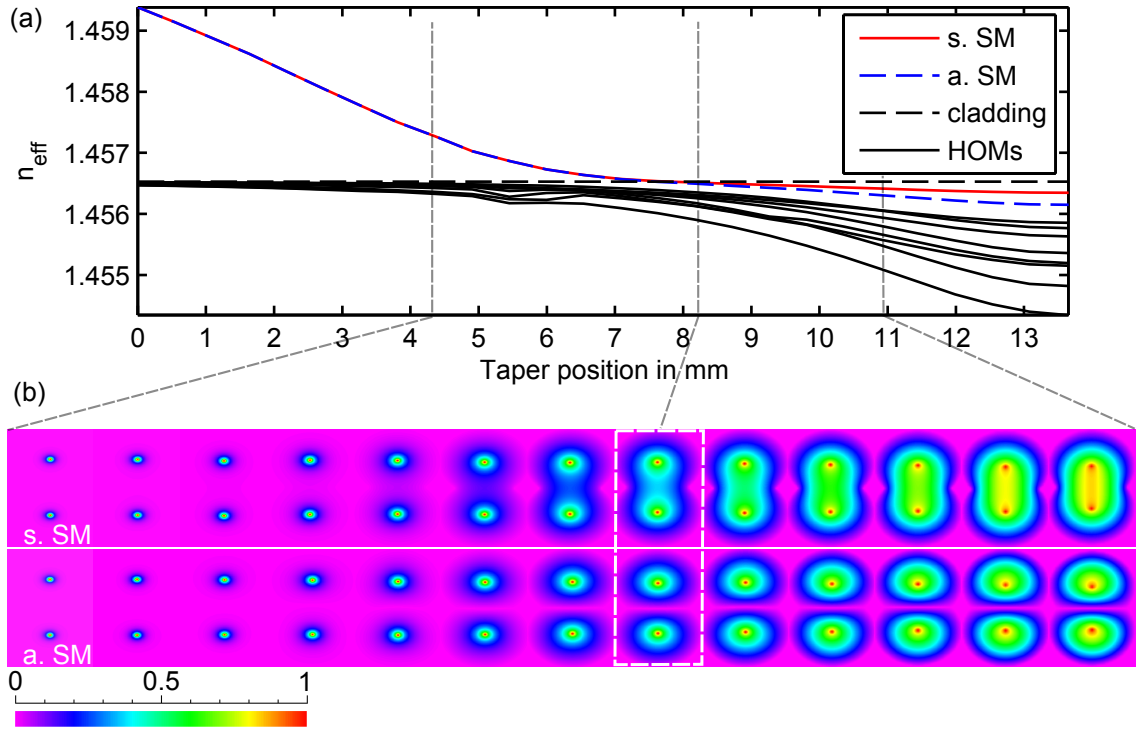


Figure 3.16: (a) Evolution of the n_{eff} of the symmetric (s. SM) and antisymmetric (a. SM) SM along the taper position of a symmetric FFC from the beginning of the taper ($z = 0$) to the taper waist ($z = 13.65$ mm). (b) Evolution of the intensity profiles of the symmetric and the antisymmetric SM at a taper position between 4.36 mm and 10.9 mm. The simulation cross section (in x and y dimension) for the eigenmode calculation in (b) is consecutively rescaled for higher taper positions.

which have also identical values of the n_{eff} . With consecutive propagation in the taper the curves split up due to the increased influence of the surrounding medium which in turn is because of the lower cladding diameter. These curves are well separated from the curves of the SMs and no mode coupling between the HOMs and the SMs should occur since a large n_{eff} difference exists [Xia11]. This means that light injected into the cores couples solely between both SMs. This behavior is further analyzed in the next section by modal decomposition.

The evolution of both SMs at a taper position between 4.36 mm and 10.9 mm is depicted in Fig. 3.16(b). The SMs evolve smoothly from core guidance to cladding guidance due to the adiabatically tapered FFC. At a taper position of approx. 8 mm both SMs expand into the whole cladding and the shape of both SMs starts to differentiate, analogous the n_{eff} curves become non-degenerated. The influence of the cores is present along the whole longitudinal taper and leads to a localization of the intensity's maxima at their position,

although the SMs are not guided by the cores anymore in the cladding guided region. The considerations in this section were conducted only for the down-taper part of the FFC. Due to the fact that the refractive index profile of the FFC is symmetric to the taper waist, the shown results are symmetric to a taper position of 13.65 mm. This means that a taper position of approx. 19 mm the light is recaptured by the cores in the up-taper.

3.4.4 Modal Decomposition

Based on the previously calculated evolution of the SMs the modal excitation of both SMs is calculated in the following. This is achieved by simulating the light propagation and the eigenmodes along a defined FFC with the parameters used in the previous section.

Figure 3.17(a) shows the result of the light propagation in the central plane of the FFC over the whole longitudinal taper length and Fig. 3.17(b) the cross section at the indicated taper positions. For better illustration the data points of each slice were normalized which is the reason why the beating seems to be abrupt. The light is injected into the core of the bottom fiber and leaves the FFC at the top fiber. Along the down-taper the light is core-guided and significant mode beating can be observed at taper positions between approx. 10 mm and 18 mm. According to Fig. 3.16 the SMs break out of the core at a taper position of approx. 8 mm. However, in order to observe a significant amount of power transfer from one side to the other, both SMs have to accumulate a notable amount of phase difference which occurs at a taper position of approx. 10 mm. From here, mode beating can be observed and due to the fact that the extension of the FFC corresponds to the second coupling maximum (cf. Fig. 3.13) the power beats three times between both sides. It should be noted, that at higher extensions the power would beat more frequently between both sides of the FFC due to the longer path with different propagation constants of the involved SMs. In the up-taper part the light is recaptured by the cores and, due to the chosen extension, the light leaves the FFC at the top fiber. Based on this simulation of the light propagation together with the calculation of the eigenmodes along the taper a modal decomposition can be performed.

The result of the modal decomposition along the complete taper is depicted in Fig. 3.18 which shows the modal weight of both SMs and the sum of the third to the tenth eigenmode. At the beginning of the taper both SMs are equally excited which is in agreement with the fact that in FFCs the number of SMs equals the number of the cores [Leo10]. Light injected into one of the cores excites both SMs and it is represented as superposition of them. The SMs are equally excited along the whole taper. Although, at a taper position between 6 mm and 9 mm, and 19 mm and 22 mm the modal weight of the HOMs increases up to a value of 20%. This corresponds in both cases to the region at which the transition

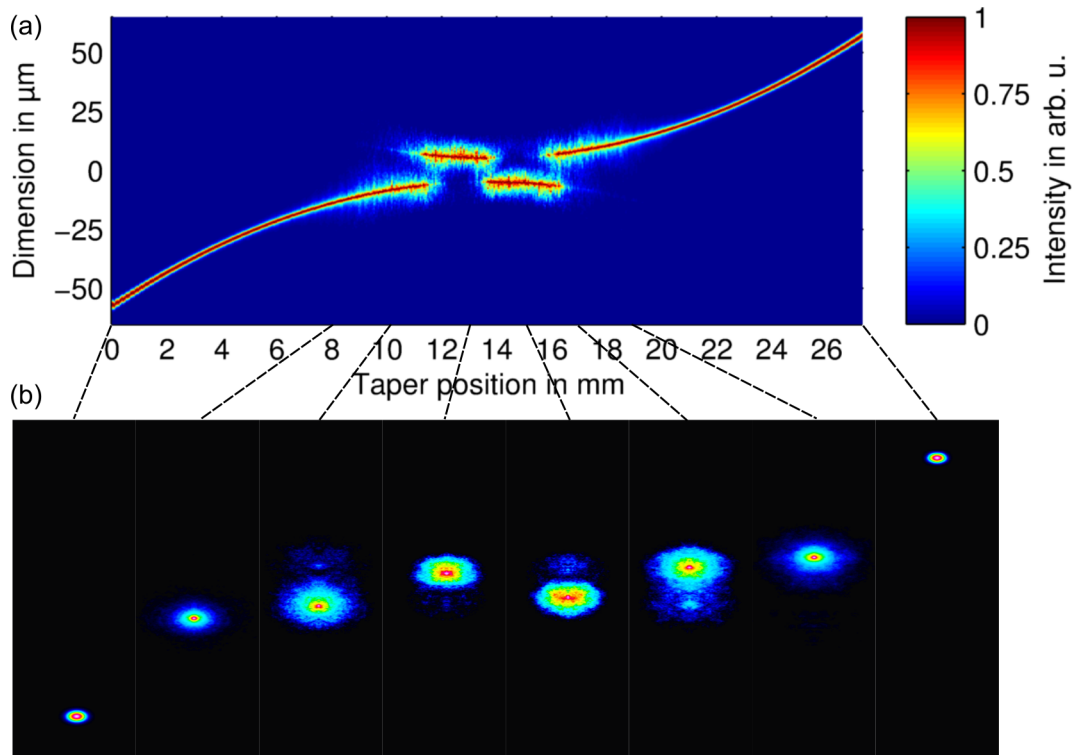


Figure 3.17: Light propagation in a symmetric FFC in the central plane over the whole longitudinal taper length (a) and the cross section at the indicated taper positions (b). The light is launched into the core of the bottom fiber. For better illustration the data points of each slice were normalized.

between core and cladding guiding occurs, just before the beginning of the power transfer and just after that.

Theoretically, if the taper transition is adiabatic and the curves of the n_{eff} do not interact or cross with each other, no mode coupling can occur [Leo14; Yer14]. A non-adiabatic taper transition would lead to mode coupling to HOMs, whereby this mode conversion is irreversible [Lov91]. The power would be irrecoverably lost increasing the insertion loss of the FFC. However, the experimental and simulated pulling signatures (cf. Fig. 3.13) do not show an increased insertion loss. In addition, the modal decomposition shows that in the taper waist, where the coupling occurs, the HOM content is negligible. Therefore, it is assumed that the local increase of the HOM content cannot be attributed to a non-adiabatic taper transition. Probably the increased HOM content comes from numerical inaccuracies of the simulated fields at the transition between core and cladding guiding. As depicted in Fig. 3.17(b) the simulated field is slightly grainy in the region of the transition and in the taper waist. This could be an explanation for the locally increased HOM content.

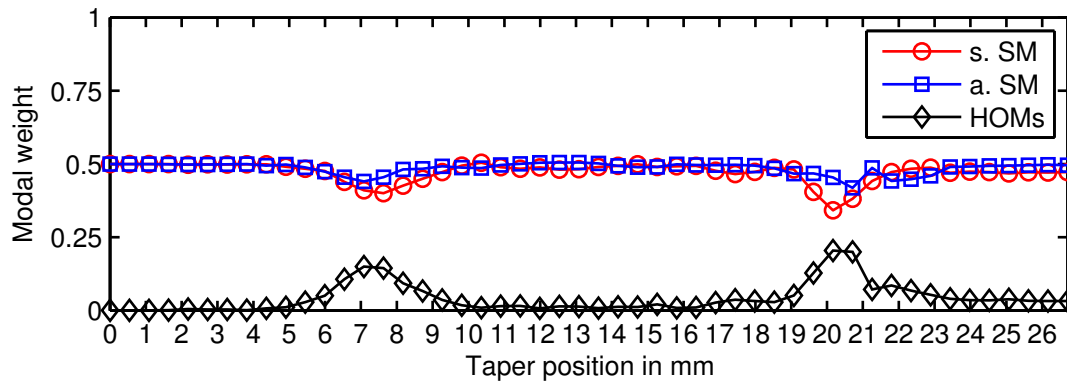


Figure 3.18: Modal excitation in a symmetric FFC. The symmetric SM (s. SM) and the antisymmetric SM (a. SM) are nearly equally excited along the whole FFC. HOMs are locally excited at a taper position between 6 mm and 9 mm and between 19 mm and 22 mm.

Nevertheless, in the central part of the FFC where the mode beating occurs only both SMs are equally excited with negligible HOM content. Therefore, the presented modal analysis confirms the common statement that in symmetric FFCs both SMs are equally excited [Oka90]. In conclusion, the presented method provides reliable information about the modal content in symmetric FFCs and can be used to study more complex asymmetric refractive index profiles.

3.5 Conclusion

In this chapter symmetric FFCs were discussed both experimentally and numerically. FFCs were fabricated by twisting two identical fibers, heating them up and pulling them while the transmission in both fibers is constantly monitored. The pulling signatures of two FFCs were recorded at a standard wavelength of 795 nm and at a less frequently used wavelength of 2 μm demonstrating the applicability of the presented fused biconical taper technique for the fabrication of FFCs in a broad wavelength region.

In order to gain insight into the coupling mechanism in FFCs, a numerical model capable to calculate the refractive index profile was elaborated. The presented model considers the parabolic taper shape, the overlap of both fibers during the fusion process and both the core-cladding and the cladding-air boundaries. Parameters as the hot zone were experimentally determined and the parabolic taper profile of the FFCs was verified. The presented numerical refractive index profile model is in relative good agreement with the real refractive index profile, although it suffers from certain limitations. Simplifications concerning the twisting and the implementation of the DOF were extensively discussed.

The presented numerical refractive index profile model was used in a self-implemented simulation tool based on the BPM algorithm to numerically characterize the experimentally

fabricated FFCs. The simulations of the pulling signature show a good agreement with the experimental data in both evaluated cases. The agreement is meant in a general qualitative way, since essential features are covered by the simulation. The beginning of the coupling and the behavior of the coupling cycles with consecutive pulling are comparable. Nevertheless, the agreement is not perfect which is due to the fact that the model suffers from certain limitations. Therefore, the simulation model cannot deliver for example the exact experimental extension for the termination of the pulling process, but it is suitable to reliably estimate the process parameters and to gain insight into the coupling mechanism. However, the pulling signatures of identically pulled FFCs differ slightly either way, because of minimal changes in the fabrication conditions.

Finally, the model was used to calculate the SMs and to perform a modal analysis in terms of n_{eff} considerations and modal decomposition in symmetric FFCs. The evaluation reveals that before the transition from core guiding to cladding guiding the symmetric and antisymmetric SMs are excited equally and have the same propagation constants. At the transition point the curves of the n_{eff} become non-degenerated and the SMs accumulate phase difference which leads to the typical mode beating in the taper waist. At the same time both SMs expand into the whole cross section and become cladding modes. A modal decomposition was performed and confirms both the fact that in symmetric FFCs the number of excited SMs corresponds to the number of fiber cores and the fact that the involved SMs are equally excited along the whole taper. Both facts are in agreement with the theory of common literature.

The results presented in this chapter show that the established numerical analysis routines are suitable for the understanding of symmetric FFCs. In the next chapters these routines are used to analyze more complex asymmetric FFCs, for example for WDM and SDM applications, which have not been investigated in terms of SMs so far.

CHAPTER 4

Asymmetric Fused Fiber Couplers for Wavelength-Division Multiplexing

Fused fiber couplers are essential components in optical data networks and fiber-based laser and amplifier systems. They enable for example the application of wavelength-division multiplexing by combining several wavelength bands in one single fiber [Eis88]. In telecommunication this is used to increase the data-carrying capacity of optical transmission systems and in fiber lasers and amplifiers to combine the pump and signal light. Typically, identical SMFs are employed for these applications, but there are cases where the use of different fibers is of interest, for example for extending the range of combinable wavelengths. In addition, such FFCs can be also useful for integrated systems or for fiber amplifiers and lasers where the pump light is outside of the single-mode range of the signal guiding fiber. The lower limit of the combinable wavelengths is given by the cut-off of the fibers. The use of a fiber guiding light below the cut-off wavelength would be undesirable since only the power fraction in the fundamental mode would be transferred to the respective other fiber. An approach for combining two widely separated wavelengths is the use of FFCs consisting of different fibers, also referred to as asymmetric FFCs due to the non-symmetric refractive index profile, whereby each fiber has single-mode guidance for one of the wavelengths. In order to control the power-splitting ratio in asymmetric FFCs Birks et al. [Bir88b] proposed to change the DOF in FFCs.

Other methods to control the power-splitting ratio in asymmetric FFCs can be transferred from the field of so called wavelength-flattened couplers [Bir95; Mor85]. These couplers show a nearly constant power-splitting ratio over a wide spectral range [Lam85b]. Such couplers are fabricated by simply employing unequal SMFs, by pre-etching [Lam85a] or by pretapering [Mor85] one fiber before the fabrication process. All these methods have in common that an asymmetry is introduced into the refractive index profile of the

coupler, either by using different fibers or by making one fiber unequal. Pretapering is a flexible and simple method to modify the refractive index profile by tapering one of the fibers before both fibers are tapered together. However neither extensive studies on the impact of pretapering on the power-splitting ratio in asymmetric FFCs nor a profound analysis of the coupling mechanism have been reported in literature so far.

In this chapter, two asymmetric FFCs designed for WDM applications are studied experimentally and numerically. It is demonstrated that by pretapering one fiber it is possible to combine two widely separated wavelengths, 633 nm and 1556 nm, and the impact of the asymmetric refractive index profile on the coupling mechanism is discussed. The application of asymmetric FFCs is analyzed for an FFC at wavelengths of 795 nm and 1980 nm which was employed for core pumping a thulium-doped fiber amplifier. Parts of the presented results were published beforehand in [Pel12; Pel14].

4.1 Fabrication and Characterization

The standard fused biconical taper technique was used for the fabrication of asymmetric FFCs as in the case of symmetric FFCs (cf. Sec. 3.1). The pulling procedure was conducted with the help of light sources emitting at wavelengths of 633 nm and 1556 nm which were injected into the pump and signal fiber, respectively. Light of the shorter wavelength of 633 nm is called pump light and light of the longer wavelength of 1556 nm is called signal light (according to the nomenclature in fiber amplifiers), although no specific laser pumping scenario is targeted in this case. The wide wavelength separation of 923 nm requires to use different fibers with single-mode guidance for the respective wavelength. The specification of the used pump fiber (630-HP) and signal fiber (1310BHP) are given in A.1.

4.1.1 Pulling Signatures at Different Pretaper Lengths

The fabrication was initiated with the pretapering process where only one fiber (in this case the signal fiber) was tapered for a certain extension, also called pretaper length (PL). Afterwards the standard fused biconical taper technique was conducted. Both fibers were twisted, heated and pulled up to their destruction, while the transmission of light at both wavelengths was monitored with the help of photodiodes. The transmission of the pump light was measured at the end of the pump fiber and the signal light at the end of the signal fiber. By doing so, only the transmission in one fiber was measured for each wavelength.

In Fig. 4.1 the transmission in an FFC at a wavelength of 633 nm at both fiber ports is depicted, whereby a PL of 4 mm was applied to the signal fiber. In addition, the sum of the transmission in both ports is plotted and reveals that the coupling is nearly complete

during the whole pulling process and exhibits only losses in the order of a few percent. Therefore, the measurement of the transmission at one fiber port is sufficient for the characterization of an FFC. The transmission in the respective other fiber port is calculated by subtracting the measured transmission from 100 %.

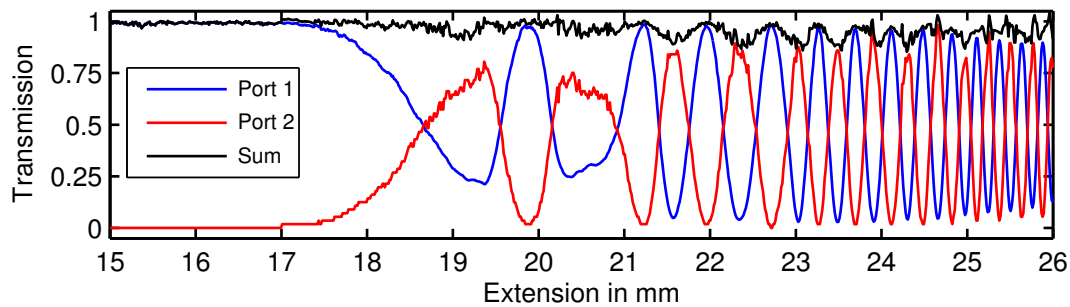


Figure 4.1: Experimental transmission in an asymmetric FFC made from 630-HP and 1310BHP (PL = 4 mm) at a wavelength of 633 nm at both fiber ports. The sum of the power in both ports equals nearly the launched power and the losses are in the order of a few percent.

An extensive study on the impact of pretapering on the pulling signatures was carried out and is depicted in Fig. 4.2. When both fibers are fused and pulled without pretapering the maximum coupled power is limited to 20 % for both wavelengths, which means that only a maximum of 20 % of the launched power coupled from one fiber to the other. In order to analyze the influence of pretapering on the coupling behavior systematically, different PLs (3 mm, 4 mm, 5 mm, 6 mm and 8 mm) were applied to the signal fiber and the respective pulling signatures were recorded, as shown in Fig. 4.2(b)-(f). By increasing the PL the maximum coupled power of both wavelengths was substantially increased up to a complete power transfer from one fiber to the other as depicted in Fig. 4.2(d) at a PL of 5 mm (both wavelengths show zero transmission which means that the light couples completely to the other fiber). Fig. 4.2(d) further illustrates that the maximum coupled power not only depends on the PL, but also on the applied extension during the pulling process.

In Fig. 4.2(d) both wavelengths show a complete power transfer at an extension of approx. 17.5 mm (see dotted line), whereas the maximum coupled power decreased with further pulling. It was further possible to combine both wavelengths in the signal fiber at a PL of 6 mm (cf. Fig. 4.2(e)) and an extension of 16.4 mm (see dotted line). The transmission was maximal for the signal light in the signal fiber and the transmission of the pump light showed a minimum in the pump fiber, which means that if the fabrication process was stopped at this extension, both wavelengths would be combined in the signal fiber with a maximum coupled power of 85 %. Besides the fact that pretapering influenced the

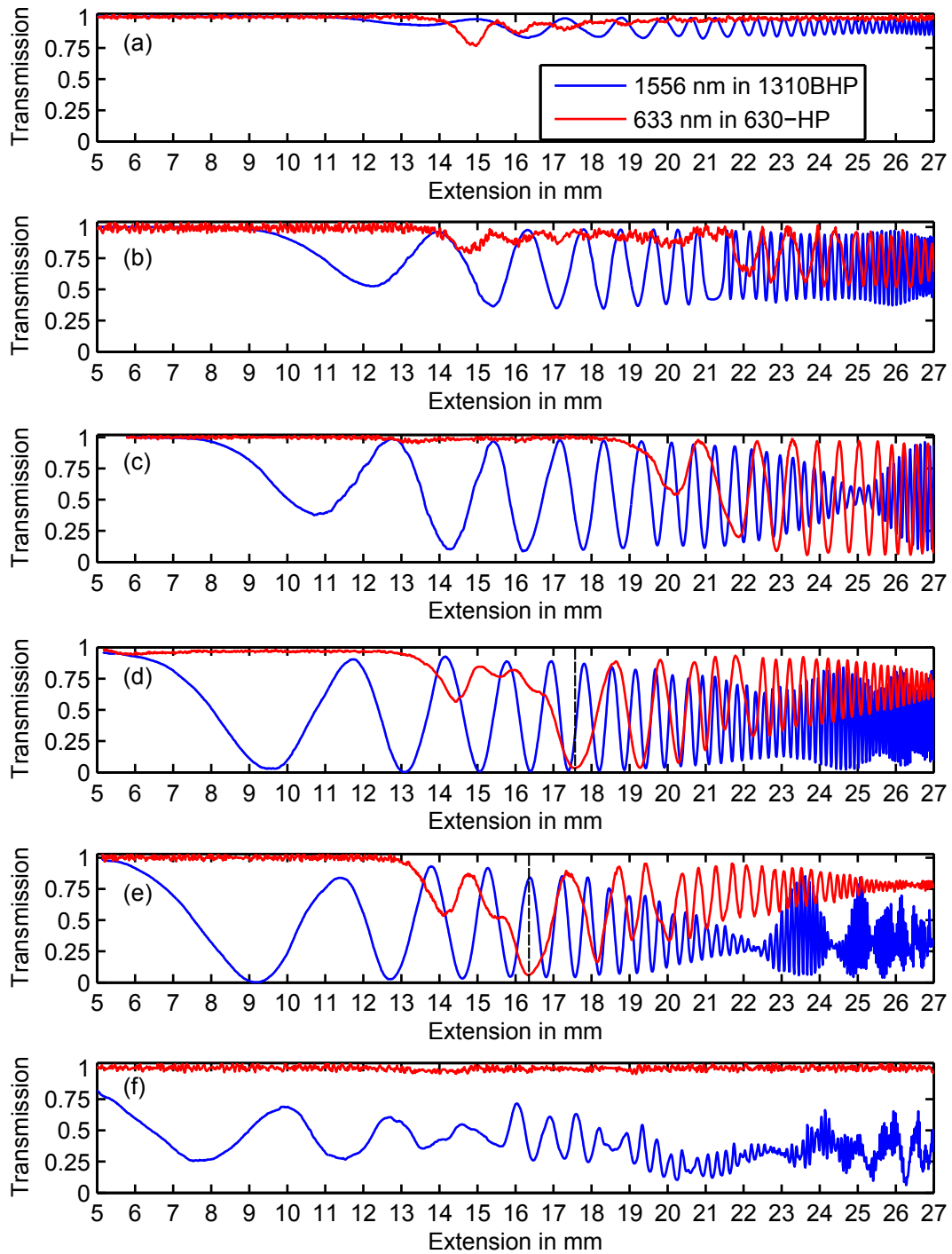


Figure 4.2: Experimental pulling signatures of the pump and signal light at different PL of the signal fiber of (a) 0 mm, (b) 3 mm, (c) 4 mm, (d) 5 mm, (e) 6 mm and (f) 8 mm.

coupling ratio, it becomes clear from Fig. 4.2 that an optimal value for the PL must be found. This can be seen in Fig. 4.2(f) at a PL of 8 mm, where the coupling ratio strongly decreased showing no coupling for the pump light, and an unpredictable coupling behavior for the signal light was observed. These results demonstrate that by pretapering one fiber it is possible to control the maximum coupled power in asymmetric FFCs.

4.1.2 Degree of Fusion

The control of the coupled power can also be achieved by etching techniques [Lam85a] or by adjusting the DOF [Bir88b]. Due to the fact that the FFCs were pulled up to the destruction for the measurements shown in Fig. 4.2 the DOF could not be measured simultaneously. For this reason two FFCs with different DOF but otherwise same parameters were pulled in order to estimate the DOF in the presented experiments and to evaluate the influence on the coupling behavior. The DOF was changed by adjusting the fuse extension at the beginning of the pulling process (cf. Sec. 3.1). FFCs were pulled up to an extension of 20 mm, cleaved at the taper waist and examined under an optical microscope.

In Fig. 4.3(a) the experimentally measured transmission of the signal light in the signal fiber at a PL of 4 mm is depicted. The DOF was measured to be 1.28 and 1.43 for the two FFCs. For comparison the curve shown in Fig. 4.2(c), for which no information about the DOF is available, is also plotted. The results show that in this configuration of a strongly fused FFC a variation of the DOF in the order of 0.15 has no significant influence on the coupling behavior (cf. Fig. A.3 for the general reproducibility). Especially, the maximum coupled power is practically the same for all three curves. However, a difference of 0.15 in the DOF compared to the maximum span of 1 is relatively low. The results further indicate that the used configuration produces FFCs with a DOF in the order between 1.28 and 1.43.

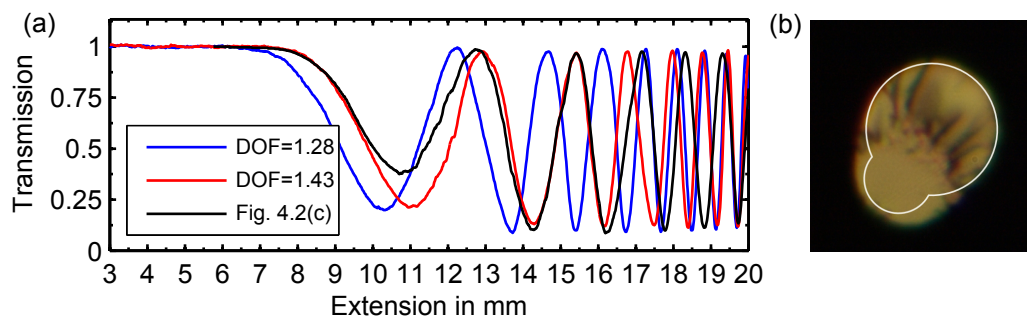


Figure 4.3: (a) Experimentally measured transmission of the signal light in the signal fiber at a PL of 4 mm. The FFCs show a DOF of 1.28 (blue curve) and 1.43 (red curve). For comparison the curve from Fig. 4.2(c) is also plotted (black curve). (b) Photograph of the cross section of the cleaved taper waist at a DOF of 1.43 (according to the red curve). The shape of the calculated refractive index cross section is indicated by the white line.

Fig. 4.3(b) shows a comparison between a photograph of the cross section at the taper waist of the FFC with a PL of 4 mm at an extension of 20 mm (according to the red curve in Fig. 4.3(a)) and the calculated cross section with a DOF of 1.43 (drawn in white). In contrast to the measured cross section the calculated one shows a non-smooth transition between both fibers, because the refractive index profile was generated by overlapping circles around the position of the cores and neglecting the material conservation.

In contrast to the work presented by Birks and Hussey [Bir88b], no significant influence on the coupling behavior due to a change in the DOF could be observed in this work, although the variation of the DOF was in a comparable order of 0.2. The difference is probably because in the here presented FFCs the effect of the cores is more pronounced since the difference in the cut-off wavelength of the fibers is about 700 nm (cf. Tab. A.1) compared to a difference in the cut-off wavelength of only 150 nm in [Bir88b]. Due to the high dissimilarity of the fibers used in this work, pretapering one of them has a stronger impact on the coupling behavior than changing the DOF.

4.1.3 Output Beam Profile

At a PL of 5 mm and an extension of 17.5 mm (cf. Fig. 4.2(d)) a complete power transfer of the pump light to the signal fiber can be achieved. An FFC fabricated at this parameter set would be highly interesting for the application in a fiber amplifier (a concrete scenario is shown in Sec. 4.4). As a consequence of the high difference between the cut-off wavelengths of both fibers, the pump light can be multimoded in the signal fiber. The V parameter for the pump light (633 nm) in the signal fiber is 5.5 which means that theoretically in total approx. 4 modes could be guided. However, it is not clear which of these modes are excited at the signal fiber output.

Therefore, the intensity beam profile was measured with a CCD camera during the pulling process simultaneously to the output power. The measurements were performed at a wavelength of 795 nm, whereby the respective V parameter is 4.4 and theoretically a total number of approx. 3 modes could be guided. Figure 4.4 shows the measured transmission in the pump and signal fiber and the respective output beam profiles at the signal fiber for each coupling maximum. The output beam profiles have the shape of the fundamental LP_{01} mode during the complete pulling process. There is no indication of an increased HOM content, as for example for the LP_{11} , LP_{02} or LP_{21} mode. Therefore, the coupling takes place from the fundamental mode in the pump fiber to the fundamental mode in the signal fiber. A more comprehensive discussion on how the modes evolve in the coupling region is given in Sec. 4.3.

In conclusion, the transmission in asymmetric FFCs was systematically tuned by modifying the refractive index profile. The modification was applied by different PLs of the

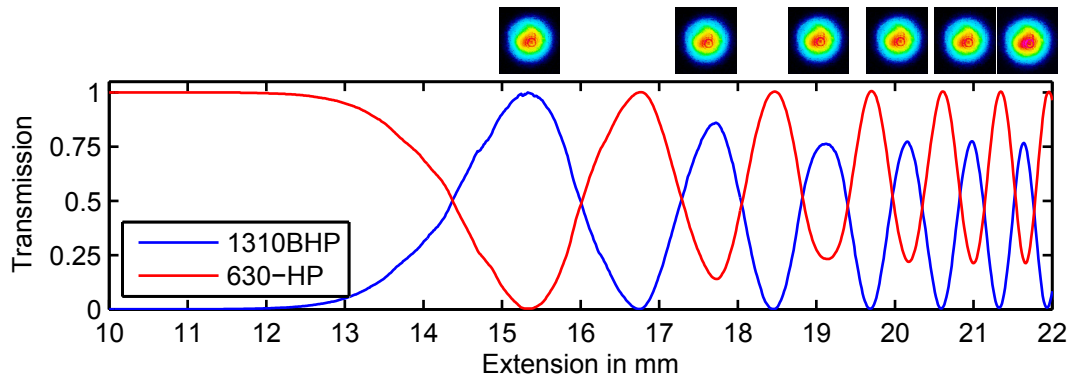


Figure 4.4: Experimentally measured transmission in the pump and signal fiber (applied PL of 5 mm) at a wavelength of 795 nm. Beam profiles at the signal fiber output during the pulling process at the coupling maxima are depicted.

signal fiber and a significant increase of the maximum coupled power was achieved. The measurement of the output beam profile reveals that in case of the pump light the coupling occurs between the fundamental mode in the pump fiber and the fundamental mode in the signal fiber.

4.2 Numerical Characterization

In the previous Sec. 4.1 asymmetric FFCs were experimentally analyzed and the coupled power was maximized at specific values of the PL and extension. The simulation of these structures can significantly improve the understanding of the coupling behavior and can be used to estimate fabrication parameters, as for example the PL.

Pulling Signatures at Different Pretaper Lengths

The transmission in the experimentally analyzed asymmetric FFCs was simulated with the help of the models presented beforehand (cf. Sec. 3.2 and 3.3) and the results are depicted in Fig. 4.5. For the simulations a DOF of 1.5 was assumed which is comprehensible, since in this case the DOF experimentally has only a minor impact on the pulling signatures and it is not completely controllable during the fabrication process.

As in the experiment when no pretaper is applied in the simulation, the coupling ratio is limited to nearly 30% for both wavelengths and no complete power transfer is possible. A gradual increase of the PL from 3 mm up to 6 mm results in an enhancement of the maximum coupled power for both wavelengths with a coupling ratio of up to 100%. A complete power transfer occurs for the signal light at a PL of 4 mm and an extension of about 15 mm (cf. Fig. 4.5(c) dotted line) and for the pump light at a PL of 6 mm and an extension of about 16.5 mm (cf. Fig. 4.5(e) dotted line). A further increase of the PL to

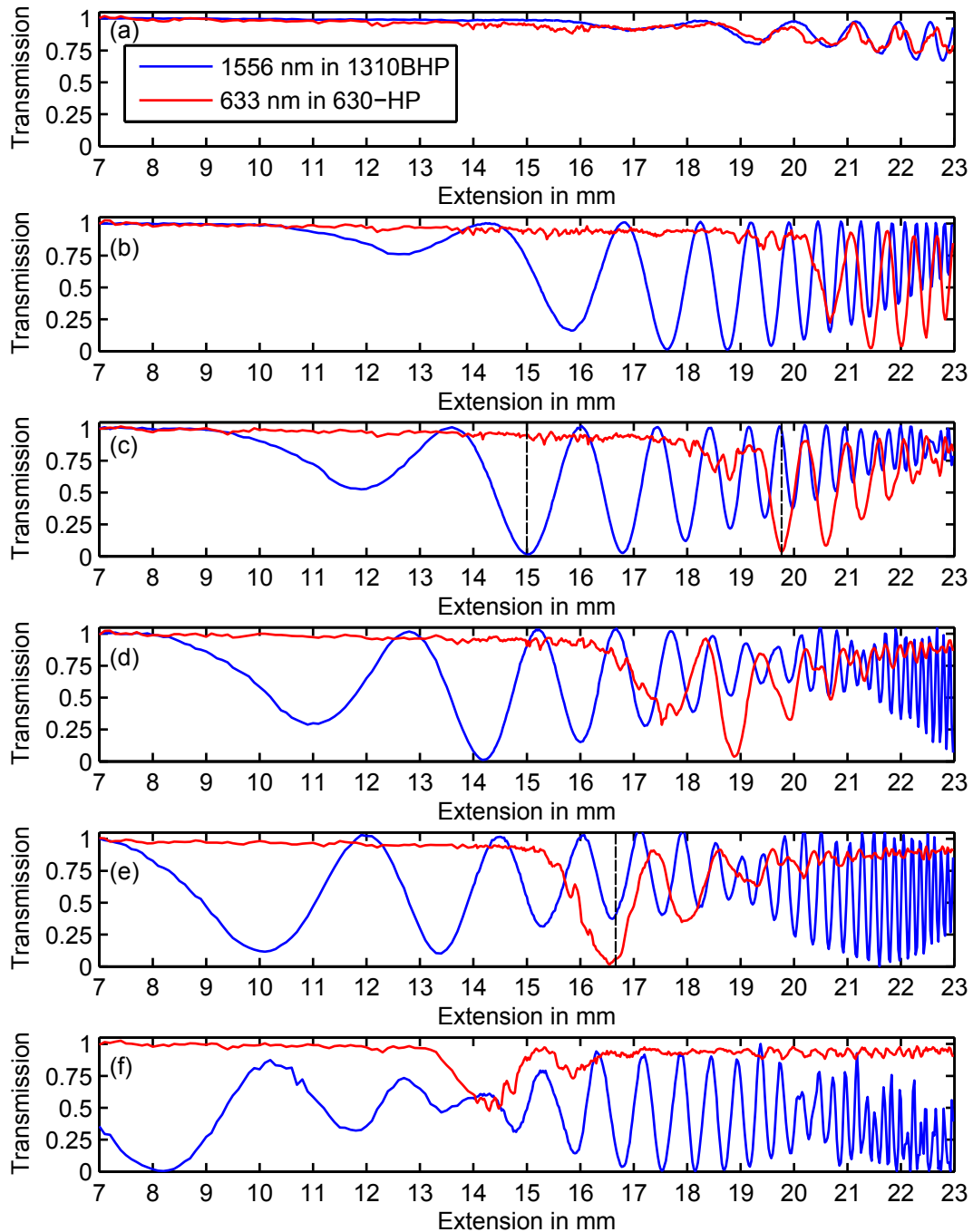


Figure 4.5: Simulated transmission of the pump and signal light at different PLs of the signal fiber of (a) 0 mm, (b) 3 mm, (c) 4 mm, (d) 5 mm, (e) 6 mm and (f) 8 mm.

8 mm results in a dramatic decrease of the coupling ratio for both wavelengths, a behavior which was also observed in the experiment. As in the experiment, the coupling ratio of both wavelengths is strongly influenced by pretapering the signal fiber. In addition, the coupling starts respectively at lower values of the extension with increasing PL and the transmission changes in dependence of the applied extension.

The simulations show that a combination of both wavelengths in the signal fiber is possible, as depicted in Fig. 4.5(c) at a PL of 4 mm and an extension of 19.7 mm. In contrast, the experimental results show that a combination can be realized at a PL of 6 mm and an extension of 16.4 mm (cf. Fig. 4.2(e)). Therefore, the simulation does not account for the exact position in terms of transmission and extension of each coupling maximum. This effect gets pronounced when long couplers with many oscillation cycles are considered which makes it nearly impossible to predict the exact value for the optimal extension. The critical aspect for this discrepancy is the transfer of the refractive index profile including exact geometry and fiber parameters of the fabricated FFCs from the experiment to the simulations (cf. discussion in Sec. 3.2.6). Although not all features of the experimental results are explained by the simulation the general agreement is good.

Parameter Scans

In order to better estimate the fabrication parameters a more accurate variation of the PL was performed, as depicted in Fig. 4.6. Here, the transmission in the signal fiber was calculated for both wavelengths for varying extension and PL. This is useful for the optimization of FFCs for the application in fiber amplifiers.

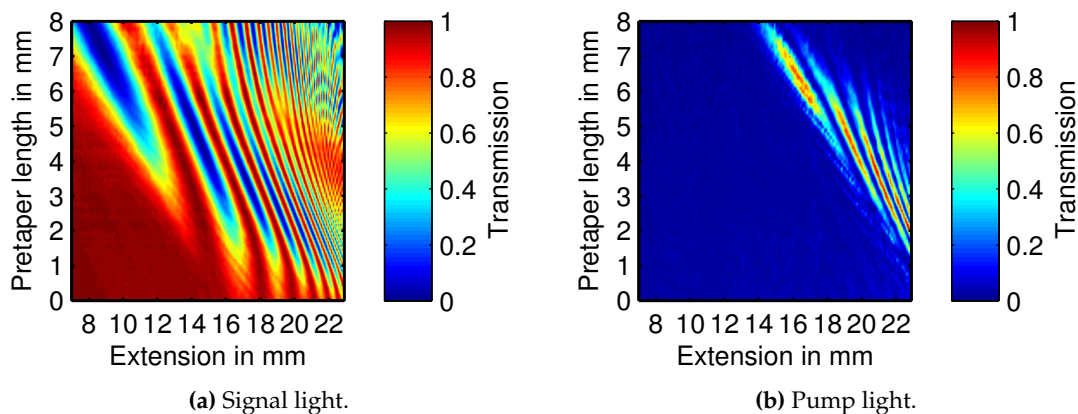


Figure 4.6: Simulated transmission in the signal fiber for PLs between 0 mm and 8 mm and extensions in the range of 7 mm and 23 mm for the signal (a) and pump light (b).

In this scenario it is desired to maximize the transmission in the signal fiber for both wavelengths. Therefore, the transmissions of the pump and signal light were multiplied

and the result is depicted in Fig. 4.7. This indicates that the product of the transmission is maximal at a PL in the range between approx. 4.5 mm and 4 mm at extensions of 19.5 mm and 20.5 mm, respectively. This corresponds to the numerical parameter set which is already determined in Fig. 4.5(c) and it proves that theoretically no better parameter set exists. It should be noted that from the manufacturing perspective it is recommended to target a broad maximum in order to facilitate the stopping point at the end of the pulling process.

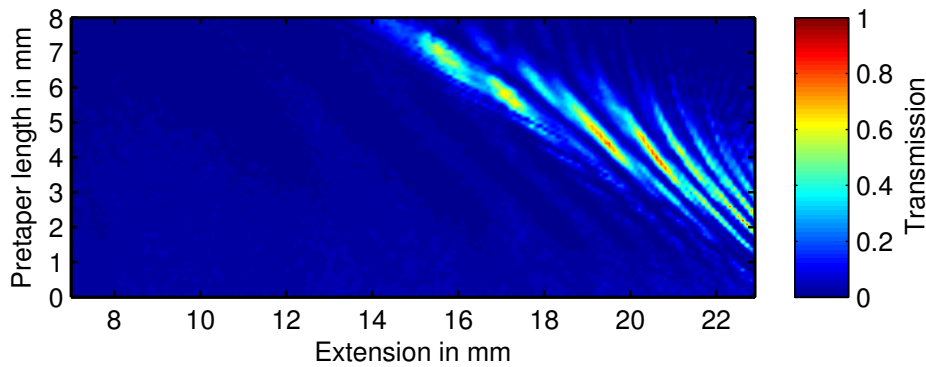


Figure 4.7: Product of the transmissions of the signal and pump light in the signal fiber.

In conclusion, the simulations can give an estimation of the PL for an experimental realization of an FFC. By consecutive experimental optimization, asymmetric FFCs, which efficiently combine two wavelengths, can be fabricated. The simulation accounts for the general qualitative behavior of the FFC performance and allows to gain insight into their operation and the underlying coupling mechanism. In the following Sec. 4.3 this routine is used to calculate the modal composition of the simulated light and to evaluate the influence of pretapering on the modal excitation of the eigenmodes of asymmetric FFCs.

4.3 Modal Analysis

According to the experimental and numerical results of the last Sec. 4.1 and 4.2 pretapering of one fiber can be used to efficiently control the coupling behavior in asymmetric FFCs enabling a complete power transfer between both fibers. In order to understand the effect of pretapering on the coupling behavior a modal analysis of asymmetric FFCs is performed in the following.

First, the guiding properties of asymmetric FFCs are generally discussed and the SMs in the taper waist of a pretapered and non-pretapered asymmetric FFC are calculated. Afterwards, it is investigated how the SMs evolve along the propagation in the taper in terms of their shape and n_{eff} for the signal and pump light, respectively. On this basis, the

modal composition in dependence of the applied PL, the extension and the taper position is analyzed, accordingly for the signal and pump light.

4.3.1 General Considerations of Guiding Properties at Different Wavelengths

In general, the impact of pretapering on the coupling behavior does not depend on the wavelength. Nevertheless, for WDM applications, especially if two widely separated wavelengths are involved, it must be considered that both wavelengths experience refractive index profiles with different guiding properties which in part result in distinct characteristics for each wavelength.

First of all, the transition between core and cladding guiding occurs at different extensions (or taper positions) for each wavelength. For the fibers used in this section (630-HP/1310BHP) the transition of the pump light occurs at an extension of 13.2 mm in the pump fiber and for the signal light at an extension of 11.8 mm in the signal fiber. The critical V parameter is $V_{cc}^p \approx 0.75$ for the pump fiber and $V_{cc}^s \approx 0.86$ for the signal fiber which means that the fiber cores become non-guiding for the respective wavelength when the given critical V parameter is reached along the taper.

As depicted in Fig. 4.2(a) without any pretapering the coupling started for both wavelengths after their respective transition point is reached. The coupling for the signal light started accordingly at lower values of the extension with increasing PL of the signal fiber since the transition point was reached earlier. Therefore, the transition point between core and cladding guiding is different for the pump and signal light. However, this is also the case in symmetric FFCs and the functional principle for WDM applications. Different wavelengths show different beat lengths which allows for the separation or combination of the wavelengths. The difference between the symmetric and asymmetric FFC is that when the light propagation in the core is considered the respective other core has different guiding properties.

At the core-cladding transition point of the pump light the signal core can influence the coupling behavior, because it can theoretically guide the pump light. The V parameter of the pump light in the signal core is about 1.8 which is well above the critical V parameter of the signal core V_{cc}^s . This means that the fundamental mode of the pump light in the signal core could be excited. Therefore the observed influence of pretapering on the coupling behavior of the pump light is mainly due to the change in core diameter of the pretapered signal fiber. This explains why the signal fiber has to be pretapered, because the influence of the signal core on the coupling behavior of the pump light is consequently reduced. Furthermore, it can be reasonably assumed that the change in the refractive index profile of the cladding due to pretapering also influences the coupling behavior of the pump light, because it directly affects the properties of the SMs.

In contrast to the pump light, the signal light cannot be guided by the pump core at the transition point, because the V parameter of the signal light in the pump core is 0.34 which is below the critical V parameter V_{cc}^p . Thus, it can be assumed that the core of the pump fiber has only a negligible influence on the signal light, and a change in core diameter of the pump fiber due to pretapering would have no significant influence on the coupling behavior of the signal light. Therefore, the influence of pretapering on the coupling behavior of the signal light is mainly due to the change in the refractive index profile of the cladding, because after the transition point the FFC effectively is a cladding-mode device [Bir88b] and coupling is dominated by the beating of the SMs.

In summary, these considerations reveal that when considering asymmetric FFCs the fiber cores cannot be simply neglected and the influence of pretapering is different for both wavelengths. For the signal light the pump core is non-guiding in the coupling region, but for the pump light the signal core can guide the fundamental mode. The shape of the refractive index profile directly affects the SMs and their coupling behavior which is further discussed in the following section.

4.3.2 Calculation of Super-Modes

The electric field of the SMs of an asymmetric FFC were calculated for an extension of 16 mm considering the non-pretapered case and the pretapered case (PL = 4 mm, cf. Fig. 4.5(c)). Figure 4.8(a)-(d) shows the calculated SMs of both wavelengths in the taper waist of a non-pretapered FFC. The signal fiber is located on the left and the pump fiber on the right side of the FFC (as in indicated in Fig. 4.8(a)). Due to the asymmetry of the refractive index profile of the FFC the SMs of the signal and pump light are remarkably different.

The symmetric SM of the signal light (cf. Fig. 4.8(a)) expands into the whole cladding, whereas the maximum is solely located at the position of the signal fiber core. The pump fiber core seems to have no influence on the excited SM, because of the lower V parameter compared to the signal fiber core. The antisymmetric SM of the signal light is nearly central symmetric (cf. Fig. 4.8(b)) and similar to the antisymmetric SM of a symmetric FFC (cf. Fig. 3.15(b)). The maximum of the symmetric SM of the pump light (cf. Fig. 4.8(c)) is only located at the position of the signal fiber core and corresponds to the fundamental core mode of the signal fiber at the pump light, because the V parameter is above V_{cc}^s . The maximum of the antisymmetric SM of the pump light is located at the position of the pump fiber core (cf. Fig. 4.8(d)). Thus, light launched into the pump fiber predominantly excites the antisymmetric SM. The SMs of the signal light are only slightly influenced by the pump core and it could be theoretically neglected in the calculation. In contrast, the

SMs of the pump light are strongly influenced by the signal core which should not be neglected in the calculations.

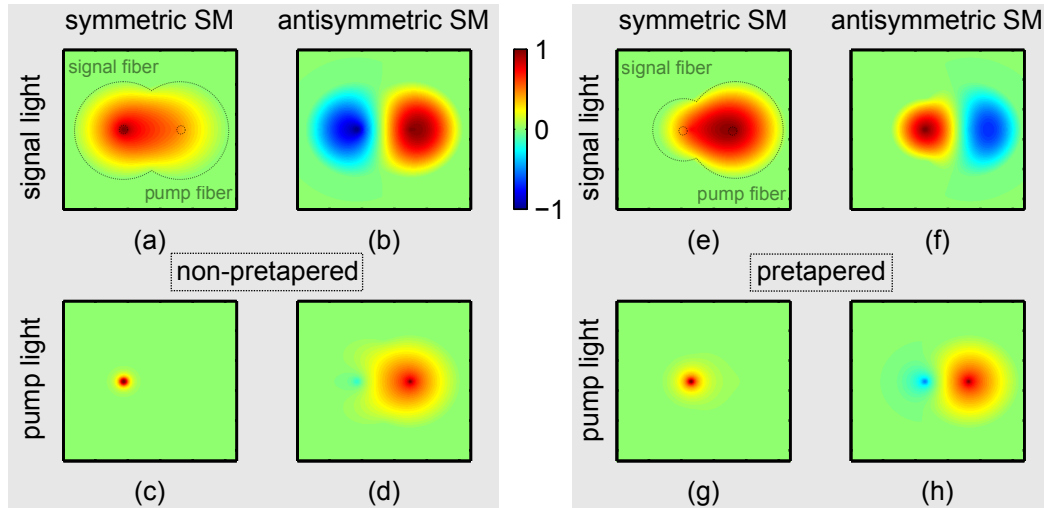


Figure 4.8: Calculated electric field of the symmetric and antisymmetric SMs of the signal (first row) and pump light (second row) in the taper waist of an FFC with an extension of 16 mm and no pretaper (a)-(d) and a PL of 4 mm (e)-(h). As indicated in (a) the signal fiber is located on the left and the pump fiber on the right side of the FFC.

Figure 4.8(e)-(h) shows the calculated SMs for the same case, but with a PL of 4 mm applied to the signal fiber (located on the left side of the FFC). The SMs of the signal light in the non-pretapered case and the pretapered case are remarkably different. In the pretapered case the maximum of the symmetric SM (cf. Fig. 4.8(e)) is located at the position of the pump fiber core and not at the position of the signal fiber core. The antisymmetric SM (cf. Fig. 4.8(f)) shows a maximum located at the position of the signal fiber core. Therefore, pretapering clearly influences the SMs of the signal light which can result in a complete power transfer, as shown in Fig. 4.5(c). The SMs of the pump light are only slightly influenced by the applied pretaper (cf. Fig. 4.8(g) and 4.8(h)). Figure 4.5(c) shows that in this configuration no power transfer occurs for the pump light and therefore the parameter set of extension and PL does not result in a complete power transfer.

4.3.3 Evolution of the Super-Modes and their Effective Refractive Index

In Sec. 3.4 the evolution of the n_{eff} along the taper of a symmetric FFC has been analyzed. It has been shown that up to the core-cladding transition both SMs have identical propagation constants β_s and β_a which split up at this transition point. Due to the difference of the propagation constants, phase difference is accumulated leading to mode beating in the coupling region. Furthermore, it is shown that both SMs are equally excited along the

complete longitudinal taper. However, in asymmetric FFCs the modal analysis has to be performed for the signal light as well as the pump light.

Signal Light

As depicted in Fig. 4.9 for the signal light the behavior of the n_{eff} curves is completely different in asymmetric FFCs, whether the signal fiber was pretapered (PL = 4 mm) (cf. Fig. 4.9(a)-(b)) or not (cf. Fig. 4.9(c)-(d)). For the signal light both SMs are core-guided at the beginning of the taper, but they have different propagation constants and the core-cladding transition of both SMs occurs at different taper positions.

In the pretapered case shown in Fig. 4.9(a) the core-cladding transition of the symmetric SM occurs at a taper position of 5 mm and for the non-pretapered case shown in Fig. 4.9(c) at a taper position of 7 mm. Up to the core-cladding transition the symmetric SM corresponds to the core mode of the signal fiber and the antisymmetric SM to the core mode of the pump fiber and any mode of a higher order is a cladding mode. The n_{eff} curve of the symmetric SM is influenced by pretapering the signal fiber and shifts to lower values of the n_{eff} which means that the fundamental mode of the signal fiber breaks out of the core earlier (cf. blue curves in Fig. 4.9(a) and (c)). The n_{eff} curve of the antisymmetric SM on the other hand is not shifted by pretapering, because it corresponds to the core mode of the pump fiber which is not significantly influenced by the pretapered signal core.

In comparison to a symmetric FFC both SMs have different progressions of the n_{eff} curves along the complete FFC and the SMs propagate at different phase velocities. However, in the asymmetric case only one SM is excited at the beginning of the FFC. Thus, in this case light injected into the signal fiber excites only the symmetric SM. If only one SM is excited along the FFC no mode beating can occur, inhibiting any power transfer to the other fiber. Therefore, pretapering is used to tune the refractive index profile in a way that the antisymmetric SM is excited along the longitudinal propagation.

In the pretapered case (cf. Fig. 4.9(a)) at a taper position of approx. 6 mm the n_{eff} curves of both SMs approach so that coupling between both SMs can occur. The coupling between the SMs is more likely between modes that are close in n_{eff} [Bir15; Lov91]. The evolution of both SMs at a taper position between 3.15 mm and 7.35 mm is depicted in Fig. 4.9(b) and reveals that at a taper position of approx. 6.3 mm, where both n_{eff} curves are closest to each other, both SMs expand into the whole cladding. In the non-pretapered case the n_{eff} curves of both SMs are well separated along the complete FFC (cf. Fig. 4.9(c)) and the evolution of the SMs does not show an expansion of the SMs into the whole cladding (cf. Fig. 4.9(d)). Therefore, it seems that the antisymmetric SM cannot be excited in the taper transition due to the fact that the n_{eff} are not similar and both SMs do not show mode

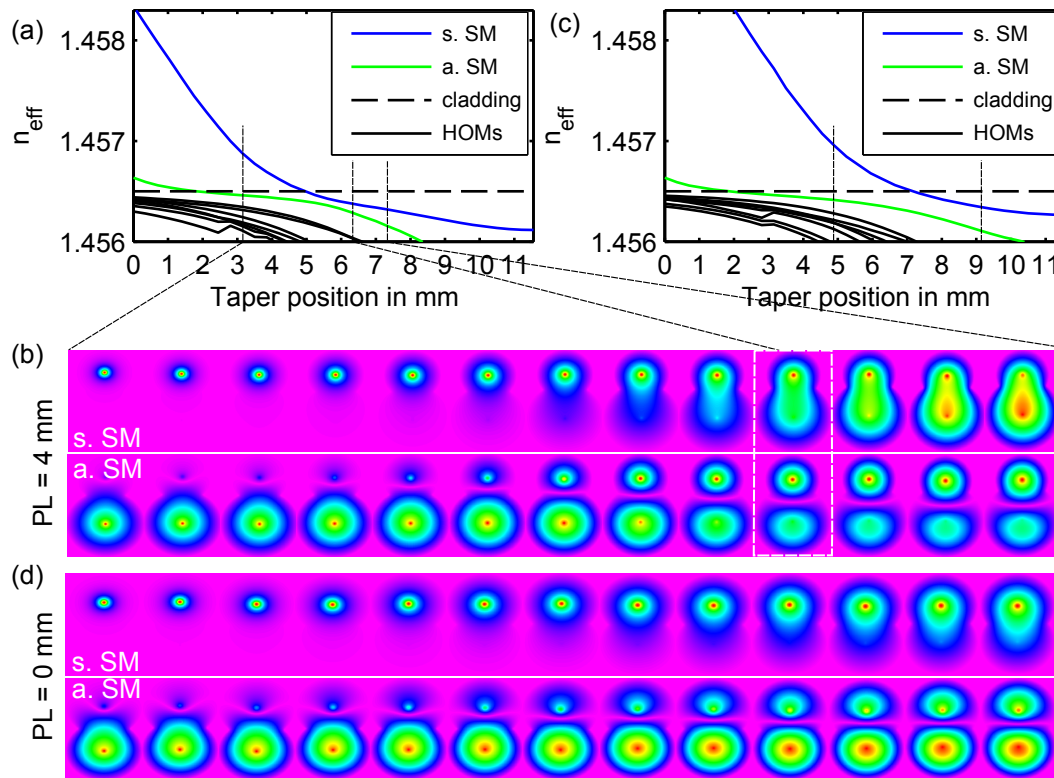


Figure 4.9: Evolution of the n_{eff} and the intensity profiles of the symmetric (s.) and antisymmetric (a.) SM along the taper position of an asymmetric FFC for the signal light. The PL was 4 mm (a)-(b) applied to the signal fiber. The non-pretapered case (c)-(d) is also shown. The simulation cross section (in x and y dimension) for the eigenmode calculation (b),(d) is consecutively rescaled for higher taper positions.

overlap. Figure 4.9 also illustrates qualitatively why it is necessary to pretaper the signal fiber in this case. Due to pretapering it can be achieved that the n_{eff} curve of the initially excited symmetric SM subsequently approaches the curve of the targeted SM which is in this case the antisymmetric SM. Then, coupling occurs from the fundamental mode in the signal fiber to the fundamental mode in the pump fiber.

Pump Light

The evolution of the n_{eff} and the SMs of the pump light is depicted in Fig. 4.10, whereby a case with a PL of 6.3 mm (a)-(b) is considered and a PL of 4 mm (c)-(d). At a PL of 6.3 mm and an extension of 16 mm a power transfer to the signal fiber was observed as depicted in Fig. 4.6(b). The n_{eff} curves for this parameter set are shown in Fig. 4.10(a), where the curves of the symmetric and antisymmetric SM approach at a taper position of approx. 9.5 mm and the respective SMs expand into the whole cladding at this position (cf. Fig. 4.10(b)).

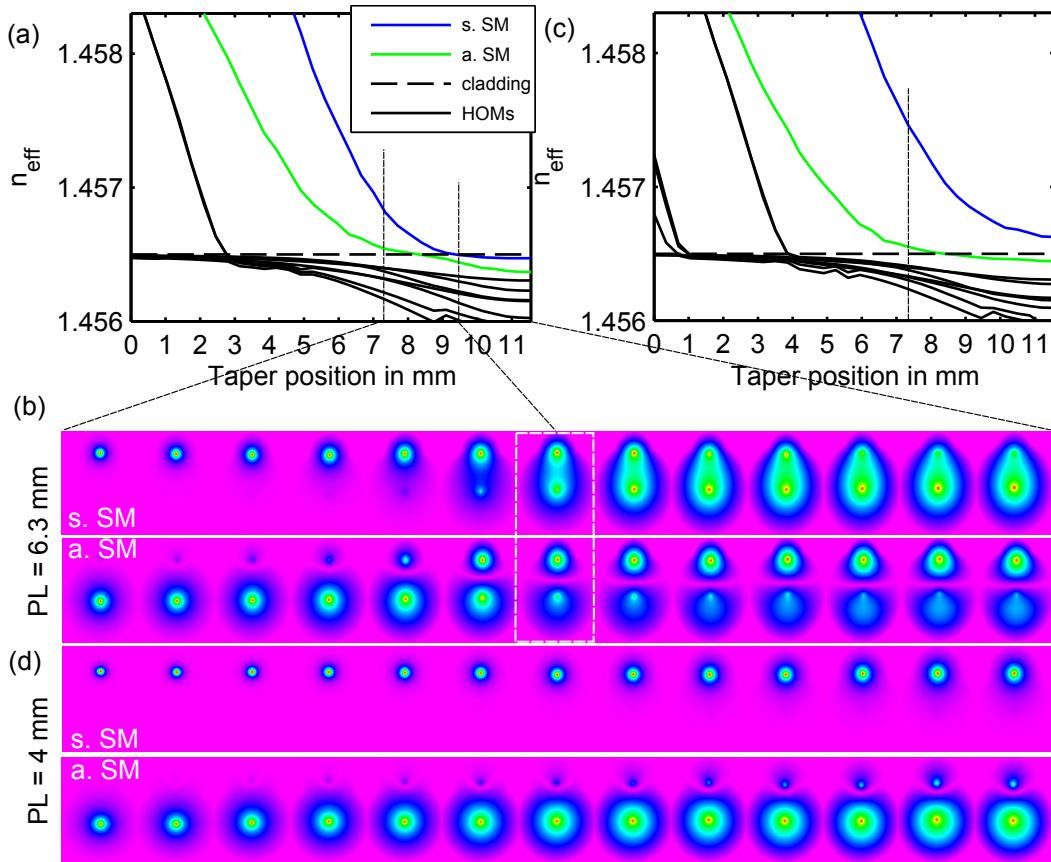


Figure 4.10: Evolution of the n_{eff} and the intensity profiles of the symmetric (s.) and antisymmetric (a.) SM along the taper position of an asymmetric FFC for the pump light. The PL was 6.3 mm (a)-(b) and 4 mm (c)-(d) applied to the signal fiber, respectively. The simulation cross section (in x and y dimension) for the eigenmode calculation (b),(d) is consecutively rescaled for higher taper positions.

At a PL of 4 mm and an extension of 16 mm, which corresponds to an optimal parameter set for the signal light, but not for the pump light, no power transfer to the signal fiber was observed as depicted in Fig. 4.6(b). The results shown in Fig. 4.10 (c)-(d) depict that the n_{eff} curves do not approach and the symmetric SM, which corresponds to the signal fiber core mode, does not break out of the core. Therefore, the symmetric SM is not excited which inhibits any power transfer. In the case that no pretaper is applied the n_{eff} curves would differ even more. In addition, the signal core would guide also more modes, since the V parameter of the signal core for the pump light is in the order of 5.5. Due to the high V parameter of the signal core for the pump light several core modes are supported at the beginning of the taper. The number of HOMs is consecutively reduced by pretapering the signal fiber.

At a PL of 6.3 mm this means that both 90°-rotated versions of the LP₁₁ mode could be excited in the signal core at the beginning of the taper. In Fig. 4.10(a) the LP₁₁ modes correspond to the curves which break out of the core at a taper position of 3 mm. In case of a PL of 4 mm the 45°-rotated versions of the LP₂₁ and LP₀₂ modes are theoretically guided which break out of the core at a taper position of approx. 1 mm.

In conclusion, pretapering one fiber has an immense impact on the evolution of the SMs in an FFC. By defined selection of the pretapered fiber and the applied PL, the n_{eff} curve of the initially excited SM and the targeted SM can be approached enabling coupling between them. In the presented case of a WDM application coupling between the fundamental modes of both fibers is desired. Therefore pretapering the signal fiber, or the fiber designed for guiding the longer wavelength, is necessary in order to tune the n_{eff} curve of the symmetric SM. Pretapering the pump fiber, or the fiber guiding the shorter wavelength, would shift the n_{eff} curve of the antisymmetric SM to lower values which is potentially interesting for SDM in order to excite HOMs. This topic is discussed in detail in Sec. 5. The considerations concerning the n_{eff} curves and the evolution of the SMs are valuable to qualitatively discuss the excitation of the SMs and the coupling between them. Although, they cannot definitely reveal if a SM is really excited or not. Therefore, a modal decomposition is performed in the following section.

4.3.4 Modal Decomposition

The coupling behavior in asymmetric FFCs, as shown by the experimental and numerical pulling signatures in Fig. 4.2 and 4.5, is mainly determined by the PL and the applied extension. Therefore, a modal decomposition is performed on the one hand at a fixed taper position and varying PL and extension and on the other hand at a fixed PL and extension, but along the longitudinal profile of an FFC.

Influence of Pretapering

Figure 4.11 shows the modal weight $|c_i|^2$ of both SMs and the first HOM in the taper waist of an FFC for varying PLs of the signal fiber. The FFC has a fixed extension of 16 mm. The signal light was launched into the signal fiber and the pump light was launched into the pump fiber. The remaining HOMs have no significant contribution, so they are not shown here. The SMs are excited unequally when no pretaper is applied which means that only a partial power transfer from one fiber to the other can be achieved. Signal light launched into the signal fiber mainly excites the symmetric SM (cf. Fig. 4.8(a)), whereas pump light launched into the pump fiber mainly excites the antisymmetric SM (cf. Fig. 4.8(d)). In general, the SM is excited, whose field is localized in the fiber core where the light was initially launched.

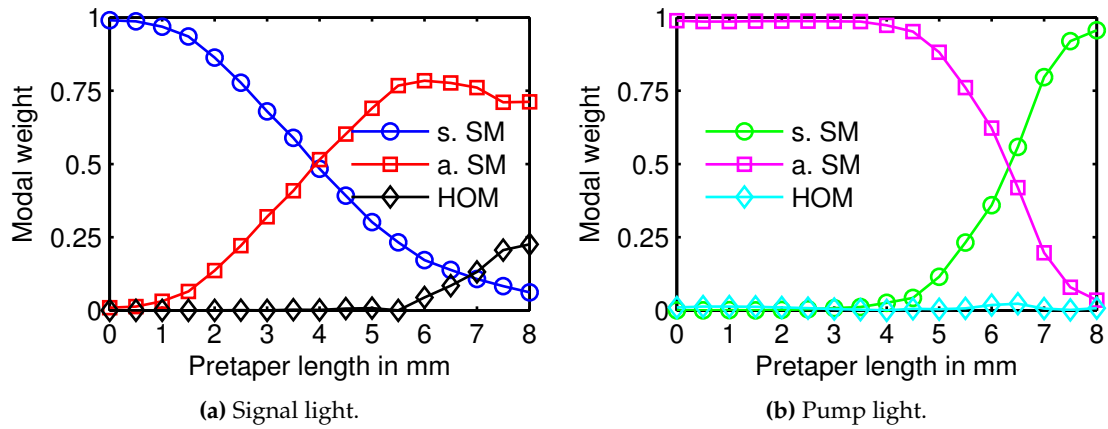


Figure 4.11: Modal weight $|c_i|^2$ of the symmetric (s.) and antisymmetric (a.) SMs and the first HOM in the taper waist of an FFC with an extension of 16 mm for different PLs of the signal fiber. The signal light (a) was launched into the signal fiber and the pump light (b) into the pump fiber.

Consecutive pretapering of the signal fiber leads to a change in the modal weight of the excited SMs in the taper waist; for the signal light the modal weight of the symmetric SM consequently decreases with increasing PL while the weight of the antisymmetric SM increases with further pretapering. At a PL of 4 mm the symmetric and antisymmetric SMs show equal modal weights. Due to the equal excitation in the taper waist a complete power transfer is possible and the output of the light is determined by the mode beating. This is in agreement with Fig. 4.5(c) (PL = 4 mm) where the signal light shows a complete power transfer¹ at an extension range of around 16 mm. Further pretapering leads to an unequal excitation of the SMs again and also to the excitation of an HOM at a PL of 6 mm. This could be the reason for the observation of an unpredictable coupling behavior of the signal light in the experiment (cf. Fig. 4.2(f)) and the simulation (cf. Fig. 4.5(f)) at higher PLs. The same matching of the modal weights can be observed for the pump light but at a different PL of 6.3 mm. Figure 4.5(e) shows a complete power transfer for the pump light at a PL of 6 mm and an extension of around 16 mm.

Influence of the Extension

The experimental and numerical pulling signatures in Fig. 4.2 and 4.5 reveal that besides the PL the applied extension also has a significant impact on the coupling behavior and the maximum coupled power for both wavelengths. In order to evaluate this effect a

¹ Coincidentally, at this extension the signal light is fully transmitted in the signal fiber. However, the coupling cycles at an extension of 15 mm and 16.8 mm show a nearly complete power transfer of the signal light.

modal decomposition in the taper waist for different extensions at a constant PL of 4 mm was performed.

The results are depicted in Fig. 4.12 and reveal a clear influence of the applied extension on the modal composition in the taper waist. An equal excitation of both SMs occurs at an extension of 16 mm for the signal light (cf. Fig. 4.12(a)) and 20 mm for the pump light (cf. Fig. 4.12(b)). This leads theoretically to a complete power transfer¹ at the respective extensions as shown by the pulling signature in Fig. 4.5(c). Therefore, as opposed to the symmetric FFCs a complete power transfer is only possible for specific values of the PL and the extension. This is reasonable since both determine the refractive index profile of the FFC in the coupling region and by that the properties of the SMs.

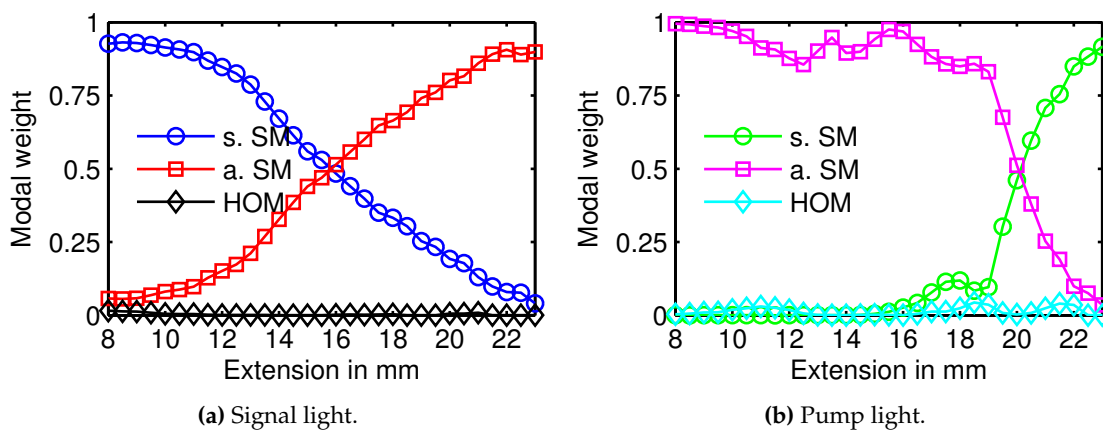


Figure 4.12: Modal weight of the symmetric (s.) and antisymmetric (a.) SM and the first HOM in the waist of an FFC with a PL of 4 mm applied to the signal fiber. The signal light (a) was launched into the signal fiber and the pump light (b) into the pump fiber.

Mode Conversion

The considerations so far show the impact of the PL and the extension on the modal excitation of the SMs, but only at one determined position in the taper (in the taper waist). In the following the mode conversion along the longitudinal propagation is discussed. In symmetric FFCs mode conversion between the SMs does not take place because the SMs are orthogonal at any position when the adiabatic conditions are satisfied [Oka90]. Therefore, the symmetric and antisymmetric SMs are excited equally over the whole length of the FFC and the power transfer is caused completely by the beat phenomena of the SMs (cf. Sec. 3.4.4). In asymmetric FFCs mode conversion between the SMs takes

¹ However, in Fig. 4.5(c) the signal light is transmitted in the signal fiber due to the resulting mode beating but the coupling cycles at an extension of 15 mm and 16.8 mm show a nearly complete power transfer.

place so that the power transfer is influenced not only by mode beating but also due to the unequal excitation of the SMs [Oka90].

Signal Light Figure 4.13(a) shows the evolution of the modal weights of the SMs along the taper position in an FFC with an extension of 16 mm and a PL of 4 mm for the signal light. At the beginning of the FFC the SMs are excited unequally, and the symmetric SM is mainly excited. In this region the SM corresponds to the fundamental core mode of the signal fiber (cf. Fig. 4.9(a)). Figure 4.13(b) depicts the respective light propagation in this configuration where the light was launched into the signal fiber (top). For better illustration the data points of each slice were normalized which is the reason why the beating seems to be abrupt.

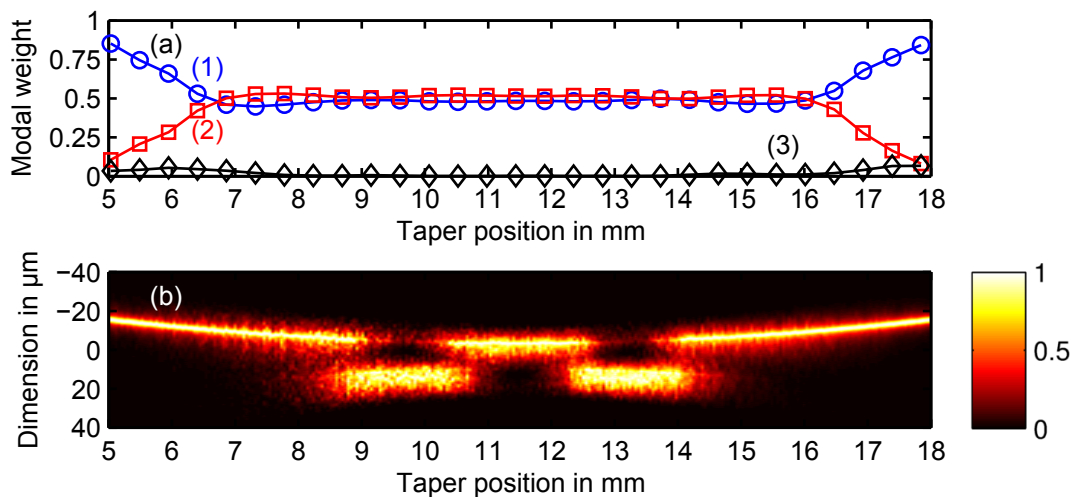


Figure 4.13: Signal light modal excitation (a) and light propagation (b) along an FFC with an extension of 16 mm and a PL of 4 mm. The light was launched into the signal fiber (top). The data points of each propagation slice were normalized. The symmetric SM is denoted with (1), the antisymmetric SM with (2) and the HOM with (3).

At a taper position of approx. 5 mm the modal weight of the symmetric SM starts to decrease and the modal weight of the antisymmetric SM starts to increase. In accordance with the results shown in Fig. 4.9(a) this corresponds to the position of the core-cladding transition of the symmetric SM. The modal weight of the SMs reaches an equal excitation at a taper position of approx. 7 mm which remains constant in the middle section of the FFC. In this section no further mode conversion takes place and a complete power transfer occurs as shown in Fig. 4.13(b). In the up-taper region the light is recaptured by the signal core (at a taper position of approx. 18 mm) and the symmetric SM becomes the dominant eigenmode of the FFC again. In this configuration the signal light is transmitted at the end of the signal fiber.

Pump Light In Fig. 4.14(a) the modal weights of an FFC with an extension of 20 mm and a PL of 4 mm for the pump light are depicted. At the beginning of the FFC the antisymmetric SM is predominantly excited, because the pump light was launched into the pump fiber (bottom) (cf. Fig. 4.14(b)). The antisymmetric SM corresponds to the fundamental core mode of the pump fiber. The modal weights equalize when the core-cladding transition occurs at a taper position of approx. 10 mm, where the mode beating starts.

In contrast to the signal light (cf. Fig. 4.13(a)) these curves show a different behavior for the up-taper region compared to the down-taper region. This is due to the fact, that the pump light is influenced by the signal core (cf. discussion in Sec. 4.3.1). The signal core becomes guiding for the pump light at a taper position of 15 mm. In Fig. 4.14(a) this leads to an increase of the modal weight of the symmetric SM, whose maximum is located in the signal core. The pump core becomes guiding for the pump light at a taper position of 17 mm which leads to an increase of the modal weight of the antisymmetric SM, whose maximum is located in the pump core. At the end of the FFC both SM are excited nearly equally and the light is guided in both cores as depicted in Fig. 4.14(b).

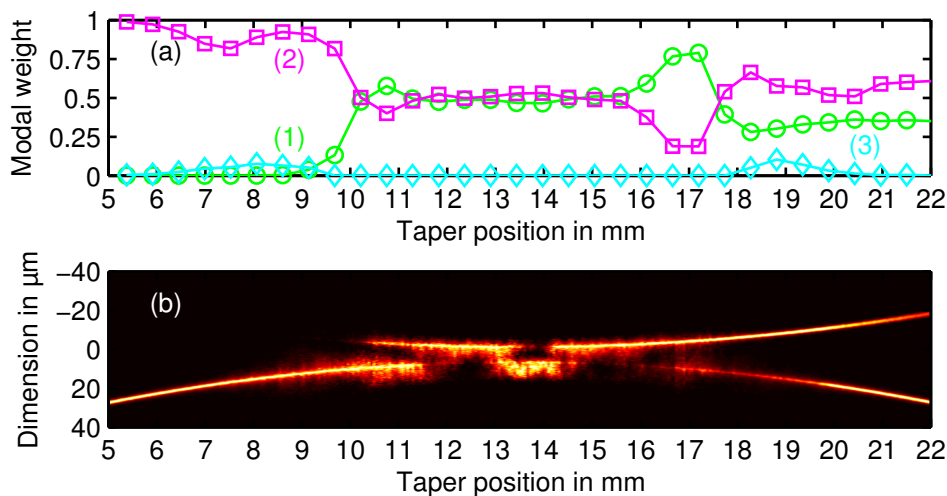


Figure 4.14: Pump light modal excitation (a) and light propagation (b) along an FFC with an extension of 20 mm and a PL of 4 mm. The pump light was launched into the pump fiber (bottom). The data points of each propagation slice were normalized. The symmetric SM is denoted with (1), the antisymmetric SM with (2) and the HOM with (3).

In conclusion, the analysis of the modal evolution in asymmetric FFCs demonstrates that by pretapering mode conversion from the originally excited SM to the second SM of the system can be achieved. The modal composition is tuned in a way that the second SM of the system becomes equally excited along the propagation in the FFC which enables a complete power transfer by mode beating. Otherwise, if the refractive index profile is not

modified, both SMs can be in general arbitrarily excited along the whole length of the FFC. Adequate pretapering tunes the mode conversion in the desired way.

4.4 Fused Fiber Couplers for Core Pumping Thulium-Doped Fibers at 795 nm

In the 630-HP/1310BHP FFC considered so far in this chapter the combination of wavelengths with a separation of 923 nm was demonstrated. However, it is possible to combine wavelengths with even higher separations, for example for applications in thulium-doped fiber amplifiers. Lasers based on thulium-doped fibers extend the directly accessible wavelengths towards the wavelength region of 2 μm . The absorption spectrum of thulium shows mainly three maxima at 1630 nm, 1210 nm and 795 nm, whereas the last absorption maximum has a nearly twice as large absorption cross section compared to the others [Jac99]. Additionally, pumping at 795 nm is favorable, as there is the possibility of direct core pumping by laser diodes. Because of the cut-off, employing equal fibers for the pump and signal light would lead to high losses [Bir88b]. To overcome this, an asymmetric FFC consisting of two different fibers with single-mode guidance for the respective wavelength was fabricated [Pel12; Say13]. Light sources at 795 nm and 1980 nm were employed, whereby as pump fiber a 780-HP and as signal fiber a SM2000 were used.

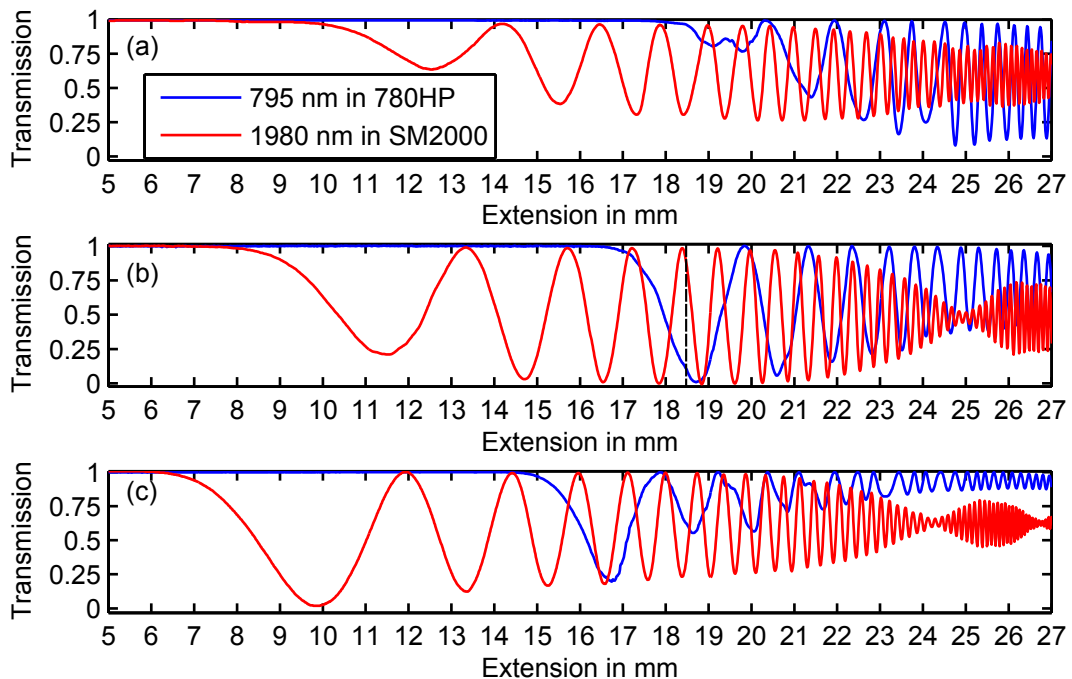


Figure 4.15: Experimental transmission of the pump and signal light at different PLs of the signal fiber of (a) 0 mm, (b) 1.8 mm and (c) 3.5 mm.

The transmission was experimentally recorded for different PLs of the signal fiber (0 mm, 1.8 mm, 3.5 mm) and the corresponding results are shown in Fig. 4.15. The pulling signa-

tures show the same characteristics as for the case of the 630-HP/1310BHP FFC shown in Fig. 4.2. When no pretaper is applied the power transfer is limited (cf. Fig. 4.15(a)) and due to consecutive pretapering a complete power transfer can be achieved (cf. Fig. 4.15(b) dotted line). At higher values of the PL the maximal power transfer decreases again (cf. Fig. 4.15(c)). Furthermore, the beginning of the coupling starts for both wavelengths at lower values of the extension with consecutive pretapering and the transmission changes in dependence of the applied extension. These characteristics correspond to those observed in the previously discussed 630-HP/1310BHP FFC (cf. Fig. 4.2), but there are also some differences. When no pretaper is applied the maximum coupled power is higher in the case of the 780-HP/SM2000 FFC and the optimal PL is in the range of 1.8 mm instead of approx. 5 mm in the case of the 630-HP/1310BHP FFC. Therefore, the exact progression of the pulling signatures depends on the specifications of the used fibers.

According to the pulling signature shown in Fig. 4.15(b) a parameter set with a high transmission of the pump and signal light in the signal fiber is at a PL of 1.8 mm and an extension of 18.5 mm. Based on these results an FFC was fabricated showing a transmission of 90 % for the pump light and 95 % for the signal light in the signal fiber. The application of this FFC was demonstrated in an all-fiber core pumped thulium-doped fiber amplifier [Pel12].

The amplifier setup consisted of the FFC, a thulium-doped fiber (OFS TmDF200, cf. Tab. A.1), a single-mode pump diode emitting at a wavelength of 795 nm and a seed source operating at a wavelength of 1980 nm. The optimal length of the thulium-doped fiber was chosen so that the residual pump light was nearly 0 %. At a seed power of 0.8 mW and a pump power of 70 mW the seed signal was amplified to 2.5 mW. The maximum achievable gain in this configuration was 5 dB, which was limited by the pump power of the commercially available laser diode. For future applications in core pumped thulium-doped fiber amplifiers, higher amplification factors should be possible with the availability of high-power single-mode laser diodes in the wavelength range of 795 nm.

4.5 Conclusion

In this chapter asymmetric fused fiber couplers, consisting of different fibers, were analyzed both experimentally and numerically. The fundamental coupling mechanisms in asymmetric FFCs were studied and a concrete WDM application was demonstrated in a fiber amplifier setup. The fundamentals of asymmetric FFCs were discussed based on experiments and simulations of an FFC consisting of 630-HP and 1310BHP fibers at wavelengths of 633 nm and 1556 nm. Both wavelengths could be combined experimentally with an efficiency of 84 % for the signal light and 94 % for the pump light. This

was achieved by systematically pretapering the fiber intended for guiding the longer wavelength. Therefore, it is shown that pretapering one fiber can be used to efficiently increase the maximum coupled power up to a complete power transfer from the fundamental mode in the original fiber to the fundamental mode in the target fiber. The same qualitative behavior in FFC characteristics was explained with help of the presented simulation tool and refractive index profile model. The simulations can give a preliminary estimation of the parameter set for an experimental realization of an FFC. By consecutive experimental optimization, asymmetric FFCs which efficiently combine two wavelengths, can be fabricated. The simulation accounts for the general qualitative behavior of the FFC performance and allows to gain insight into their operation and the underlying coupling mechanism.

It was shown that the fiber cores may not be simply neglected when asymmetric FFCs are considered, since the fiber core of one fiber can be non-guiding for its original wavelength while still showing guidance for the other wavelength. Both wavelengths experience refractive index profiles with different guiding properties. The calculation of the symmetric and antisymmetric SMs of the FFC reveal that the SMs of the signal and pump light are remarkably different and directly influenced by the refractive index profile of the FFC. Therefore, the influence of pretapering is different for both wavelengths. The SMs of the signal light are quasi not influenced by the pump core, whereas the SMs of the pump light are dominated by the signal core. The calculation of the n_{eff} and the evolution of the SMs along the taper reveal that pretapering has an immense impact on those. By defined selection of the pretapered fiber and the applied PL, the n_{eff} curve of the symmetric SM and the antisymmetric SM can be approached in order to theoretically enable coupling between both. In the presented case of a WDM application coupling between the fundamental modes of both fibers is desired. Therefore pretapering the fiber designed for guiding the longer wavelength is necessary in order to tune the n_{eff} curve of the symmetric SM. Pretapering the fiber guiding the shorter wavelength is potentially interesting for SDM in order to excite HOMs. This topic is discussed in detail in the following Chapter 5.

An in-depth analysis of the modal composition of the light was carried out in simulations in order to determine the excitation of the SMs. Mode conversion in asymmetric FFCs takes place and leads to a change of the modal weight of the excited SMs. Without any modification of the refractive index profile both SMs can be in general arbitrarily excited along the complete taper. However, in the central part of the FFC where the mode beating occurs an unequal modal excitation of the SMs inhibits a complete power transfer. By pretapering mode conversion from the originally excited SM to the other SM of the

system can be achieved. The modal composition is tuned in a way that the second SM of the system becomes equally excited along the propagation in the FFC which enables a complete power transfer. These findings improve the understanding of FFCs consisting of different fibers and enable the fabrication of novel and special fused fiber components. Therefore, it was possible to fabricate an FFC capable of multiplexing wavelengths in the range of 795 nm and 1980 nm with a transmission of 90% for both wavelengths in the signal fiber which was employed in a core pumped 2 μm thulium-doped fiber amplifier.

CHAPTER 5

Asymmetric Mode-Selective Fiber Couplers for Space-Division Multiplexing

Single-mode fibers guiding only one single spatial mode are rapidly approaching their transmission capacity limit [Ess10]. In order to delay this capacity crunch [Win14] various approaches have been completely optimized including wavelength-division multiplexing (WDM) and polarization-division multiplexing (PDM). Currently, the concept of space-division multiplexing (SDM) has come into focus to increase the data-carrying capacity of optical fibers [Ric13]. This approach uses a fiber or waveguide design capable of guiding several higher-order spatial modes instead of using a single-mode waveguide which is intrinsically limited to one spatial mode. The use of the spatial dimension as additional degree of freedom can highly increase the number of data channels.

Current devices for the application of SDM cover both fiber-based and waveguide-based approaches in order to realize spatial mode multiplexer and demultiplexer. Such waveguide-based devices include asymmetric Y-junctions [Lov12b], tapered velocity mode-selective couplers [Rie13] and integrated asymmetric mode-selective devices [Gro14; Han13; Rie14]. Recently, Gross et al. [Gro14] reported 3D tapered mode-selective couplers which were written directly in a photonic chip by using a femtosecond laser. These devices exhibit extremely efficient one-to-one mode mapping with an ultra-high bandwidth. In order to implement SDM in future fiber optical networks successfully fiber-based components are predestinated in order to achieve a high degree of compatibility with existent telecommunication systems. Despite waveguide-based approaches have strongly advanced in recent years, fiber-based solutions have still a good potential for the future and are currently in active development. Few-mode erbium doped fiber amplifiers [Jun11] have been presented which currently support up to 6 spatial modes [Jun14]. Multiplexing devices can be realized by, for example, planar lightwave circuits [Han14], acousto-optic

devices [Son14] or fiber devices which include photonic lanterns [Leo10; Leo05; Leo14; Noo09; Vel15; Yer14], photonic crystal fiber devices [Cai15; Lai07; Wit08], long-period fiber gratings [Ami11; Li12a; Li12b; Li13], multicore fibers [Mat12; Zhu12] or mode-selective fiber couplers (MSFCs).

MSFCs can be implemented with the help of FMFs guiding several spatial modes. Such MSFCs can be realized as fused-type multi-mode couplers [Jun13; Sho99], weakly-fused directional couplers [Ism14], twisted fused couplers [Wit08] or fused-type fiber couplers [Son00; Son02; Son03]. Song et al. [Son02] demonstrated a weakly-fused MSFC which couples the LP_{11} mode in one fiber and the LP_{01} mode in the other using a special elliptical core two-mode fiber and an SMF. A numerical analysis was carried out according to the evanescent field coupling approach assuming independent waveguides. Also the LP_{02} mode [Son03] and the LP_{1m} cladding modes [Lee05] could be selectively excited by adequate tuning of the coupler geometry in terms of reduced cladding diameter and pretapering. However, the results presented by Song et al. [Son00; Son03] lack profound numerical characterization and they do not present a versatile model to describe the coupling mechanism in arbitrarily fused MSFCs. Ismaeel et al. [Ism14] discuss the coupling mechanism in weakly-fused MSFCs based on inter-modally phase-matching the propagation constants, but this model is not applicable to well- and strongly-fused MSFCs, because both fibers cannot be considered as isolated.

In this chapter, fused-type MSFCs exciting the LP_{11} mode are investigated experimentally and numerically by the use of the same techniques as in Chapter 3 and 4. First, the fabrication of MSFCs and the pretreatment of the fibers by etching is introduced. Afterwards, the experimental characterization of the fabricated MSFCs is presented and the impact of tuning the coupler geometry in terms of cladding diameter reduction, pretapering and fusion on the transmission and the HOM excitation are discussed. The transmission in the experimentally analyzed MSFCs was simulated with the help of the models presented beforehand (cf. Sec. 3.2 and 3.3). Finally, the modal evolution of the SMs in arbitrarily fused MSFCs is analyzed by calculations of the n_{eff} and by modal decomposition. Parts of the presented results were published beforehand in [Pel15].

5.1 Fabrication

The standard fused biconical taper technique [Kaw81] was used for the fabrication of MSFCs (cf. Sec. 3.1). The pulling procedure was conducted at a wavelength of 795 nm using different standard circular-core fibers, 630-HP and 1310BHP which are the same fibers already used in Chapter 4 for WDM applications. The specifications of the used fibers are given in A.1. At a wavelength of 795 nm the 630-HP guides only the fundamental

LP_{01} mode and acts therefore as SMF. At this wavelength the 1310BHP guides the LP_{01} mode and several HOMs and acts therefore as FMF. Figure 5.1(a) illustrates the function of an MSFC, where the LP_{01} mode launched into the SMF selectively excites an HOM in the FMF, i. e. the LP_{11} mode or the LP_{21} mode.

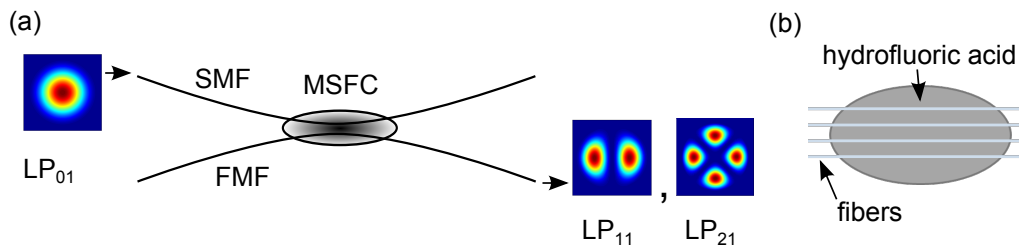


Figure 5.1: (a) Mode-selective fiber coupler (MSFC) consisting of an SMF and an FMF. The fundamental LP_{01} mode is launched into the SMF and can selectively excite HOMs in the FMF, i. e. the LP_{11} mode or the LP_{21} mode. (b) Arrangement of fibers and hydrofluoric acid for the etching process.

Etching

Prior to the MSFC fabrication both fibers were etched by 40 % hydrofluoric acid to reduce the cladding diameter. This is required in order to split up the n_{eff} curves of the HOMs and to achieve a selective excitation of the LP_{11} mode. The theoretical details are discussed in-depth in Sec. 5.4. Before the etching process, a section of the fibers of approx. 35 mm was stripped, cleaned and a group of 4 fibers was arranged in parallel positions as indicated in Fig. 5.1(b). A hydrofluoric acid drop of 1 ml was dosed by a syringe and positioned in a way that the stripped section of the fibers was equally covered in order to achieve homogeneous etching. The final cladding diameter is set by adjusting the etching time, whereby the etching rate is non-linear and increases with time. In this configuration an etching time of (45 ± 2) min produces cladding diameters in the order of (60 ± 5) μm and an etching time of (53 ± 2) min results in cladding diameters of (40 ± 5) μm . The etching process was stopped by filling up to 10l of water into the reservoir to dilute the hydrofluoric acid. After the etching process, the fibers were dried, cleaned, checked for damages and the cladding diameter was measured with the help of an optical microscope.

Figure 5.2(a)-(b) shows SEM images of a fiber tip which was etched to a diameter of 60.75 μm . The surface of the etched fibers is smooth and the etching seems to be homogeneous as also indicated by an optical microscope image shown in Fig. 5.2(c). Rarely, the etched fibers showed damages as indicated in Fig. 5.2(d) which can be attributed to the etching process. It is assumed that the surface damage is due to unfavorable changes of the environmental conditions during the etching process. Typically, etching processes are sensitive to variations of the ambient temperature and humidity. These parameters

could not be adjusted reliably in the laboratory so that the etching results differ in terms of quality and cladding diameter for each etching procedure. This makes it necessary to inspect each fiber after the etching process to ensure the use of non-damaged fibers for the MSFC fabrication process. In conclusion, the general quality of the etched fibers was verified to be good and only fibers without visible damage were used for the performed experiments.

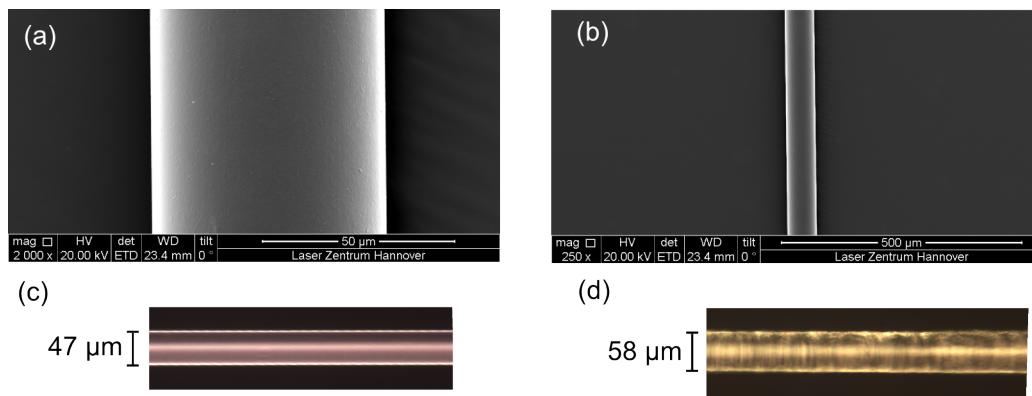


Figure 5.2: SEM images (a)-(b) of an etched fiber tip and optical microscope images of a well etched (c) and badly etched (d) fiber section.

Pulling Procedure

The pulling procedure of the MSFCs started with the pretapering process where only the SMF was pretapered for a specific PL. It should be mentioned that in comparison to the FFCs for WDM applications discussed in Chapter 4 the fiber designed for guiding the shorter wavelength (pump fiber) was pretapered instead of the fiber designed for guiding the longer wavelength (signal fiber). Etched cladding diameter and PL were estimated based on simulations which are discussed later on (cf. Sec. 5.3). Afterwards both fibers were twisted, heated and pulled, while the transmission at both fiber outputs was monitored with photodiodes. In addition, the near-field output intensity pattern at the output of the FMF was monitored simultaneously to the transmitted power with the aid of a focusing lens, a beam splitter and a CCD camera.

To consider the modified fiber diameter due to etching, the fuse and pulling process was conducted completely manually, whereby the pulling speed was set to 0.02 mm/s during the fusion process and 0.04 mm/s during the pulling process and the gas pressure was set to 42 mbar. Furthermore, the burner height which directly determines the temperature in the crucible has to be adapted to the reduced fiber diameter. Otherwise the temperature would be too high for the reduced glass volume of the fibers and would destroy them.

The optimal burner height was determined by measuring the DOF of the pulled FFC and consecutive adaption of the burner height afterwards. A preliminary burner height was obtained by determining the maximum burner height during the automatically conducted pretapering process which the equipment determines by measuring the axial tension on the fiber.

A basic proof of the fabrication of FFCs with etched fibers is given in Fig. 5.3. The pulling signature of a symmetric FFC consisting of two 780-HP fibers etched to a diameter of $65\ \mu\text{m}$ each shows that the coupling starts at an extension of $(10.5 \pm 0.5)\ \text{mm}$ which is 3 mm less compared to the case with non-etched $125\ \mu\text{m}$ fibers (cf. Fig. 3.3). It is assumed that this is due to evanescent field coupling between both fiber cores before the core-cladding transition. Since both fibers have a reduced cladding, the cores are closer to each other which can enable direct coupling between them. However, evanescent field coupling is overtaken by SM coupling, because the core-cladding transition occurs at an extension of approx. 13.5 mm which is still before the first coupling maximum.

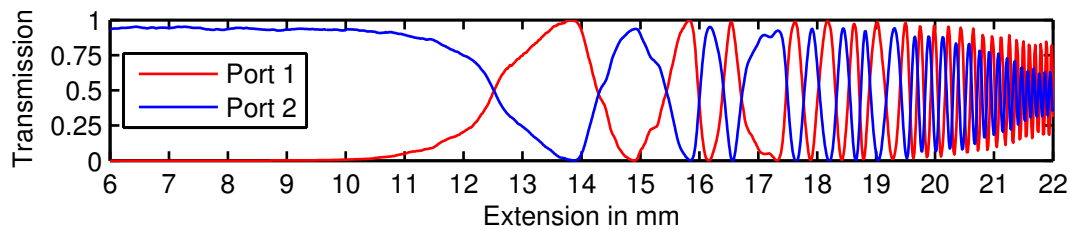


Figure 5.3: Pulling signature in a symmetric FFC made from $65\ \mu\text{m}$ etched 780-HP fibers at a wavelength of 795 nm.

5.2 Experimental Characterization

In this section MSFCs are experimentally characterized by analyzing the impact of the cladding diameter, the PL and the DOF on the transmission and the selective excitation of HOMs. Pulling signatures are presented for MSFCs made from unetched fibers at different PLs and for MSFCs made from fibers etched to a diameter of $(40 \pm 5)\ \mu\text{m}$ at different PLs and DOF.

5.2.1 Impact of the Cladding Diameter and the Pretaper Length

Unetched Fibers

Figure 5.4 shows pulling signatures of MSFCs made from unetched $125\ \mu\text{m}$ fibers. The experiments were performed at a wavelength of 795 nm and the outputs at the SMF (solid lines) and the FMF (dotted lines) were measured for different PLs of 0 mm, 2 mm, 4 mm and 6 mm, which were applied to the SMF. The near-field output intensity pattern of the

FMF was measured simultaneously and is depicted for the indicated extensions. The measured DOF for all pulling signatures is 1.2.

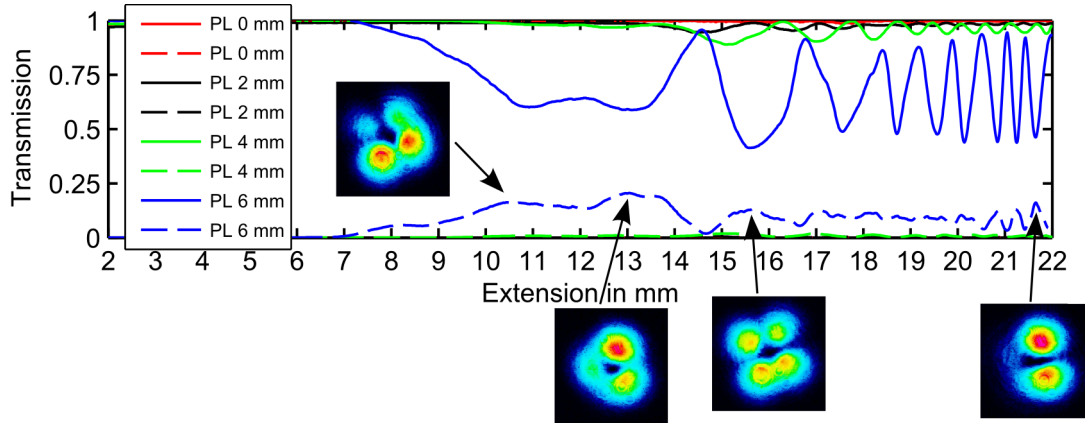


Figure 5.4: Experimentally measured transmission at a wavelength of 795 nm at the output of the SMF (solid lines) and FMF (dotted lines) during the fabrication process for different PLs of 0 mm, 2 mm, 4 mm and 6 mm applied to the SMF. Both fibers are non-etched and have the standard cladding diameter of 125 μm . The insets show the output intensity pattern of the FMF at the indicated extension.

The results show that a maximal transmission of 20% in the FMF can be achieved by pretapering the SMF with a PL of 6 mm. At lower PLs no significant power transfer to the FMF was observed. However, at a PL of 6 mm the transmission in the FMF is irregular and shows a flat profile instead of regular coupling cycles with minima and maxima. The corresponding transmission in the SMF exhibits on the other hand regular coupling cycles. The sum of the transmission at both fiber ports is not complete and accordingly the insertion loss is relatively high. The minimum of the SMF transmission is in the order of 45%, whereby the transmission in the FMF is in the order of maximal 10% and the losses are approx. 45%. The maximal transmission of 20% in the FMF is achieved at an extension of 13 mm and the corresponding output intensity pattern cannot be clearly assigned to a typical LP fiber mode. The intensity patterns at other extensions are different, whereby the pattern at an extension of 15.6 mm has the shape of an LP_{21} mode and the pattern at an extension of 21.6 mm the shape of an LP_{11} mode.

Therefore, it seems that several HOMs are undefinedly excited and no selective excitation of a specific HOM, as the LP_{11} , occurs. The excitation of higher-order cladding modes is probably the reason for the high losses at the transmission minima of the SMF. If higher-order cladding modes are excited in the down-taper, they are not recaptured by the cores in the up-taper and they tend to be absorbed by the fiber coating. In order to enable a selective excitation of HOMs, etched fibers with a reduced cladding diameter are used and characterized.

Etched Fibers

Theoretically, an increased selectivity is achieved by reducing the cladding diameter of the fibers. A lower limit for the cladding diameter is given by the mechanical handling of the fibers during the etching and pulling process. In accordance with preliminary experiments and simulations a cladding diameter in the order of $(40 \pm 5) \mu\text{m}$ was identified as a reliable value, whereby thinner fibers can practically not be handled.

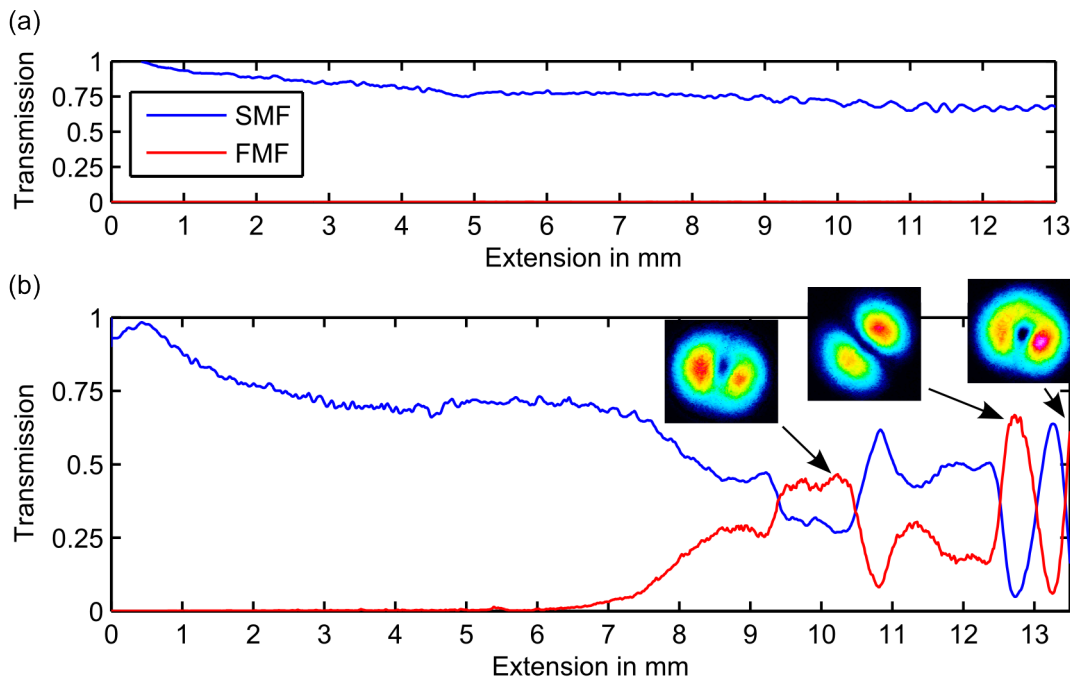


Figure 5.5: Experimentally measured transmission at a wavelength of 795 nm at the output of the SMF and FMF during the fabrication process for the non-pretapered case (a) and for the case that a PL of 3.5 mm is applied to the SMF (b). The insets in (b) are showing the output intensity pattern of the FMF at the indicated extension.

In Fig. 5.5 the experimentally recorded pulling signatures at the output of the SMF and FMF, both having a cladding diameter of $(40 \pm 5) \mu\text{m}$, are depicted. In the non-pretapered case (cf. Fig. 5.5(a)) no power is coupled to the FMF which is analogous to the case with non-etched fibers. When a PL of 3.5 mm was applied to the SMF (cf. Fig. 5.5(b)) a substantial increase of the maximum coupled power from the LP_{01} mode guided in the SMF to the LP_{11} mode in the FMF was observed. At the beginning of the pulling process a maximum at an extension ranging from 7 mm to 12 mm was detected with a transmitted power of maximal 45%. The intensity pattern shows a selective excitation of the LP_{11} mode. At an extension of 12.7 mm the transmission in the LP_{11} mode was 66%. Considering the overall losses at the beginning of the tapering process in the order

of 30 %, this corresponds quasi to the complete remaining power. At this extension the initially launched LP_{01} mode is nearly completely converted into the LP_{11} mode. A further coupling cycle was detected at 13.5 mm extension showing a more annular mode rather than a two-lobed LP_{11} mode. Due to the fact that a circular-core FMF was used, mode coupling between the 90° -rotated versions of the LP_{11} modes can occur [Yer14]. The ring-shaped intensity patterns in Fig. 5.5(b) indicate this coupling behavior.

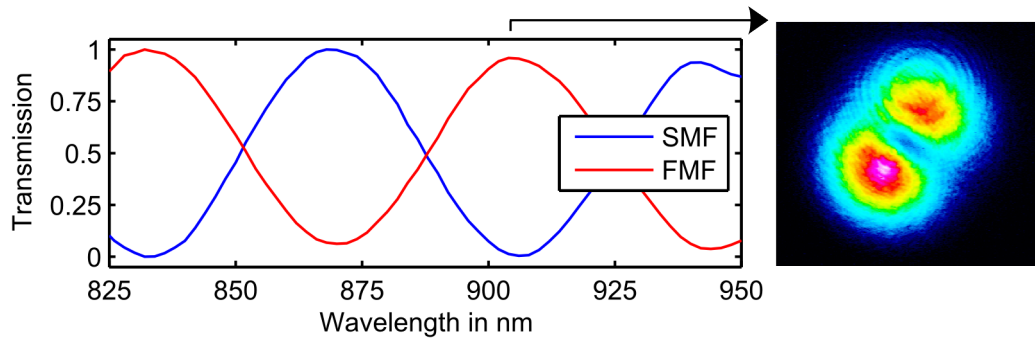


Figure 5.6: Wavelength dependence of the fabricated MSFC. The data points were normalized to the overall transmitted power. At a wavelength of 905 nm 80 % of the injected power was transmitted in the FMF. The output intensity pattern indicate the excitation of an LP_{11} mode.

The pulling process was stopped at an extension of 13.55 mm for further packaging of the MSFC. Upon completion of the pulling process the coupling ratio changed, so that 60 % of the overall transmitted power was in the FMF and 40 % in the SMF. Therefore this MSFC is not suitable for an efficient LP_{11} -excitation at a wavelength of 795 nm. The spectral characteristics of this MSFC were measured with an optical fiber analysis system (Photon Kinetics 2500) and the results are shown in Fig. 5.6. The transmission is maximal in the FMF at wavelengths of 832 nm and 905 nm. The selective LP_{11} -excitation was verified at a wavelength of 905 nm (cf. intensity pattern in Fig. 5.6) and it was measured that 80 % of the injected power was transmitted in the FMF.

In conclusion, the reduction of the cladding diameter and the application of an adequate pretaper substantially increase the power transfer and enables the selective excitation of, for example, the LP_{11} mode. The impact of pretapering is analogous to the impact discussed in Chapter 4 and it enables the power transfer between both fibers. However, the choice of the fiber to pretaper defines which mode is excited. By pretapering the FMF or signal fiber the fundamental LP_{01} mode is excited (cf. Chapter 4) and by pretapering the SMF or pump fiber the LP_{11} mode is excited in the FMF (cf. Chapter 5). Only by pretapering it is not possible to achieve a complete power transfer and a defined HOM excitation. Reducing the cladding diameter of the fibers to $(40 \pm 5) \mu\text{m}$ further increases the power transfer and allows for a selective excitation of the LP_{11} mode.

5.2.2 Discussion of the Loss Mechanisms

The pulling signatures in Fig. 5.5 show in both cases, non-pretapered and pretapered, that at the beginning of the tapering process a part of the launched power is irrecoverably lost. It was measured that the power transmitted in the SMF decreases during the pulling process to less than 75 %, although no power is coupled to the FMF. This loss during the pulling process was observed in several of the performed experiments with etched fibers, but not in the experiments with unetched fibers. Therefore, it is assumed that the loss might be attributed to fiber damage during the etching process [Zho13], microbends [Mar84], core dopant diffusion [McL88] or a combination of these loss mechanisms.

The general quality of the etched fibers was verified with SEM images to be good and only fibers without visible damage were used for the performed experiments (cf. Fig. 5.2(a)-(c)). Nevertheless, it cannot be excluded that fiber damage introduced by the etching process leads to losses during the fabrication. In addition, microscopic bends [Mar84] of the fibers can occur during the fusion process leading to bending losses. These microbending losses get pronounced in etched fibers, because they are very thin and more susceptible to deformations.

Another source of losses can be the diffusion of core dopants due to the application of a high temperature and axial tension which reduces the core-cladding index difference and increases the core diameter [McL88; Sho99]. Pickett et al. [Pic88] identified this effect as loss mechanism which occurs in the fabrication of tapered fibers due to nonadiabatic transitions of the core-guided mode at the input and output sections of the fiber taper. The transition must be adiabatic in order to prevent uncontrollable mode coupling to higher-order cladding modes and to be low loss. It was tried to minimize the influence of this effect by running the tapering process at the lowest possible temperature. However, temperature change also affects the resulting DOF which is why the reduction of the temperature is limited. In addition the DOF directly influences the coupling behavior as discussed in the following.

5.2.3 Impact of the Degree of Fusion

The non-pretapered MSFC realized for Fig. 5.5(a) was pulled up to an extension of 13.7 mm, cleaved at the taper waist and examined under an optical microscope, measuring a DOF of 1.75. For the pulling signature in Fig. 5.5(b) no information about the DOF is available, since the coupler was housed for further characterization. Based on experiments with the same parameters the DOF was estimated to be in the order of (1.70 ± 0.05) and therefore well-fused.

In order to evaluate the influence of the DOF on the coupling behavior, the pulling signature of a weakly-fused MSFC with a DOF of 1.98 was recorded and is depicted in

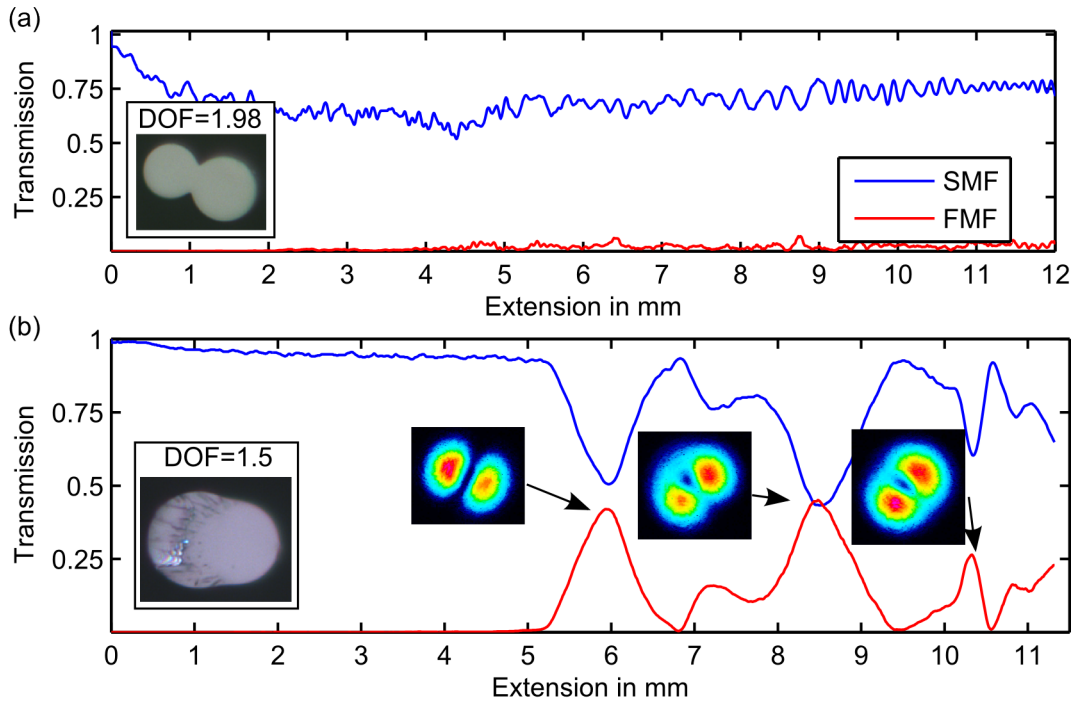


Figure 5.7: Experimentally measured transmission at a wavelength of 795 nm at the output of the SMF and FMF during the fabrication process for a PL of 3 mm with a DOF of 1.98 (a) and for a PL of 3.5 mm and a DOF of 1.5 (b). The insets show a photograph of the cleaved taper waist. The insets in (b) show the intensity pattern at the FMF end at the indicated extension.

Fig. 5.7(a). No coupling was detected in the weakly-fused case in comparison to the MSFC with a DOF of (1.70 ± 0.05) and nearly the same PL (cf. Fig. 5.5(b)). The applied PL on the SMF was 3 mm for the MSFC shown in Fig. 5.7(a) and 3.5 mm for the MSFC shown in Fig. 5.5(b). Therefore the applied PL is not exactly equal, but this difference in terms of the PL should have only a minor influence on the coupling behavior. In addition, a strongly-fused MSFC applying a PL of 3.5 mm was pulled with a DOF of 1.5 whose pulling signature is depicted in Fig. 5.7(b). In this case the LP_{11} mode could be selectively excited at extensions of 6 mm and 8.5 mm with more than 40% transmission. Compared to the pulling signature for the case with a DOF of (1.70 ± 0.05) (cf. Fig. 5.5(b)) this one is different in terms of transmission and extension of each coupling maximum. Although, for the fabrication of all MSFCs a quasi identical PL of 3.5 mm was applied to the SMF, the pulling signatures are remarkably different due to the varying DOF in the range between 1.98 and 1.5.

These results point out how sensitive the fabrication of MSFCs is to variations of the coupler geometry. Besides a cladding diameter reduction and an appropriate PL, also the

right choice of the DOF is crucial for an efficient excitation of HOMs. Ismael et al. [Ism14] discussed weakly-fused couplers based on inter-modally phase-matching the propagation constants in each arm of the asymmetric fused coupler. In the weakly-fused case both arms can be considered isolated and due to the small fused region the fields in both arms can overlap. As stated in [Ism14] a stronger fusion makes it more difficult to find the right phase matching condition in terms of the evanescent field coupling approach since both fibers become a combined structure and cannot be considered isolated. The pulling signature shown in Fig. 5.7(b) demonstrates that it is also possible to achieve the right conditions to selectively excite HOMs in strongly-fused MSFCs.

A modal analysis in terms of the SM coupling approach, as performed in Chapter 3 and 4, is used in the following to analyze the impact of the DOF on the coupling behavior in MSFCs. So far in literature this has only been analyzed by the evanescent field coupling approach which is restricted to the assumption of independent waveguides [Ism14; Lee05; Son02; Son03].

5.3 Numerical Characterization

In the previous Sec. 5.2 MSFCs were experimentally analyzed and the impact of cladding diameter reduction, pretapering and fusion was discussed. In order to execute the presented experiments, numerical studies were performed beforehand to obtain detailed information about the fabrication parameters.

Unetched Fibers

Therefore, the transmission in the FME, when light was launched into the SMF, was calculated depending on the PL of the SMF and the extension. First, standard cladding diameters of 125 μm for both fibers were assumed and the well-fused case with a DOF of 1.7 (cf. Fig. 5.8(a)) was considered.

In the non-pretapered case no power is coupled to the FME, but at a PL of 6 mm the maximal transmission is in the order of 40% in the FME (cf. Fig. 5.8(b)). However, the respective output beam profile at an extension of 11 mm seems to be a superposition of different LP modes. In addition, the sum of the transmission in the SMF and FME is not complete for the pulling process and therefore the insertion loss is quite high which could be attributed to the excitation of lossy higher-order cladding modes. These features correspond qualitatively to those observed in the experiments shown in Fig. 5.4.

Impact of the Degree of Fusion

In order to analyze the impact of the cladding diameter reduction, diameters of 45 μm for both fibers were assumed and the well-fused case with a DOF of 1.7 (cf. Fig. 5.9(a)-(b))

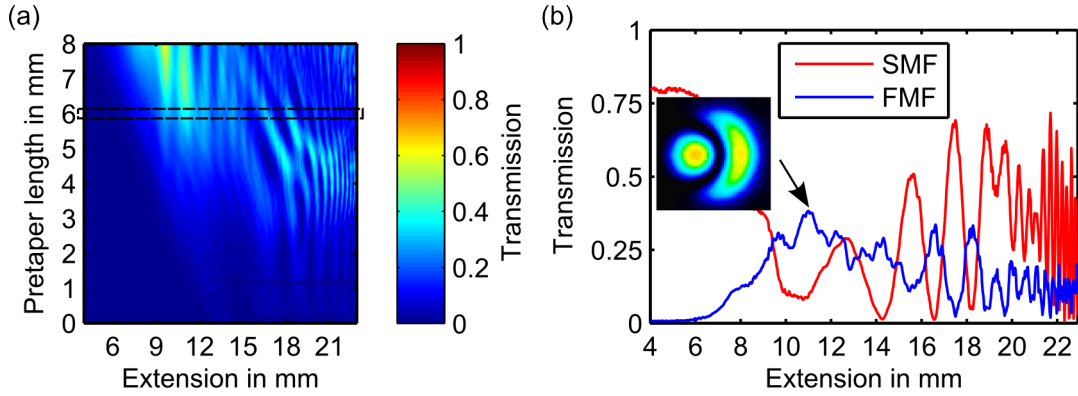


Figure 5.8: Simulated transmission in the FMF, when light was launched into the SMF, for cladding diameters of $125\ \mu\text{m}$ for both fibers. The well-fused case with a DOF of 1.7 is considered for varying PL (a) and the pulling signature at a PL of 6 mm with the output beam profile at an extension of 11 mm is depicted.

and the weakly-fused case with a DOF of 1.95 (cf. Fig. 5.9(c)-(d)) were chosen. In the non-pretapered case no power is coupled to the FMF no matter if the MSFC was well-fused or weakly-fused. By increasing the PL to values between 2 mm and 5 mm the maximum coupled power from the SMF to the FMF was substantially increased in the well-fused case. In Fig. 5.9(b) the pulling signature at a PL of 3.5 mm is depicted, demonstrating a complete power transfer and excitation of the LP_{11} mode at an extension of 10.6 mm. In the weakly-fused case the PL must be further increased to values between 4.5 mm and 5.5 mm in order to achieve a significant power transfer. The respective pulling signature at a PL of 5.37 mm is depicted in Fig. 5.9(d) and shows a transmission of 80 % in the FMF at an extension of 11.6 mm exciting the LP_{11} mode. In comparison to the well-fused case the coupling behavior is different with respect to the number and the position of the coupling cycles. Therefore, the optimal PL for achieving a complete power transfer and an LP_{11} -excitation depends sensitively on the DOF.

In conclusion, the simulations confirm qualitatively the experimentally observed impact of reduced cladding diameter, pretapering and the DOF on the transmission and the selective excitation of the LP_{11} mode. A comparison of the experimental (cf. Fig. 5.5 and 5.7) and simulation (cf. Fig. 5.9) results shows a qualitative agreement between both, since the essential features, as LP_{11} -excitation and maximum coupled power, are explained by the simulation. Although, the simulation does not account for the exact position, in terms of transmitted power and extension, of each coupling maximum. This is due to the simplified refractive index profile model for the simulation, which neglects the material conservation, and the fact that it is difficult to take all experimental parameters

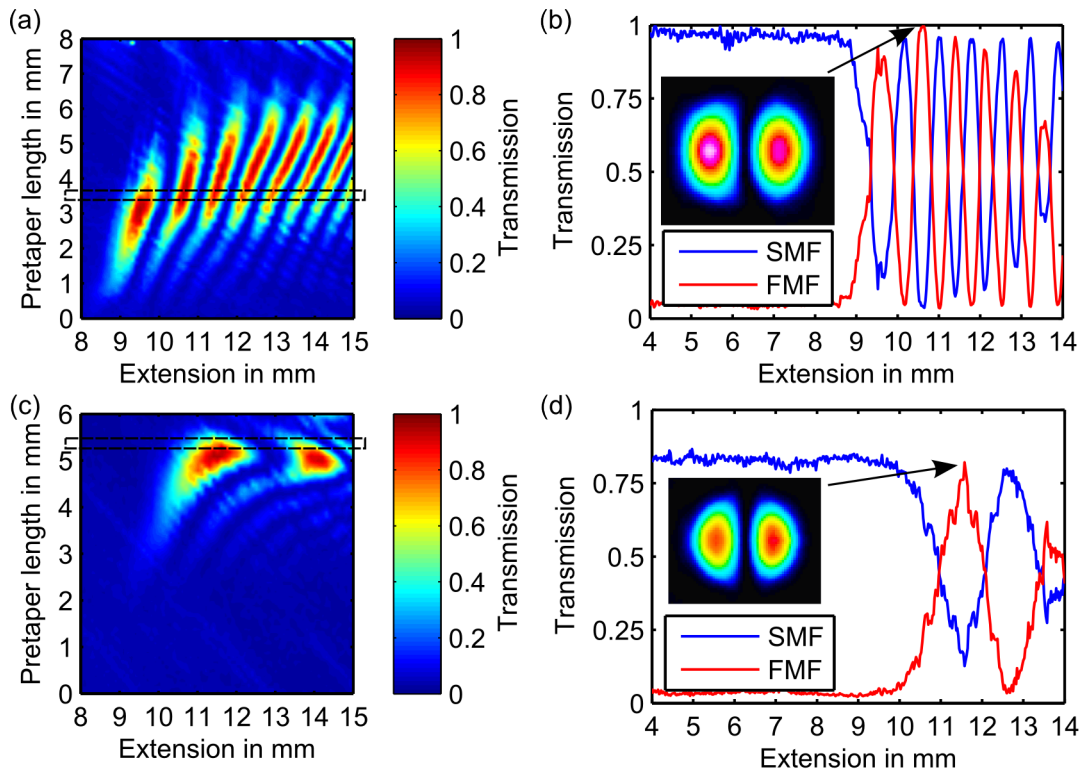


Figure 5.9: Simulated transmission in the FMF, when light was launched into the SMF, for cladding diameters of $45\ \mu\text{m}$ for both fibers. Well-fused case with a DOF of 1.7 (a) and weakly-fused case with a DOF of 1.95 (c). Pulling signatures at a PL of 3.5 mm in the well-fused case (b) and at a PL of 5.37 mm in the weakly-fused case (d) are depicted.

into account. The agreement is comparable to the agreement shown in Chapter 3 and 4 for symmetric and asymmetric FFCs.

5.4 Modal Analysis

In weakly-fused MSFCs both fibers can be considered isolated and due to the small fused region coupling between the fields in both fibers can occur. Ismaeel et al. [Isma14] discussed these types of MSFCs based on inter-modally phase-matching the propagation constants, but at the same time emphasizing the difficulty to find the right conditions in strongly-fused MSFCs in which both fibers cannot be considered as isolated. In order to understand the coupling behavior in well and strongly-fused MSFCs a modal analysis is performed in terms of the SM coupling approach.

First, the SMs of an MSFC at the beginning of the taper and the taper waist are calculated. Afterwards, it is investigated how the SMs evolve along the propagation in the taper in terms of their shape and n_{eff} for a well- and weakly-fused MSFC. On this basis, the modal composition in dependence of the cladding diameter and the DOF is analyzed.

5.4.1 Calculation of Super-Modes

Figure 5.10 shows the six lowest-order SMs at the beginning of the taper and the taper waist, defined by the respective propagation constant in descending order. The eigenmodes were calculated for an MSFC with the same parameters as used for Fig. 5.9(b) (PL of 3.5 mm and DOF of 1.7) and at an extension of 10.6 mm.

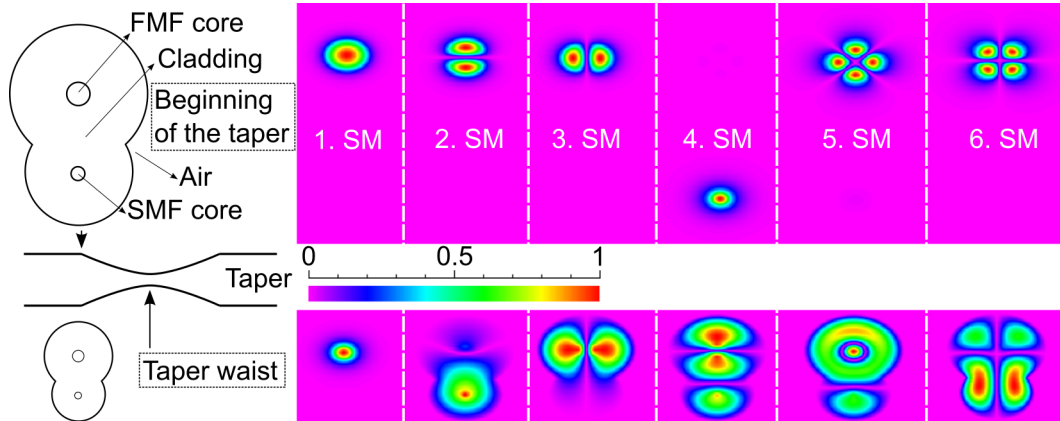


Figure 5.10: Intensity profiles of the six lowest-order SMs of the cross section at the beginning of the taper and the taper waist, defined by the respective propagation constant in descending order. The eigenmodes were calculated for an MSFC with the same parameters used in Fig. 5.9(b) (PL of 3.5 mm and DOF of 1.7) and at an extension of 10.6 mm.

At the beginning of the taper the first SM corresponds to the LP_{01} mode of the FMF and the second and third SMs are the two 90° -rotated versions of the LP_{11} mode. The fourth SM corresponds to the LP_{01} mode of the SMF. The fifth and sixth SMs correspond to the two 45° -rotated¹ versions of the LP_{21} mode of the FMF. The seventh SM (not shown here) corresponds to the LP_{02} mode guided in the FMF core and all further eigenmodes are cladding modes.

In symmetric fiber devices, as FFCs and photonic lanterns, light launched into one fiber core excites all SMs or in other words the guided core mode is a superposition of all SMs. The number of the excited SMs equals the number of the fiber cores [Leo10]. In the asymmetric case, where the cores have different radii and numerical apertures, the SMs at the beginning of the taper correspond to the respective core modes of the fibers. The number of the overall core guided modes depends on the V parameter of both cores. In this case the FMF core guides up to 6 different modes, whereby the LP_{11} and LP_{21} are represented by two different orientations. The SMF core guides only one mode, so that in total 7 SMs exist in this configuration. Light launched into the SMF only excites SMs with

1 The orthogonal orientation state of an LP_{lm} mode is obtained by rotation of $\frac{\pi}{2l}$ [Lov12a].

non-zero intensity in the SMF core which is here only fulfilled by the fourth SM. Since for an MSFC the idea is to achieve mode coupling, for example to the LP_{11} mode (respectively to the second SM), this mode has to be excited along the propagation in the MSFC.

As long as the SMs are core guided each of them can be easily assigned to an LP mode. Along the propagation to the taper waist the SMs consecutively evolve into cladding modes (except for the first SM in this case) which are remarkably different from the SMs at the beginning of the taper so that the corresponding LP_{lm} mode cannot be simply assigned (cf. Fig. 5.10). Therefore, the further discussion is based on the numeration, i. e. the fourth mode instead of LP_{01} mode in the SMF, as clarified in Fig. 5.10.

5.4.2 Evolution of the Super-Modes and their Effective Refractive Index

Well-Fused MSFCs

In the following the n_{eff} of the six lowest-order SMs along the propagation in the taper of a well-fused MSFC with a DOF of 1.7 are calculated (cf. Fig. 5.11(a)). The parameters of the MSFC are the same used for the calculation of the SMs in the previous Sec. 5.4.1.

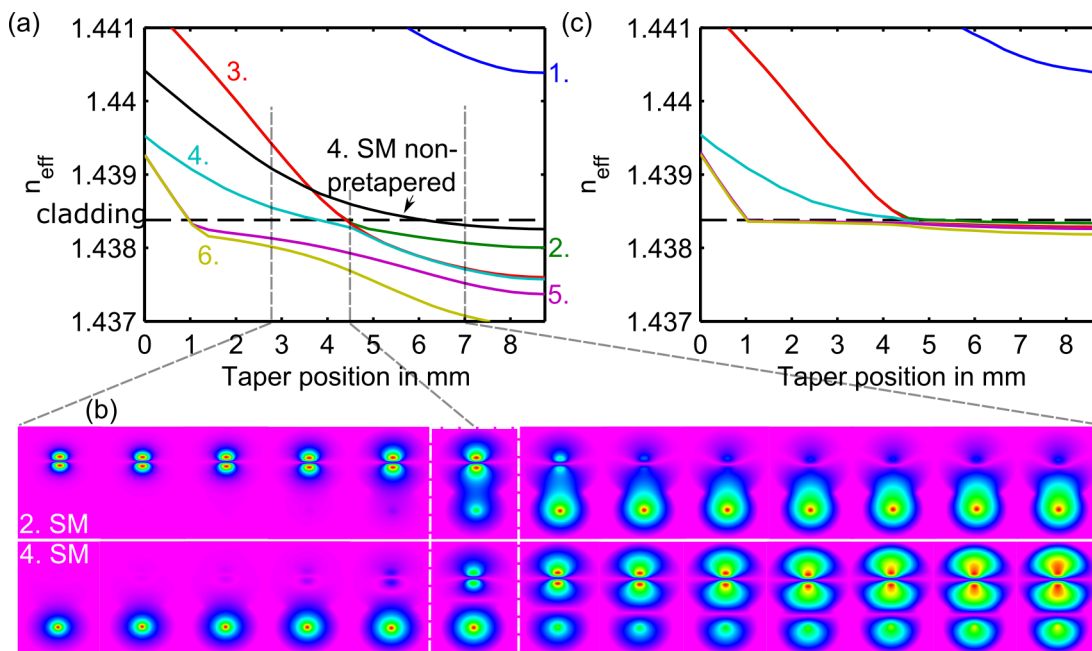


Figure 5.11: (a) Evolution of the n_{eff} and the intensity profiles of the n -th SM along the taper position for an MSFC with the same parameters used in Fig. 5.10 and (c) with a cladding diameter of $125 \mu\text{m}$. (b) Intensity profiles of the second and fourth SM at a taper position between 2.8 mm and 7 mm are depicted. The simulation cross section (in x and y dimension) for the eigenmode calculation (b) is consecutively rescaled for higher taper positions.

Since light is launched into the SMF, the fourth SM is excited at the beginning of the taper. At a taper position of 3.8 mm the n_{eff} of the fourth SM equals the cladding refractive

index which means that the SM is not guided anymore in the core and becomes a cladding mode. With further progression the n_{eff} approaches the n_{eff} curves of the 90°-rotated versions of the LP₁₁ mode (2. and 3. SM) at a taper position of 4.5 mm. If the n_{eff} of the SM cross or interact with each other during the taper transition, mode coupling between the respective SMs can occur [Leo14]. Or in other words, coupling is more likely between modes that are close in n_{eff} [Bir15; Lov91].

Therefore, in the pretapered-case mode coupling between the fourth SM and the LP₁₁ mode set, which correspond to the second and third SM, can occur if both SMs spatially overlap to a high degree. At this position the LP₁₁ mode set becomes non-degenerated, because both SMs evolve into cladding modes of a non-circular refractive index profile. Figure 5.11(b) shows the evolution of the second and fourth SM at a taper position between 2.8 mm and 7 mm. At the taper position of 4.5 mm where the n_{eff} curves are closest to each other, both SMs expand into the whole cladding. The second and fourth SM show visually a high degree of mode overlap. Both SMs seem to be a combination of the LP₁₁ mode located at the FMF and the LP₀₁ mode located at the SMF.

In Fig. 5.11(a) the n_{eff} curve of the fourth SM in the non-pretapered case is also depicted¹. In this case the fourth SM breaks out of the core at a higher value of the taper position of 6.1 mm and the n_{eff} curve does not approach any other n_{eff} curve of a higher-order SM after the core-cladding transition. At a taper position of 3.7 mm the n_{eff} curve crosses the n_{eff} curves of the LP₁₁ mode set and becomes the second SM. Note, that at this intersection the LP₀₁ mode in the SMF is core guided and that a power transfer to the FMF can take place only due to evanescent field coupling. For this, the cores have to be in near proximity which is apparently not the case, since no coupling occurs (cf. Fig. 5.5(a)).

The fact that the fourth SM becomes the second SM seems to be contradictory, since it is well known from the field of photonic lanterns (cf. Sec. 2.3.2) (and in the down-taper part an FFC is effectively a two-fiber photonic lantern), that the n-th SM evolves into the n-th SM in the taper waist as long as the transition is adiabatic [Leo14]. However in this case, the involved SMF (V parameter = 1.80) and FMF (V parameter = 4.37) are more different in terms of V parameter than typically mode-selective photonic lanterns are, as e. g. investigated by Leon-Saval et al. [Leo14]. Due to the large difference of the V parameter the propagation constants of the SMs cross or interact with each other during the transition so that mode coupling could theoretically occur.

¹ The impact of pretapering the SMF on the SMs guided by the FMF is negligible compared to the impact on the fourth SM. This is because pretapering the SMF affects mainly the SMs guided in the SMF core. Vice versa, pretapering the FMF would affect mainly the SMs guided in the FMF core. Therefore, it is reasonable to depict the n_{eff} curve of the fourth SM for the pretapered and non-pretapered case together with the n_{eff} curves of the remaining SMs of the pretapered case.

As a reminder, in Chapter 4 the fiber designed for guiding the longer wavelength was pretapered in order to couple the LP_{01} modes in both fibers. Figure 5.11(a) also illustrates qualitatively why in this case it is necessary to pretaper the SMF or the fiber designed for guiding the shorter wavelength. Due to pretapering it can be achieved that the initially excited SM breaks out of the core earlier and subsequently approaches the n_{eff} curves of the targeted SM; in this case the LP_{11} mode which corresponds to the second SM. In general, by pretapering the SMF the n_{eff} curves of the SMs guided in the SMF are shifted to lower taper positions, whereby the curves of the SMs guided in the FMF are fixed. Vice versa, by pretapering the FMF the n_{eff} curves of the SMs guided in the FMF are shifted to lower taper positions, whereby the curves of the SMs guided in the SMF are fixed. Further pretapering of the SMF could therefore result in the excitation of SMs having a higher order, but is practically limited by the mechanical handling of a strongly pretapered fiber. Alternatively, an FMF with a higher V parameter could be used which would shift the n_{eff} curves of the HOMs to higher values of the taper position while the n_{eff} curves of the SMs guided in the SMF remain at their position. By this, the practically inconvenient strong pretapering of the SMF could be avoided.

These findings are valid for arbitrary wavelengths and can be easily transferred to telecommunication wavelengths. However, the progression of the n_{eff} curves changes according to the considered wavelength. For higher wavelengths the n_{eff} curves shift to lower taper positions because the SMs break out of the core at lower taper positions and also the progression itself changes due to the modified cladding diameter in the cladding guided region. The limit for increasing the wavelength is given by the guidance of the fundamental mode in the SMF and the LP_{11} mode in the FMF. The behavior for shorter wavelengths is considered, respectively.

In addition to an adequate choice of the PL, it is necessary for the fabrication of MSFCs to reduce the cladding diameter of typical fibers with 125 μm cladding diameter for example by etching which was experimentally shown in Sec. 5.2. The evolution of the n_{eff} along the taper position for fibers with a 125 μm cladding diameter is depicted in Fig. 5.11(c). In comparison to the case with 45 μm cladding diameter all n_{eff} curves overlap after the core-cladding transition which results in strong coupling between all these SMs making it impossible to selectively excite one of them. A reduction of the cladding diameter enhances the impact of the refractive index of the surrounding material (in this case air) and therefore the n_{eff} curves split up allowing a selective excitation of the desired SM.

Weakly-Fused MSFCs

Besides the cladding diameter reduction and the applied PL the DOF has an immense impact on the characteristics of MSFCs. Therefore, fusion and pretaper must be well-matched in order to achieve an HOM excitation. In the following the modal evolution in a weakly-fused MSFC with a DOF of 1.95 is analyzed. In Fig. 5.12 the evolution of the n_{eff} is depicted with the same PL as in the well-fused case (cf. Fig. 5.11) and at a modified PL of 5.37 mm as obtained from the simulations shown in Fig. 5.9(c)-(d).

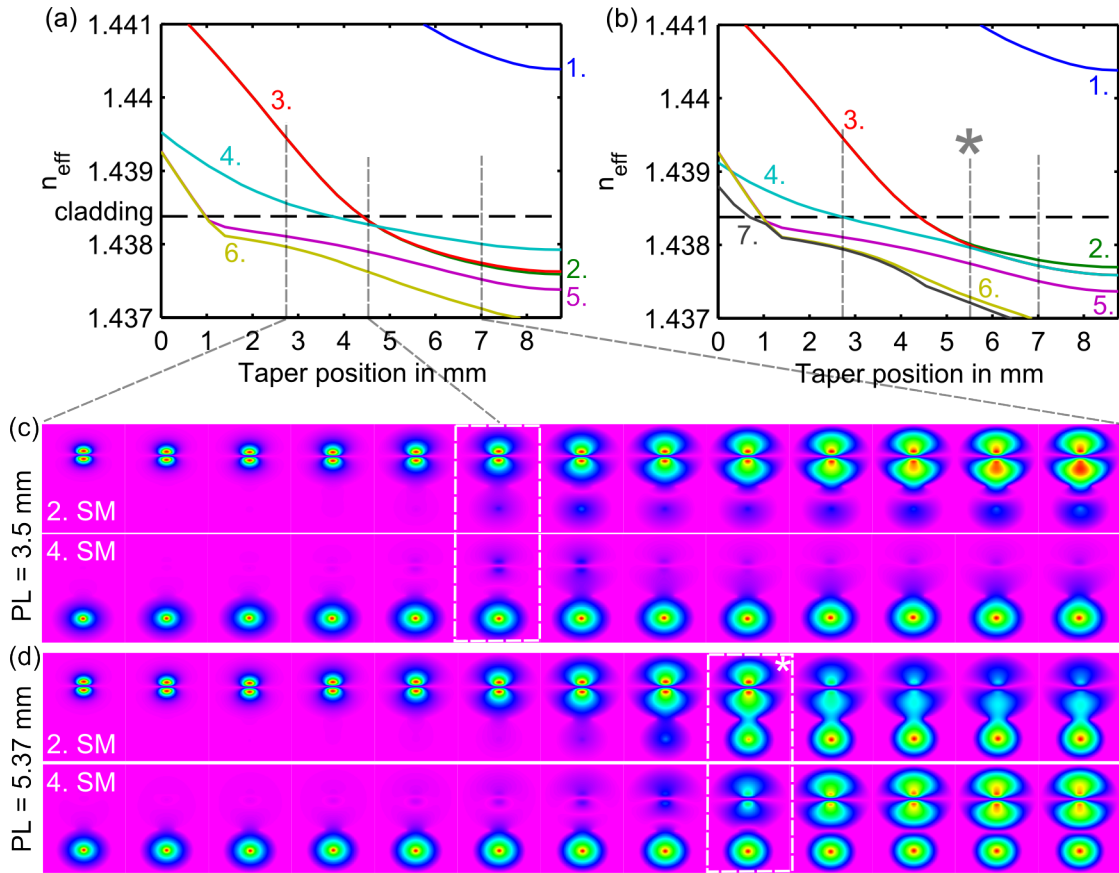


Figure 5.12: Evolution of the n_{eff} and the intensity profiles of the n -th SM along the taper position for an MSFC with a DOF of 1.95 and a PL of (a) 3.5 mm and (b) 5.37 mm and otherwise with the same parameters used in Fig. 5.10. Intensity profiles of the second and fourth SM along the propagation in the MSFC for a PL of 3.5 mm (c) and 5.37 mm (d) are depicted. The simulation cross section (in x and y dimension) for the eigenmode calculation (c)-(d) is consecutively rescaled for higher taper positions.

The trend of the n_{eff} curves in Fig. 5.12(a) is similar to the well-fused case, although the fourth SM shows the same behavior as the n_{eff} curve of the non-pretapered case in Fig. 5.11(a). The n_{eff} curve of the initially fourth SM becomes the second SM and intersects

the n_{eff} curves of the LP₁₁ mode set at a position of 4.5 mm, but no coupling occurs at this taper position, as can be seen from low transmission values in Fig. 5.9(c). The evolution of the second and fourth SM is depicted in Fig. 5.12(c) and reveals that along the taper the respective SMs remain localized in the fiber where they were initially excited. Therefore, the chosen PL of 3.5 mm seems to be inappropriate for this DOF, although the n_{eff} curves of the fourth and second SM intersect with each other.

A change of the PL to 5.37 mm leads to the fact that the fourth SM breaks out of the core at a lower taper position of 2.8 mm (cf. Fig. 5.12(b)). The fourth SM and the LP₁₁-corresponding mode set approach each other at a taper position of 5.6 mm. In contrast to the case with a PL of 3.5 mm the LP₁₁ mode set becomes non-degenerated at this position. The evolution of the second and fourth SM, shown in Fig. 5.12(d), demonstrates that at this position both SMs expand into the whole cladding and show visually a high degree of mode overlap. Therefore, light launched into the SMF should excite both SMs at this position. This is further investigated quantitatively in the following by modal decomposition.

5.4.3 Modal Decomposition

The considerations concerning the n_{eff} curves of MSFCs are valuable to qualitatively discuss the excitation of the SMs and the coupling between them. Although, they cannot definitely reveal if a SM is excited or not, e.g. at the taper positions where the n_{eff} curves of the SMs approach. Therefore, a modal decomposition of the simulated light field in different MSFCs is performed. MSFCs with standard 125 μm diameter fibers are considered and compared to the case with reduced cladding diameter.

Well-fused MSFCs with 125 μm Diameter Fibers

As discussed in Sec. 5.2 and 5.3 MSFCs made from standard 125 μm diameter fibers suffer from low transmission in the FMF and no selective HOM excitation. A modal decomposition was performed for a well-fused MSFC with the same parameters used in Fig. 5.8 (DOF=1.7, extension=11 mm, PL=6 mm) and the results are shown in Fig. 5.13. The modal weights of 10 calculated SMs are depicted, whereby the order of the SMs is not allocated due to the fact that the order changes multiple times along the propagation¹. This circumstance is pronounced in the case of standard 125 μm fibers since the n_{eff} values of the SMs are close to each other. Nevertheless, it becomes clear from Fig. 5.13(a) that

¹ In addition to the fact that the order of the SMs changes multiple times along the propagation in the MSFC, BeamPROP does not calculate the eigenmodes according to their order. This complicates the calculation of the modal excitation.

multiple SMs become excited along the propagation. At the beginning of the taper only the fundamental mode of the SMF is excited. After that in the down-taper mainly three SMs are excited in the central part of the MSFC and in the up-taper part even more SMs are excited. The excitation of several SMs is also illustrated in Fig. 5.13(b) where the light propagation is depicted. Especially in the up-taper part of the MSFC an interference pattern in the FMF core demonstrates the beating of several SMs. Therefore, in MSFC with 125 μm diameter fibers no selective HOM excitation occurs since several SMs are excited along the propagation.

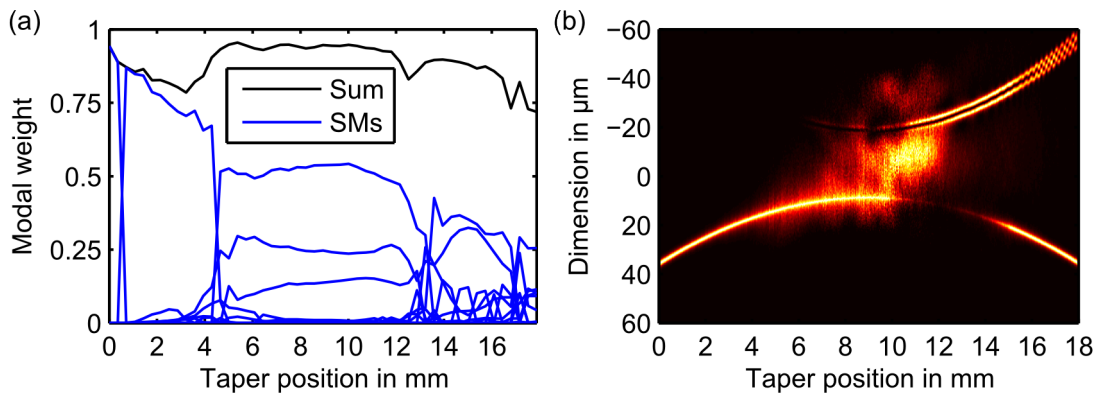


Figure 5.13: Modal excitation (a) and light propagation (b) along a well-fused (DOF=1.7) MSFC with an extension of 11 mm, a PL of 6 mm and cladding diameter of 125 μm . The light was launched into the SMF (bottom).

Well-Fused MSFCs with 45 μm Diameter Fibers

The selective HOM excitation is achieved by reducing the fiber cladding to diameters in the order of 45 μm . In Fig. 5.14(a) the modal excitation along the well-fused MSFC with the same parameters (PL=3.5 mm, DOF=1.7) used in Fig. 5.10 and 5.11 is depicted. At the beginning of the taper up to a taper position of 4 mm only the fourth SM is excited, since the light was launched into the SMF exciting the LP₀₁ mode in the SMF. At a taper position of 4 mm the modal weight changes up to the point at 4.6 mm where the second and fourth SM are equally excited. This zone corresponds to the part in Fig. 5.11(a) where the fourth SM breaks out of the core and the n_{eff} curves approach each other. On the up-taper part at a taper position of 13.6 mm the light is recaptured by the cores and mainly the LP₁₁-corresponding second SM persists excited. The corresponding light propagation is shown in Fig. 5.14(b) demonstrating the mode conversion from the LP₀₁ mode to the LP₁₁ mode and the beating between both SMs in the taper waist. At the cladding-core transition around a taper position of 13 mm the residual mode content has a maximum of approx. 25%. This was also observed at the modal decomposition of symmetric FFCs shown in Fig. 3.18 which was mainly attributed to numerical inaccuracies.

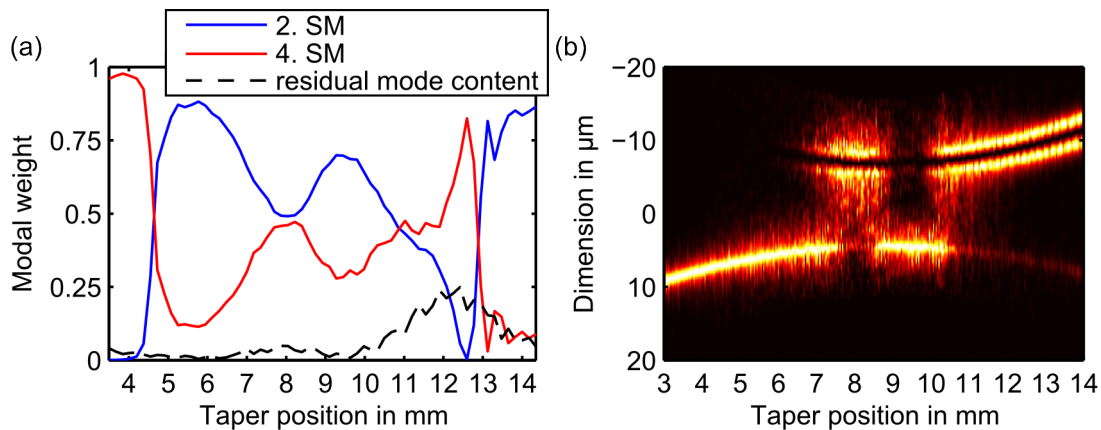


Figure 5.14: Modal excitation (a) and light propagation (b) along a well-fused (DOF=1.7) MSFC with an extension of 10.6 mm, a PL of 3.5 mm and cladding diameter of 45 μm . The light was launched into the SMF (bottom).

The modal weighting of the involved SMs in the central part of the coupler between 4.6 mm and 12.8 mm changes along the taper position. This is different to the behavior observed in asymmetric FFCs shown in Fig. 4.13 and 4.14 where the modal weights remain constant in the central part. The changing modal weights are due to the fact that the refractive index profile of an MSFC with a low coupling cycle number at short extensions is considered (cf. Fig. 5.9). Therefore, a modal decomposition in an MSFC at a higher extension at the fifth coupling cycle (PL=4.5 mm, extension=13.3 mm) was performed (cf. Fig. 5.15) which demonstrates that the modal weights remain constant in the central part of the MSFC. At the core-cladding and cladding-core transition of the SMs the modal weights change on a millimeter scale and between these points the modal weights remain constant. This constant section is only visible if refractive index profiles with several coupling cycles are considered.

The presented results show that due to adequate pretapering and fusion mode conversion from the LP_{01} mode to the LP_{11} mode is achieved. Theoretically, it is possible to operate the MSFC the other way around to convert an HOM into the fundamental LP_{01} mode. When the LP_{11} mode is launched into the FMF mode conversion to the LP_{01} mode also occurs for the presented configuration. This was verified by simulations and corresponds to the light propagation shown in Fig. 5.14(b) when light is launched into the FMF (top fiber, launched on the right). In order to experimentally verify the mode conversion from the LP_{11} mode to the LP_{01} mode it is necessary to reliably excite only the LP_{11} mode which is not easy feasible. It was tried to excite HOMs by butt-coupling an SMF and an FMF with slightly offset center positions. However, by this method it was not

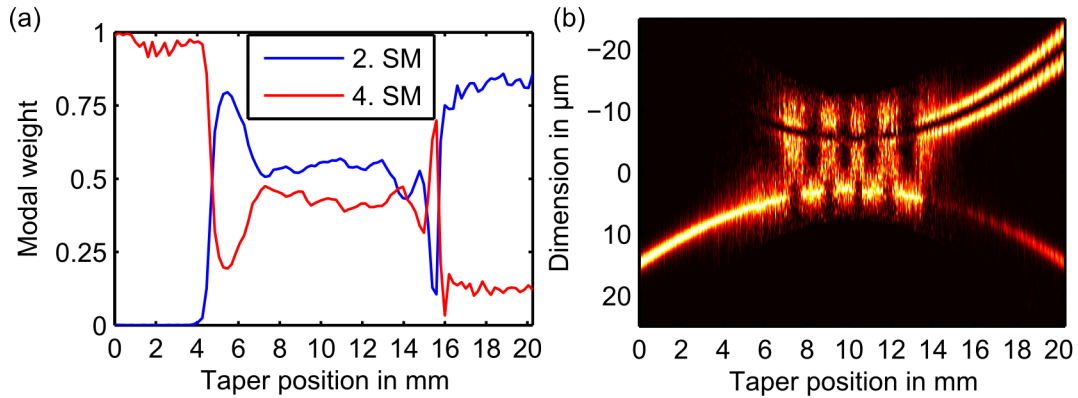


Figure 5.15: Modal excitation (a) and light propagation (b) along a well-fused (DOF=1.7) MSFC with an extension of 13.3 mm, a PL of 4.5 mm and cladding diameter of 45 μm . The light was launched into the SMF (bottom).

possible to generate solely the LP_{11} . The employment of a spatial light modulator which was not accessible could enable the LP_{11} mode excitation.

Weakly-Fused MSFCs with 45 μm Diameter Fibers

According to the previously discussed results DOF and PL must be well-matched in order to achieve a low-loss HOM-excitation. In Fig. 5.16(a) the modal excitation along the weakly-fused (DOF=1.95) MSFC with the same parameters used in Fig. 5.12(b) is depicted. Due to the application of a PL of 5.37 mm on the SMF an excitation of the LP_{11} mode can be achieved.

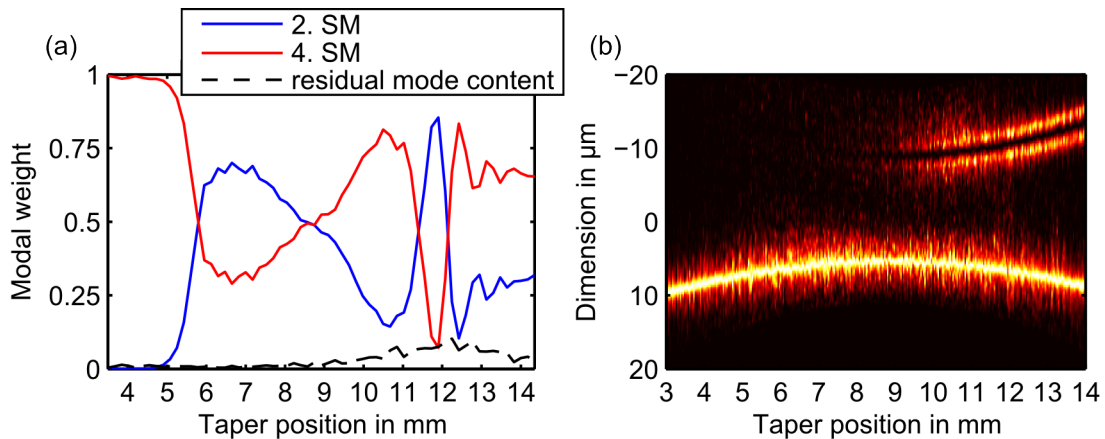


Figure 5.16: Modal excitation (a) and light propagation (b) along a weakly-fused (DOF=1.95) MSFC with an extension of 10.6 mm and a PL of 5.37 mm. The light was launched into the SMF (bottom).

From the beginning of the taper up to a taper position of 5 mm only the fourth SM is excited, since the light was launched into the SMF exciting the LP_{01} mode. According

to Fig. 5.12(b) the fourth SM breaks out of the core at a taper position of 2.8 mm, so that the fourth SM persists excited after the core-cladding transition. The modal weight does not change until the n_{eff} curves approach at a taper position of 5 mm. At this position the modal weight of both SMs is first equal and then oscillates up to a taper position of 12.6 mm where the modal weight remains constant. The LP_{11} mode in the FMF is recaptured by the core at a taper position of 13 mm and the LP_{01} mode in the SMF at a taper position of 14.8 mm. At the end of the taper the LP_{11} mode is excited with a ratio of 30 % which is also visible in the respective light propagation (cf. Fig. 5.16(b)). In this case no mode beating occurs, since it is the beginning of the first coupling cycle.

In conclusion, the performed modal decomposition reveals that the LP_{11} -corresponding SM is excited in the presented well-fused and weakly-fused MSFCs. At the taper position where the n_{eff} curves approach the modal weights of the corresponding SMs change dramatically and coupling between them occurs. At this position the involved SMs expand into the whole cladding showing mode overlap to a high degree. This is a direct result of the application of the correct amount of pretaper and fusion. Due to the cladding diameter reduction the amount of excited SMs is decreased enabling a selective excitation of the LP_{11} mode. Therefore, the simulation results confirm the experimental observation that the coupling behavior is very sensitive to variations of the refractive index profile, whereby all three parameters must be chosen adequately for the fabrication. The cladding diameter of the fibers can be measured exactly prior to the fabrication process and also the PL can be applied reliably. However, the DOF is difficult to control during the fabrication and cannot be simply adjusted, since it depends on the heat distribution in the crucible during the fusion process. Therefore, it is challenging to find the correct parameter set and to successfully apply it.

5.5 Conclusion

In this chapter fused-type MSFCs which selectively excite HOMs were experimentally and numerically analyzed. The fundamental coupling mechanisms were studied and a versatile model is presented to describe arbitrarily fused MSFCs. A concrete application for SDM was demonstrated by exciting the LP_{11} mode at wavelengths of 795 nm and 905 nm.

Experimental pulling signatures of different MSFCs were recorded to analyze the impact of the cladding diameter, the PL and the DOF on the transmission and the excitation of HOMs. MSFCs with standard cladding diameter of 125 μm were pulled which showed low transmission in the FMF and an undefined excitation of HOMs. Therefore, both

fibers were etched to a cladding diameter of 45 μm , in order to separate the n_{eff} of the SMs in the coupling region. An MSFC was successfully realized which showed a selective LP₁₁-excitation and a transmission of 80% in the FMF at a wavelength of 905 nm. This was achieved by defined tuning of the coupler geometry in terms of cladding diameter reduction, adequate pretapering and fusion. It was shown that the DOF has a major impact on the coupling behavior and as a consequence the applied PL on the SMF has to be adapted. The recorded pulling signatures reveal that it is possible to achieve the right conditions to selectively excite HOMs even in strongly-fused MSFCs.

Numerical simulations were performed to estimate fabrication parameters and to discuss the impact of variations in the coupler geometry. Simulations of MSFCs with standard fibers of 125 μm diameter reveal that the transmission in the FMF is low and the corresponding output beam profile does not correspond to an LP₁₁ mode. Therefore, simulations were performed with reduced fiber diameters of 45 μm . For specific values of the PL and the DOF the simulations demonstrate that a high transmission in the FMF with simultaneous LP₁₁-excitation can be achieved. The simulations confirm qualitatively the experimentally observed impact of reduced cladding diameter, pretapering and the DOF on the transmission and the selective excitation of the LP₁₁ mode.

In order to understand the coupling mechanisms in MSFCs a modal analysis is performed by analyzing the n_{eff} and the SMs of the whole cladding structure. The evolution of the SMs along the propagation in the taper showed that it can be achieved by adequate pretapering and appropriate fusion that the n_{eff} curves of the initially excited SM and the targeted SM approach once the SMs become cladding modes of the tapered structure enabling coupling between them. In the presented case of an SDM application the fundamental mode in the SMF and the LP₁₁-corresponding SM in the FMF expand into the whole cross section showing mode overlap to a high degree which is achieved by pretapering the fiber with the lower V parameter. The properties of the SMs in terms of n_{eff} and shape are determined by the refractive index profile which in turn is defined by the cladding diameter, the PL and the DOF.

An in-depth analysis of the modal composition of the simulated light was carried out in order to reveal if a specific SM is excited or not at the taper position where the n_{eff} curves approach. It is shown that in MSFCs made from standard fibers with 125 μm cladding diameter several SMs are excited along the propagation inhibiting the selective excitation of the LP₁₁ mode. By reducing the cladding to diameters in the order of 45 μm selective mode conversion from the LP₀₁ mode to the LP₁₁ mode is achieved. The mode conversion is initiated at the taper position where the n_{eff} curves approach and the shape of the SMs overlap. The performed modal decomposition reveals that the LP₁₁-corresponding SM is excited along the propagation in the presented MSFCs.

CHAPTER 6

Summary and Outlook

Fiber-based multiplexing devices consisting of different types of fibers are widely used in the field of fiber optics to exploit new functionalities. This includes, among others, devices consisting of N fibers which are fused together and pulled in order to enable coupling of light from one or several input fibers to one or several output fibers. These asymmetric fused fiber couplers (FFCs) are commonly described in terms of the coupled mode theory or in terms of eigenmodes (also called super-modes (SMs)). However, the description based on the coupled mode theory is limited to the assumption of independent waveguides whereas the description based on SMs allows for the modeling of FFCs in general. The aim of this work was to analyze arbitrarily fused asymmetric 2×2 FFCs including the experimental tuning of the coupler characteristics by changing the degree of dissimilarity between the fibers and the numerical modeling of the coupling mechanisms in terms of SMs.

To get a general idea of the coupling mechanisms in FFCs, symmetric devices were discussed both experimentally and numerically first. Therefore, a numerical model capable to describe the refractive index profile of such tapered fibers was elaborated in order to calculate the light propagation and the properties of the SMs. The essential features of the experimental characteristics are in agreement with the simulation, so that the modeling can be reliably employed to estimate process parameters and can be used to perform a complete analysis in terms of SMs. The evaluation of the coupling in symmetric FFCs reveals both the fact that in symmetric FFCs the number of excited SMs corresponds to the number of fiber cores and the fact that the symmetric and antisymmetric SM are equally excited along the whole longitudinal taper. Both findings are in agreement with the theory in literature which means that the established numerical analysis routines are suitable for discussing the coupling in FFCs in general. In the next step the analysis was extended

to asymmetric FFCs for wavelength-division multiplexing (WDM) and space-division multiplexing (SDM).

Asymmetric FFCs for increasing the range of combinable wavelengths in WDM applications were realized and discussed based on experiments and simulations at wavelengths of 633 nm and 1556 nm. Both wavelengths could be combined experimentally with an efficiency of 84 % for the signal light and 94 % for the pump light. This was achieved by systematically pretapering the fiber intended for guiding the signal light to a specific value. Therefore, it is shown that pretapering one fiber can be used to efficiently increase the maximum coupled power up to a complete power transfer from the original fiber to the target fiber. A concrete application of an FFC capable of combining two widely separated wavelengths in the range of 795 nm and 1980 nm was demonstrated which exhibits a transmission of 90 % for both wavelengths in the signal fiber. It was used in a core pumped thulium-doped fiber amplifier emitting at a wavelength of 2 μm [Pel12].

The simulation accounts for the general qualitative behavior of the FFC performance and it can give an estimation of the PL for further experimental optimization. The calculation of the SMs and their n_{eff} along the taper reveal that pretapering has a significant impact on the SMs of both wavelengths. By defined selection of the pretapered fiber and the applied PL, the n_{eff} curve of the symmetric SM and the antisymmetric SM can be approached in order to theoretically enable coupling between both. Therefore, pretapering the fiber designed for guiding the longer (signal) wavelength is necessary in order to tune the n_{eff} curve of the symmetric SM and to achieve coupling between the fundamental mode in the original fiber and the fundamental mode in the target fiber. However, the choice of the fiber to pretaper defines which SMs are excited, so that pretapering the fiber guiding the shorter (pump) wavelength is potentially interesting for exciting HOMs. An in-depth analysis of the modal composition of the simulated light field was carried out in order to determine the excitation of the SMs. It was shown that mode conversion in asymmetric FFCs takes place and that by pretapering the modal composition can be tuned in a way that the symmetric and antisymmetric SM are equally excited in the central part of the FFC enabling a complete power transfer [Pel14].

The capabilities of asymmetric FFCs were consecutively exploited for selectively coupling from the fundamental mode in an SMF to an HOM in an FMF. A fused-type MSFC was successfully realized which showed a selective excitation of the LP_{11} mode and a transmission of 80 % in the FMF at a wavelength of 905 nm. This was achieved by defined tuning of the coupler geometry in terms of cladding diameter reduction, adequate pretapering and fusion. Therefore, both fibers were etched to a cladding diameter of 45 μm , in

order separate the n_{eff} of the SMs in the coupling region. It was shown that the DOF has a major impact on the coupling behavior and as a consequence the applied PL on the SMF has to be adapted. The recorded pulling signatures reveal that it is possible to achieve the right conditions to selectively excite HOMs even in strongly-fused MSFCs which has not been reported so far [Ism14].

The process parameters were estimated by simulations of the MSFCs which also confirm qualitatively the experimentally observed impact of reduced cladding diameter, pretapering and the DOF on the transmission and the selective excitation of the LP₁₁ mode. The evolution of the SMs along the propagation in the taper showed that it can be achieved by adequate pretapering and appropriate fusion that the n_{eff} curves of the initially excited SM and the targeted SM approach once the SMs become cladding modes enabling coupling between them. An in-depth analysis of the modal composition revealed that in the presented case mode conversion from the fundamental mode in the SMF to the SM which corresponds to the LP₁₁ mode in the FMF occurs. The mode conversion is initiated at the taper position where the SMs expand into the whole cross section showing mode overlap to a high degree. The properties of the SMs in terms of n_{eff} and shape are determined by the geometric structure which in turn are defined by the refractive index profile, the PL and the DOF [Pel15].

All in all, the presented results show a general analysis of asymmetric FFCs in terms of SMs for the first time. The potential of asymmetric FFCs is exploited in order to achieve a combination of widely separated wavelengths and the selective excitation of an HOM which is of major interest for WDM and SDM. Due to the universal description of the coupling in terms of SMs, these findings significantly improve the understanding of asymmetric FFCs in general.

Outlook

Spatial multiplexing has a huge potential for avoiding the capacity crunch in telecommunication or for the use in fiber lasers and amplifiers for mode-selective filtering and amplification. Current devices for the application of SDM cover both fiber-based and waveguide-based approaches in order to realize spatial mode multiplexers and demultiplexers. As recently published in [Gro14] such waveguide-based devices include 3D tapered mode-selective couplers which were directly written by using a femtosecond laser writing into a photonic chip. These devices exhibit extremely efficient one-to-one mode mapping with an ultra-high bandwidth. However, fiber-based components, as MSFCs, feature a high degree of compatibility with existent fiber-based telecommunication and laser systems. In order to increase the applicability of MSFCs, as discussed in this work, the fabrication and characterization processes have to be improved in the future.

In the presented work, the experimental excitation of the LP_{11} mode was demonstrated. However, it was not investigated to selectively excite higher-order LP modes, as the LP_{21} or LP_{02} mode, although the theoretical considerations showed that mode conversion is possible by further tuning of the coupler geometry in terms of pretapering for example. Nevertheless, the mechanical handling of strongly pretapered and etched fibers is difficult and time-consuming so that the fabrication could be significantly facilitated by avoiding these process steps. Therefore, it would be necessary to have access to custom-designed fibers, instead of being restricted to commercial fibers with fixed fiber parameters. This way, it is for example possible to choose fibers with the appropriate V parameter in order to excite the corresponding LP_{lm} mode and to choose fibers with adequate cladding diameter to avoid etching. Furthermore, it would be desirable to implement an element for discriminating both rotation versions of an LP_{lm} mode. This could be realized for example by introducing an elliptical core enabling the selective access to both rotation versions.

In addition to improvements in terms of fabrication the characterization of the fabricated MSFCs has to be enhanced, too. In order to reliably fabricate MSFCs for different LP_{lm} modes the detection has to be modified in a way that also the modal content can be quantitatively measured, optimally during the fabrication process itself. Several modal decomposition techniques exist as for example S^2 imaging [Nic08], but they require time-consuming post-data processing or intense experimental measurements. Recently, a numerical technique for real-time modal decomposition was presented [Hua15b] which would enable the modal characterization during the fabrication process.

Bibliography

- [Ami11] A. A. AMIN, A. LI, S. CHEN, X. CHEN, G. GAO, and W. SHIEH: “Dual-LP₁₁ mode 4×4 MIMO-OFDM transmission over a two-mode fiber”. *Optics Express* (2011), vol. 19(17): pp. 16672–16679.
- [Bil88] F. BILODEAU, K. O. HILL, S. FAUCHER, and D. C. JOHNSON: “Low-loss highly overcoupled fused couplers: fabrication and sensitivity to external pressure”. *Journal of Lightwave Technology* (1988), vol. 6(10): pp. 1476–1482.
- [Bir88a] T. A. BIRKS: “Practical tuning mechanism for fused-tapered couplers”. *Optics Letters* (1988), vol. 13(12): pp. 1126–1128.
- [Bir89] T. A. BIRKS: “Twist-induced tuning in tapered fiber couplers”. *Applied Optics* (1989), vol. 28(19): pp. 4226–4233.
- [Bir95] T. A. BIRKS, D. O. CULVERHOUSE, S. G. FARWELL, and P. ST. J. RUSSELL: “All-fiber polarizer based on a null taper coupler”. *Optics Letters* (1995), vol. 20(12): pp. 1371–1373.
- [Bir15] T. A. BIRKS, I. GRIS-SÁNCHEZ, S. YEROLATSITIS, S. G. LEON-SAVAL, and R. R. THOMSON: “The photonic lantern”. *Adv. Opt. Photon.* (2015), vol. 7(2): pp. 107–167.
- [Bir88b] T. A. BIRKS and C. D. HUSSEY: “Control of power-splitting ratio in asymmetric fused-tapered single-mode fiber couplers”. *Optics Letters* (1988), vol. 13(8): pp. 681–683.
- [Bir92] T. A. BIRKS and Y. W. LI: “The shape of fiber tapers”. *Journal of Lightwave Technology* (1992), vol. 10(4): pp. 432–438.
- [Bir12] T. A. BIRKS, B. J. MANGAN, A. DÍEZ, J. L. CRUZ, and D. F. MURPHY: ““Photonic lantern” spectral filters in multi-core fiber”. *Optics Express* (2012), vol. 20(13): pp. 13996–14008.

- [Bla86] R. J. BLACK and R. BOURBONNAIS: "Core-mode cutoff for finite-cladding lightguides". *Optoelectronics, IEE Proceedings J* (1986), vol. 133(6): pp. 377–384.
- [Bla09] J. BLAND-HAWTHORN and P. KERN: "Astrophotonics: a new era for astronomical instruments". *Optics Express* (2009), vol. 17(3): pp. 1880–1884.
- [Bri85] T. BRICHENO and V. BAKER: "All-fibre polarisation splitter/combiner". *Electronics Letters* (1985), vol. 21(6): pp. 251–252.
- [Bri84] T. BRICHENO and A. FIELDING: "Stable low-loss single-mode couplers". *Electronics Letters* (1984), vol. 20(6): pp. 230–232.
- [Bur09] J. BURES: *Guided Optics*. Wiley-VCH, 2009.
- [Bur83] J. BURES, S. LACROIX, and J. LAPIERRE: "Analyse d'un coupleur bidirectionnel a fibres optiques monomodes fusionnees". *Applied Optics* (1983), vol. 22(12): pp. 1918–1822.
- [Bur87] W. K. BURNS and M. ABEBE: "Coupling model for fused fiber couplers with parabolic taper shape". *Applied Optics* (1987), vol. 26(19): pp. 4190–4192.
- [Bur85] W. K. BURNS, M. ABEBE, and C. A. VILLARRUEL: "Parabolic model for shape of fiber taper". *Applied Optics* (1985), vol. 24(17): pp. 2753–2755.
- [Cai15] S. CAI, S. YU, M. LAN, L. GAO, S. NIE, and W. GU: "Broadband Mode Converter Based on Photonic Crystal Fiber". *IEEE Photonics Technology Letters* (2015), vol. 27(5): pp. 474–477.
- [Cha14] S. H. CHANG, H. S. CHUNG, N. K. FONTAINE, R. RYF, K. J. PARK, K. K., J. C. LEE, J. H. LEE, B. Y. KIM, and Y. K. KIM: "Mode division multiplexed optical transmission enabled by all-fiber mode multiplexer". *Optics Express* (2014), vol. 22(12): pp. 14229–14236.
- [Cha15] S. H. CHANG, H. S. CHUNG, R. RYF, N. K. FONTAINE, C. HAN, K. J. PARK, K. KIM, J. C. LEE, J. H. LEE, B. Y. KIM, and Y. K. KIM: "Mode- and wavelength-division multiplexed transmission using all-fiber mode multiplexer based on mode selective couplers". *Optics Express* (2015), vol. 23(6): pp. 7164–7172.
- [Chi86] K. S. CHIANG: "Analysis of fused couplers by the effective-index method". *Electronics Letters* (1986), vol. 22(23): pp. 1221–1222.
- [Chi87] K. S. CHIANG: "Effects of cores in fused tapered single-mode fiber couplers". *Optics Letters* (1987), vol. 12(6): pp. 431–433.
- [Cis14] CISCO SYSTEMS, INC.: *The Zettabyte Era: Trends and Analysis*. White Paper. 2014.

- [Eis88] M. EISENMANN and E. WEIDEL: "Single-mode fused biconical couplers for wavelength division multiplexing with channel spacing between 100 and 300 nm". *Journal of Lightwave Technology* (1988), vol. 6(1): pp. 113–119.
- [Ess10] R. ESSIAMBRE, G. KRAMER, P. J. WINZER, G. J. FOSCHINI, and B. GOEBEL: "Capacity Limits of Optical Fiber Networks". *Journal of Lightwave Technology* (2010), vol. 28(4): pp. 662–701.
- [Ess12] R. ESSIAMBRE and R. W. TKACH: "Capacity Trends and Limits of Optical Communication Networks". *Proceedings of the IEEE* (2012), vol. 100(5): pp. 1035–1055.
- [Fon12] N. K. FONTAINE, R. RYF, J. BLAND-HAWTHORN, and S. G. LEON-SAVAL: "Geometric requirements for photonic lanterns in space division multiplexing". *Optics Express* (2012), vol. 20(24): pp. 27123–27132.
- [Gro14] S. GROSS, N. RIESEN, J. D. LOVE, and M. J. WITHFORD: "Three-dimensional ultra-broadband integrated tapered mode multiplexers". *Laser & Photonics Reviews* (2014), vol. 8(5): pp. L81–L85.
- [Han13] N. HANZAWA, K. SAITOH, T. SAKAMOTO, T. MATSUI, K. TSUJIKAWA, M. KOSHIBA, and F. YAMAMOTO: "Two-mode PLC-based mode multi/demultiplexer for mode and wavelength division multiplexed transmission". *Optics Express* (2013), vol. 21(22): pp. 25752–25760.
- [Han14] N. HANZAWA, K. SAITOH, T. SAKAMOTO, T. MATSUI, K. TSUJIKAWA, M. KOSHIBA, and F. YAMAMOTO: "Mode multi/demultiplexing with parallel waveguide for mode division multiplexed transmission". *Optics Express* (2014), vol. 22(24): pp. 29321–29330.
- [Hua15a] B. HUANG, N. K. FONTAINE, R. RYF, B. GUAN, S. G. LEON-SAVAL, R. SHUBOCHKIN, Y. SUN, R. LINGLE, and G. LI: "All-fiber mode-group-selective photonic lantern using graded-index multimode fibers". *Optics Express* (2015), vol. 23(1): pp. 224–234.
- [Hua15b] L. HUANG, S. GUO, J. LENG, H. LÜ, P. ZHOU, and X. CHENG: "Real-time mode decomposition for few-mode fiber based on numerical method". *Optics Express* (2015), vol. 23(4): pp. 4620–4629.
- [Iga15] K. IGARASHI, D. SOUMA, K. TAKESHIMA, and T. TSURITANI: "Selective mode multiplexer based on phase plates and Mach-Zehnder interferometer with image inversion function". *Optics Express* (2015), vol. 23(1): pp. 183–194.

- [Ism14] R. ISMAEEL, T. LEE, B. ODURO, Y. JUNG, and G. BRAMBILLA: "All-fiber fused directional coupler for highly efficient spatial mode conversion". *Optics Express* (2014), vol. 22(10): pp. 11610–11619.
- [Jac99] S. D. JACKSON and T. A. KING: "Theoretical modeling of Tm-doped silica fiber lasers". *Journal of Lightwave Technology* (1999), vol. 17(5): pp. 948–956.
- [Jun11] Y. JUNG, S. ALAM, Z. LI, A. DHAR, D. GILES, I. P. GILES, J. K. SAHU, F. POLETTI, L. GRÜNER-NIELSEN, and D. J. RICHARDSON: "First demonstration and detailed characterization of a multimode amplifier for space division multiplexed transmission systems". *Optics Express* (2011), vol. 19(26): B952–B957.
- [Jun13] Y. JUNG, R. CHEN, R. ISMAEEL, G. BRAMBILLA, S. U. ALAM, I. P. GILES, and D. J. RICHARDSON: "Dual mode fused optical fiber couplers suitable for mode division multiplexed transmission". *Optics Express* (2013), vol. 21(20): pp. 24326–24331.
- [Jun14] Y. JUNG, E. L. LIM, Q. KANG, T. C. MAY-SMITH, N. H. L. WONG, R. STANDISH, F. POLETTI, J. K. SAHU, S. U. ALAM, and D. J. RICHARDSON: "Cladding pumped few-mode EDFA for mode division multiplexed transmission". *Optics Express* (2014), vol. 22(23): pp. 29008–29013.
- [Kac87] P. KACZMARSKI, P. LAGASSE, and J. VANDEWEGE: "Propagating-beam model for a single-mode-fibre fused coupler". *Optoelectronics, IEE Proceedings J* (1987), vol. 134(2): pp. 111–116.
- [Kao66] K. C. KAO and G. A. HOCKHAM: "Dielectric-fibre surface waveguides for optical frequencies". *Proceedings of the Institution of Electrical Engineers* (1966), vol. 113(7): pp. 1151–1158.
- [Kaw81] B. S. KAWASAKI, K. O. HILL, and R. G. LAMONT: "Biconical-taper single-mode fiber coupler". *Optics Letters* (1981), vol. 6(7): pp. 327–328.
- [Kec73] D. B. KECK, R. D. MAURER, and P. C. SCHULTZ: "On the ultimate lower limit of attenuation in glass optical waveguides". *Applied Physics Letters* (1973), vol. 22(7): pp. 307–309.
- [Koe64] C. J. KOESTER and E. SNITZER: "Amplification in a Fiber Laser". *Applied Optics* (1964), vol. 3(10): pp. 1182–1186.
- [Lac94] S. LACROIX, F. GONTHIER, and J. BURES: "Modeling of symmetric 2×2 fused-fiber couplers". *Applied Optics* (1994), vol. 33(36): pp. 8361–8369.

- [Lai07] K. LAI, S. G. LEON-SAVAL, A. WITKOWSKA, W. J. WADSWORTH, and T. A. BIRKS: "Wavelength-independent all-fiber mode converters". *Optics Letters* (2007), vol. 32(4): pp. 328–330.
- [Lam85a] R. G. LAMONT, K. O. HILL, and D. C. JOHNSON: "Fabrication of fused twin biconical taper singlemode fiber splitters: effect of unequal cladding diameters". *Optical Fiber Communication*. Optical Society of America, 1985: TUQ22.
- [Lam85b] R. G. LAMONT, K. O. HILL, and D. C. JOHNSON: "Tuned-port twin biconical-taper fiber splitters: fabrication from dissimilar low-mode-number fibers". *Optics Letters* (1985), vol. 10(1): pp. 46–48.
- [Lee05] S. H. LEE, K. Y. SONG, and B. Y. KIM: "Fused bitapered single-mode fiber directional coupler for core and cladding mode coupling". *IEEE Photonics Technology Letters* (2005), vol. 17(12): pp. 2631–2633.
- [Leo10] S. G. LEON-SAVAL, A. ARGYROS, and J. BLAND-HAWTHORN: "Photonic lanterns: a study of light propagation in multimode to single-mode converters". *Optics Express* (2010), vol. 18(8): pp. 8430–8439.
- [Leo05] S. G. LEON-SAVAL, T. A. BIRKS, J. BLAND-HAWTHORN, and M. ENGLUND: "Multimode fiber devices with single-mode performance". *Optics Letters* (2005), vol. 30(19): pp. 2545–2547.
- [Leo14] S. G. LEON-SAVAL, N. K. FONTAINE, J. R. SALAZAR-GIL, B. ERCAN, R. RYF, and J. BLAND-HAWTHORN: "Mode-selective photonic lanterns for space-division multiplexing". *Optics Express* (2014), vol. 22(1): pp. 1036–1044.
- [Li12a] A. LI, X. CHEN, A. A. AMIN, and W. SHIEH: "Fused Fiber Mode Couplers for Few-Mode Transmission". *IEEE Photonics Technology Letters* (2012), vol. 24(21): pp. 1953–1956.
- [Li12b] A. LI, X. CHEN, A. A. AMIN, J. YE, and W. SHIEH: "Space-Division Multiplexed High-Speed Superchannel Transmission Over Few-Mode Fiber". *Journal of Lightwave Technology* (2012), vol. 30(24): pp. 3953–3964.
- [Li13] A. LI, J. YE, X. CHEN, and W. SHIEH: "Fabrication of a Low-Loss Fused Fiber Spatial-Mode Coupler for Few-Mode Transmission". *IEEE Photonics Technology Letters* (2013), vol. 25(20): pp. 1985–1988.

- [Li14] G. LI, N. BAI, N. ZHAO, and C. XIA: "Space-division multiplexing: the next frontier in optical communication". *Adv. Opt. Photon.* (2014), vol. 6(4): pp. 413–487.
- [Lov85] J. D. LOVE and M. HALL: "Polarisation modulation in long couplers". *Electronics Letters* (1985), vol. 21(12): pp. 519–521.
- [Lov86] J. D. LOVE and W. M. HENRY: "Quantifying loss minimisation in single-mode fibre tapers". *Electronics Letters* (1986), vol. 22(17): pp. 912–914.
- [Lov91] J. D. LOVE, W. M. HENRY, W. J. STEWART, R. J. BLACK, S. LACROIX, and F. GONTHIER: "Tapered single-mode fibres and devices. I. Adiabaticity criteria". *Optoelectronics, IEE Proceedings J* (1991), vol. 138(5): pp. 343–354.
- [Lov12a] J. D. LOVE and N. RIESEN: "Mode-selective couplers for few-mode optical fiber networks". *Optics Letters* (2012), vol. 37(19): pp. 3990–3992.
- [Lov12b] J. D. LOVE and N. RIESEN: "Single-, Few-, and Multimode Y-Junctions". *Journal of Lightwave Technology* (2012), vol. 30(3): pp. 304–309.
- [Mai60] T. H. MAIMAN: "Stimulated Optical Radiation in Ruby". *Nature* (1960), vol. 187(4736): pp. 493–494.
- [Mar84] D. MARCUSE: "Microdeformation losses of single-mode fibers". *Applied Optics* (1984), vol. 23(7): pp. 1082–1091.
- [Mat12] S. MATSUO, Y. SASAKI, T. AKAMATSU, I. ISHIDA, K. TAKENAGA, K. OKUYAMA, K. SAITOH, and M. KOSIHBABA: "12-core fiber with one ring structure for extremely large capacity transmission". *Optics Express* (2012), vol. 20(27): pp. 28398–28408.
- [McL88] M. N. MCLANDRICH: "Core dopant profiles in weakly fused single-mode fibres". *Electronics Letters* (1988), vol. 24(1): pp. 8–10.
- [Men06] A. MENDEZ and T. MORSE: *Specialty Optical Fibers Handbook*. Academic Press, 2006.
- [Mit05] F. MITSCHKE: *Glasfasern - Physik und Technologien*. Elsevier GmbH, 2005.
- [Mor85] D. B. MORTIMORE: "Wavelength-flattened fused couplers". *Electronics Letters* (1985), vol. 21(17): pp. 742–743.
- [Mor90a] D. B. MORTIMORE: "Theory and fabrication of 4×4 single-mode fused optical fiber couplers". *Applied Optics* (1990), vol. 29(3): pp. 371–374.

- [Mor90b] D. B. MORTIMORE and J. W. ARKWRIGHT: "Theory and fabrication of wavelength flattened $1 \times N$ single-mode couplers". *Applied Optics* (1990), vol. 29(12): pp. 1814–1818.
- [Nic08] J. W. NICHOLSON, A. D. YABLON, S. RAMACHANDRAN, and S. GHALMI: "Spatially and spectrally resolved imaging of modal content in large-mode-area fibers". *Optics Express* (2008), vol. 16(10): pp. 7233–7243.
- [Noo09] D. NOORDEGRAAF, P. M. SKOVGAARD, M. D. NIELSEN, and J. BLAND-HAWTHORN: "Efficient multi-mode to single-mode coupling in a photonic lantern". *Optics Express* (2009), vol. 17(3): pp. 1988–1994.
- [Nuf14a] NUFERN: *630-HP data sheet*. 2014. URL: http://www.nufern.com/pam/optical_fibers/882/630-HP/ (visited on 10/21/2014).
- [Nuf14b] NUFERN: *780-HP data sheet*. 2014. URL: http://www.nufern.com/pam/optical_fibers/883/780-HP/ (visited on 03/06/2014).
- [NVI12] NVIDIA CORPORATION: *NVIDIA CUDA Programming Guide Version 5.0*. 2012.
- [OFS14] OFS: *TmDF200 data sheet*. 2014. URL: <http://fiber-optic-catalog.ofsoptics.com/item/all-categories/tterbium-and-thulium-doped-fibers-for-fiber-lasers/tmdf200?&bc=100%7C1060> (visited on 05/11/2014).
- [Oka90] K. OKAMOTO: "Theoretical investigation of light coupling phenomena in wavelength-flattened couplers". *Journal of Lightwave Technology* (1990), vol. 8(5): pp. 678–683.
- [Oka06] K. OKAMOTO: *Fundamentals of Optical Waveguides*. Academic Press, 2006.
- [Opt08] SIFAM FIBER OPTICS: *Single-mode tapering rig manual*. 2008.
- [Ott15] C. OTTENHUES, T. THEEG, K. HAUSMANN, M. WYSMOLEK, H. SAYINC, J. NEUMANN, and D. KRACHT: "Single mode monolithic fiber laser with 200 W output power at a wavelength of 1018 nm". manuscript in preparation. 2015.
- [Pal03] B. PAL: "Fabrication and Modeling of Fused Biconical Tapered Fiber Couplers". *Fiber and Integrated Optics* (2003), vol. 22(2): pp. 97–117.
- [Pas08] R. PASCHOTTA: *Encyclopedia of Laser Physics and Technology*. Wiley-VCH, 2008.
- [Pau12] M. PAURISSE, L. LÉVÈQUE, M. HANNA, F. DRUON, and P. GEORGES: "Complete measurement of fiber modal content by wavefront analysis". *Optics Express* (2012), vol. 20(4): pp. 4074–4084.

- [Pay85a] F. P. PAYNE, C. D. HUSSEY, and M. S. YATAKI: "Modelling fused single-mode-fibre couplers". *Electronics Letters* (1985), vol. 21(11): pp. 461–462.
- [Pay85b] F. P. PAYNE, C. D. HUSSEY, and M. S. YATAKI: "Polarisation analysis of strongly fused and weakly fused tapered couplers". *Electronics Letters* (1985), vol. 21(13): pp. 561–563.
- [Pel12] G. PELEGRINA-BONILLA, K. HAUSMANN, K. LIU, H. SAYINC, U. MORGNER, J. NEUMANN, and D. KRACHT: "Matching of the propagation constants in an asymmetric single-mode fused fiber coupler for core pumping thulium-doped fiber at 795 nm". *Optics Letters* (2012), vol. 37(11): pp. 1844–1846.
- [Pel15] G. PELEGRINA-BONILLA, K. HAUSMANN, H. SAYINC, U. MORGNER, J. NEUMANN, and D. KRACHT: "Analysis of the modal evolution in fused-type mode-selective fiber couplers". *Optics Express* (2015), vol. 23(18): pp. 22977–22990.
- [Pel14] G. PELEGRINA-BONILLA, K. HAUSMANN, H. TÜNNERMANN, P. WESSELS, H. SAYINC, U. MORGNER, J. NEUMANN, and D. KRACHT: "Analysis of the Coupling Mechanism in Asymmetric Fused Fiber Couplers". *Journal of Lightwave Technology* (2014), vol. 32(13): pp. 2382–2391.
- [Pic88] C. W. PICKETT, W. K. BURNS, and C. A. VILLARRUEL: "Dopant diffusion loss mechanism in high-birefringent-fiber fused couplers". *Optics Letters* (1988), vol. 13(10): pp. 835–837.
- [Pis13] M. PÍSAŘÍK, P. PETERKA, S. ZVÁNOVEC, Y. BARAVETS, F. TODOROV, I. KAŠÍK, and P. HONZÁTKO: "Fused fiber components for "eye-safe" spectral region around 2 μm ". *Optical and Quantum Electronics* (2013), vol. 46(4): pp. 603–611.
- [Pol14] M. N. POLYANSKIY: *Refractive index database*. 2014. URL: <http://refractiveindex.info> (visited on 09/04/2014).
- [Pon04a] E. PONE, X. DAXHELET, and S. LACROIX: "Refractive index profile of fused-fiber couplers cross-section". *Optics Express* (2004), vol. 12(6): pp. 1036–1044.
- [Pon04b] E. PONE, X. DAXHELET, and S. LACROIX: "Refractive index profile of fused-tapered fiber couplers". *Optics Express* (2004), vol. 12(13): pp. 2909–2918.
- [Qia12] D. QIAN, M. F. HUANG, E. IP, Y. K. HUANG, Y. SHAO, J. HU, and T. WANG: "High Capacity/Spectral Efficiency 101.7-Tb/s WDM Transmission Using PDM-128QAM-OFDM Over 165-km SSMF Within C- and L-Bands". *Journal of Lightwave Technology* (2012), vol. 30(10): pp. 1540–1548.

- [Rei97] G. A. REIDER: *Photonik - Eine Einführung in die Grundlagen*. Springer-Verlag, 1997.
- [Ric13] D. J. RICHARDSON, J. M. FINI, and L. E. NELSON: "Space-division multiplexing in optical fibres". *Nature Photonics* (2013), vol. 7(5): pp. 354–362.
- [Ric10] D. J. RICHARDSON, J. NILSSON, and W. A. CLARKSON: "High power fiber lasers: current status and future perspectives". *J. Opt. Soc. Am. B* (2010), vol. 27(11): B63–B92.
- [Rie14] N. RIESEN, S. GROSS, J. D. LOVE, and M. J. WITHFORD: "Femtosecond direct-written integrated mode couplers". *Optics Express* (2014), vol. 22(24): pp. 29855–29861.
- [Rie13] N. RIESEN and J. D. LOVE: "Tapered Velocity Mode-Selective Couplers". *Journal of Lightwave Technology* (2013), vol. 31(13): pp. 2163–2169.
- [RSo10] RSOFT DESIGN GROUP: *BeamPROP 8.2*. 2010.
- [Sal07] B. E. A. SALEH and M. C. TEICH: *Fundamentals of Photonics*. Wiley Series in Pure and Applied Optics, 2007.
- [Say13] H. SAYINC, G. PELEGRINA-BONILLA, and K. HAUSMANN: "Method for manufacturing a coupling arrangement, coupling arrangement and amplifier". EP2618192 A1. 2013.
- [Sca00] R. SCARMOZZINO, A. GOPINATH, R. PREGLA, and S. HELFERT: "Numerical techniques for modeling guided-wave photonic devices". *IEEE Journal of Selected Topics in Quantum Electronics* (2000), vol. 6(1): pp. 150–162.
- [Sho99] Y. SHOU, J. BURES, S. LACROIX, and X. DAXHELET: "Mode Separation in Fused Fiber Coupler Made of Two-Mode Fibers". *Optical Fiber Technology* (1999), vol. 5(1): pp. 92–104.
- [Sni61] E. SNITZER: "Proposed Fiber Cavities for Optical Masers". *Journal of Applied Physics* (1961), vol. 32(1): pp. 36–39.
- [Sny72] A. W. SNYDER: "Coupled-mode theory for optical fibers". *J. Opt. Soc. Am.* (1972), vol. 62(11): pp. 1267–1277.
- [Soh04] D. B. S. SOH, J. NILSSON, S. BAEK, C. CODEMARD, Y. JEONG, and V. PHILIPPOV: "Modal power decomposition of beam intensity profiles into linearly polarized modes of multimode optical fibers". *J. Opt. Soc. Am. A* (2004), vol. 21(7): pp. 1241–1250.

- [Son14] D. R. SONG, H. S. PARK, B. Y. KIM, and K. Y. SONG: "Acoustooptic Generation and Characterization of the Higher Order Modes in a Four-Mode Fiber for Mode-Division Multiplexed Transmission". *Journal of Lightwave Technology* (2014), vol. 32(23): pp. 3932–3936.
- [Son00] K. Y. SONG, I. K. HWANG, S. H. YUN, and B. Y. KIM: "High performance fused-type mode selective coupler for two-mode fiber devices". *Optical Fiber Communication Conference*. Paper TuB5-1. 2000.
- [Son02] K. Y. SONG, I. K. HWANG, S. H. YUN, and B. Y. KIM: "High performance fused-type mode-selective coupler using elliptical core two-mode fiber at 1550 nm". *IEEE Photonics Technology Letters* (2002), vol. 14(4): pp. 501–503.
- [Son03] K. Y. SONG and B. Y. KIM: "Broad-band LP₀₂ mode excitation using a fused-type mode-selective coupler". *IEEE Photonics Technology Letters* (2003), vol. 15(12): pp. 1734–1736.
- [Sor86] W. V. SORIN, B. Y. KIM, and H. J. SHAW: "Highly selective evanescent modal filter for two-mode optical fibers". *Optics Letters* (1986), vol. 11(9): pp. 581–583.
- [Tan13] S. TANNER. private communication. 2013.
- [Tew86] R. TEWARI and K. THYAGARAJAN: "Analysis of tunable single-mode fiber directional couplers using simple and accurate relations". *Journal of Lightwave Technology* (1986), vol. 4(4): pp. 386–390.
- [The12] T. THEEG, H. SAYINC, J. NEUMANN, L. OVERMEYER, and D. KRACHT: "Pump and signal combiner for bi-directional pumping of all-fiber lasers and amplifiers". *Optics Express* (2012), vol. 20(27): pp. 28125–28141.
- [Tho14a] THORLABS: *1310BHP data sheet*. 2014. URL: <http://www.thorlabs.de/thorcat/13900/1310BHP-SpecSheet.pdf> (visited on 21/10/2014).
- [Tho14b] THORLABS: *SM2000 data sheet*. 2014. URL: <http://www.thorlabs.de/thorcat/21000/SM2000-SpecSheet.pdf> (visited on 02/09/2014).
- [Tom08] W. J. TOMLINSON: "Evolution of Passive Optical Component Technologies for Fiber-Optic Communication Systems". *Journal of Lightwave Technology* (2008), vol. 26(9): pp. 1046–1063.
- [Tün13] H. TÜNNERMANN: *Self-implemented BPM algorithm based on the CUDA architecture*. 2013.

- [Vel15] A. M. VELAZQUEZ-BENITEZ, J. C. ALVARADO, G. LOPEZ-GALMICHE, J. E. ANTONIO-LOPEZ, J. HERNÁNDEZ-CORDERO, J. SANCHEZ-MONDRAGON, P. SILLARD, C. M. OKONKWO, and R. AMEZCUA-CORREA: “Six mode selective fiber optic spatial multiplexer”. *Optics Letters* (2015), vol. 40(8): pp. 1663–1666.
- [Win14] P. J. WINZER: “Making spatial multiplexing a reality”. *Nature Photonics* (2014), vol. 8(5): pp. 345–348.
- [Wit08] A. WITKOWSKA, S. G. LEON-SAVAL, A. PHAM, and T. A. BIRKS: “All-fiber LP₁₁ mode convertors”. *Optics Letters* (2008), vol. 33(4): pp. 306–308.
- [Xia11] C. XIA, N. BAI, I. OZDUR, X. ZHOU, and G. LI: “Supermodes for optical transmission”. *Optics Express* (2011), vol. 19(17): pp. 16653–16664.
- [Yer14] S. YEROLATSITIS, I. GRIS-SÁNCHEZ, and T. A. BIRKS: “Adiabatically-tapered fiber mode multiplexers”. *Optics Express* (2014), vol. 22(1): pp. 608–617.
- [Zhe86] X. H. ZHENG: “Finite-element analysis for fused couplers”. *Electronics Letters* (1986), vol. 22(15): pp. 804–805.
- [Zho13] N. ZHONG, Q. LIAO, X. ZHU, Y. WANG, and R. CHEN: “High-quality fiber fabrication in buffered hydrofluoric acid solution with ultrasonic agitation”. *Applied Optics* (2013), vol. 52(7): pp. 1432–1440.
- [Zhu12] T. ZHU, F. XIAO, L. XU, M. LIU, M. DENG, and K. S. CHIANG: “Pressure-assisted low-loss fusion splicing between photonic crystal fiber and single-mode fiber”. *Optics Express* (2012), vol. 20(22): pp. 24465–24471.

APPENDIX A

Fiber Specifications and Fused Fiber Coupler Fabrication

A.1 Fiber Parameters and Refractive Index Profiles

Table A.1: Fiber parameters.

Fiber	780-HP	SM2000	630-HP	1310BHP	TmDF200
Datasheet	[Nuf14b]	[Tho14b]	[Nuf14a]	[Tho14a]	[OFS14]
Core diameter in μm	4.4	11	3.5	8.5	4 (estimated)
Cladding diameter in μm	125	125	125	125	125
Numerical aperture	0.13	0.126 [Tan13]	0.13	0.13	0.26
Cut-off wavelength in nm	730 ± 30	1700	570 ± 30	1260 ± 30	1350

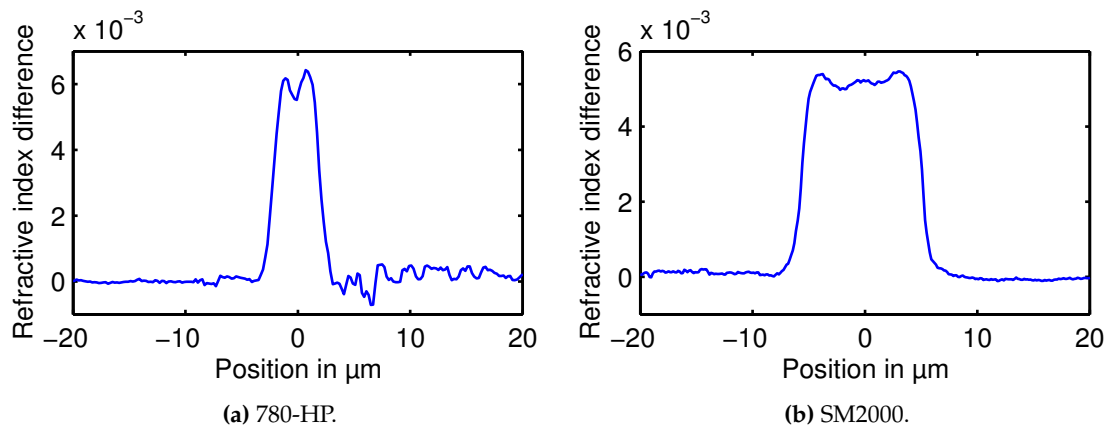


Figure A.1: Refractive index profiles measured with an S14 Refractive Index Profiler (Photon Kinetics).

A.2 Wavelength-Dependent Numerical Aperture

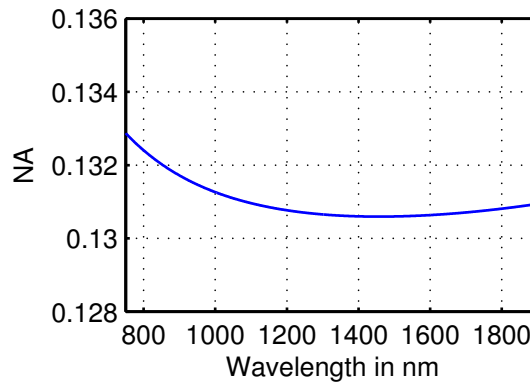


Figure A.2: Dependency of the NA on the wavelength based on the dispersion of undoped fused silica in the cladding and germanium-doped fused silica (4 mol %) in the core [Men06].

A.3 Reproducibility of the Fused Fiber Coupler Fabrication

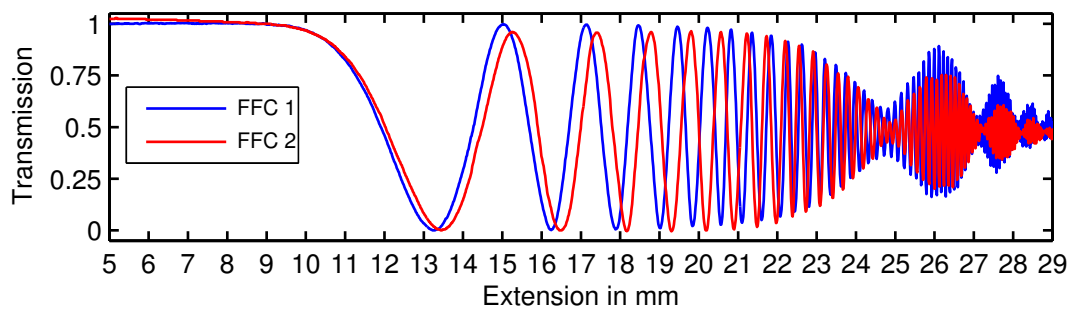


Figure A.3: Pulling signatures at one fiber port of two identically pulled symmetric FFCs made from SM2000 at a wavelength of 1980 nm.

APPENDIX B

Listings

B.1 Calculation of the Refractive Index Profile

B.1.1 Parabolic Taper Shape

```
1   # Diameter of the cores
2   # Pump fiber
3   a3_p=(di_p-df_p)/(-L/2)**2
4   dia_clad_p=a3_p*(z-L/2)**2+df_p
5
6   # Signal fiber
7   a3_s=(di_s-df_s)/(-(L_pre+delta_z)/2)**2
8   dia_clad_s=a3_s*(z-(L_pre+delta_z)/2+pre/2)**2+df_s
```

B.1.2 Position of the Fiber Cores

```
1   # Pump fiber
2   d_p=L/2
3   e_p=(di_p/2-df_p/2)
4   a_p=e_p/d_p**2
5   core_pos_p=a_p*(z-d_p)**2+df_p/2-ul/2
6
7   # Signal fiber
8   d_s=(L_pre+delta_z)/2
9   e_s=(-di_s/2-df_s/2+ul)
10  a_s=(-di_s+ul-e_s)/d_s**2
11  core_pos_s=a_s*(z+pre/2-d_s)**2-df_s/2+ul/2
```

B.1.3 Derivation of the Separation of the Fiber Cores

The width of the overlapped region is

$$w_{\text{ol}} = (X + Y - Z) \quad \text{with} \quad \text{DOF} = \frac{2 \cdot Z}{X + Y} \Leftrightarrow Z = \frac{\text{DOF} \cdot (X + Y)}{2} \quad (\text{B.1})$$

$$w_{\text{ol}} = (X + Y) \left(1 - \frac{\text{DOF}}{2}\right). \quad (\text{B.2})$$

The actual separation of the cores d is the initial separation of the cores d_i minus the overlapped region w_{ol} :

$$d = d_i - w_{\text{ol}} \quad (\text{B.3})$$

$$= \frac{Y}{2} + \frac{X}{2} - (X + Y) \left(1 - \frac{\text{DOF}}{2}\right) \quad (\text{B.4})$$

$$= \frac{(X + Y)}{2} (\text{DOF} - 1). \quad (\text{B.5})$$

Publications

Publications in peer-reviewed journals

1. **G. PELEGRINA-BONILLA**, K. HAUSMANN, K. LIU, H. SAYINC, U. MORGNER, J. NEUMANN, and D. KRACHT: "Matching of the propagation constants in an asymmetric single-mode fused fiber coupler for core pumping thulium-doped fiber at 795 nm". *Optics Letters* (2012), vol. 37(11): pp. 1844–1846.
2. **G. PELEGRINA-BONILLA**, K. HAUSMANN, H. TÜNNERMANN, P. WESSELS, H. SAYINC, U. MORGNER, J. NEUMANN, and D. KRACHT: "Analysis of the Coupling Mechanism in Asymmetric Fused Fiber Couplers". *Journal of Lightwave Technology* (2014), vol. 32(13): pp. 2382–2391.
3. **G. PELEGRINA-BONILLA**, K. HAUSMANN, H. SAYINC, U. MORGNER, J. NEUMANN, and D. KRACHT: "Analysis of the modal evolution in fused-type mode-selective fiber couplers". *Optics Express* (2015), vol. 23(18): pp. 22977–22990.

Publications

1. **G. PELEGRINA-BONILLA**, K. HAUSMANN, K. LIU, H. SAYINC, U. MORGNER, J. NEUMANN, and D. KRACHT: "Asymmetric fused fiber coupler consisting of different single-mode glass fibers". *Photonik International* (2012), vol. 1: pp. 48–50.
2. **G. PELEGRINA-BONILLA**, K. HAUSMANN, K. LIU, H. SAYINC, U. MORGNER, J. NEUMANN, and D. KRACHT: "Asymmetrische Faserkoppler aus unterschiedlichen Singlemode-Glasfasern". *Photonik* (2012), vol. 3: pp. 54–56.

Patent applications

1. H. SAYINC, **G. PELEGRINA-BONILLA**, and K. HAUSMANN: "Method for manufacturing a coupling arrangement, coupling arrangement and amplifier". EP2618192 A1. 2013.

2. H. SAYINC, G. PELEGRINA-BONILLA, and K. HAUSMANN: "Method for manufacturing a coupling arrangement, coupling arrangement and amplifier". US-2013-0222891-A1. 2013.

Submissions to international conferences

1. G. PELEGRINA-BONILLA, K. HAUSMANN, K. LIU, H. SAYINC, U. MORGNER, J. NEUMANN, and D. KRACHT: "Asymmetric single-mode fused fiber coupler for core pumping thulium-doped fiber at 795 nm". *5th EPS-QEOD Europhoton Conference*. Paper FrB.7. 2012.
2. G. PELEGRINA-BONILLA, K. HAUSMANN, K. LIU, H. SAYINC, U. MORGNER, J. NEUMANN, and D. KRACHT: "Single-mode WDM for core pumping thulium-doped fiber at 795 nm". *SPIE Photonics West*. Paper 8237-81. 2012.
3. T. THEEG, K. HAUSMANN, G. PELEGRINA-BONILLA, H. SAYINC, J. NEUMANN, and D. KRACHT: "High power single mode optical fiber coupler with enhanced mode field diameter". *SPIE Photonics West*. Paper 8237-89. 2012.
4. G. PELEGRINA-BONILLA, K. HAUSMANN, H. TÜNNERMANN, P. WESSELS, H. SAYINC, U. MORGNER, J. NEUMANN, and D. KRACHT: "Experimental and numerical investigations on asymmetric fused fibre couplers consisting of different single-mode fibres". *CLEO/Europe-IQEC*. Paper CE-4.2. 2013.
5. G. PELEGRINA-BONILLA, A. SCHWENKE, H. SAYINC, U. MORGNER, J. NEUMANN, B. CHICHKOV, L. SAJTI, and D. KRACHT: "Optical amplification at 1.06 μm from laser ablated neodymium nanoparticles embedded in a polymer host". *SPIE Photonics West*. Paper 8609-13. 2013.
6. G. PELEGRINA-BONILLA, K. HAUSMANN, H. SAYINC, U. MORGNER, J. NEUMANN, and D. KRACHT: "Modal Analysis in Fused-Type Mode-Selective Fiber Couplers". *Advanced Photonics*. Paper SoW2B.3. 2014.
7. G. PELEGRINA-BONILLA, K. HAUSMANN, H. TÜNNERMANN, P. WESSELS, H. SAYINC, U. MORGNER, J. NEUMANN, and D. KRACHT: "Modal Decomposition in Asymmetric Wavelength-Selective Fused Fiber Couplers". *Advanced Photonics*. Paper JM5A.6. 2014.
8. H. SAYINC, T. THEEG, G. PELEGRINA-BONILLA, K. HAUSMANN, H. TÜNNERMANN, P. WESSELS, J. NEUMANN, and D. KRACHT: "New Pump and Signal Combiners". *Advanced Photonics*. Paper SoW1B.2. 2014.

-
9. U. THOMBANSEN, P. ABELS, S. KAIERLE, J. NEUMANN, and G. PELEGRINA-BONILLA: “Accelerated innovation through laser-based equipment assessment”. *The Industrial Laser Applications Symposium (ILAS)*. 2015.

Curriculum Vitae

Personal Data

Name Gabriel Pelegrina Bonilla
Date of birth 02.12.1985
Place of birth Münster, Germany
Nationality Spanish

Education

2005 Abitur (German university entrance qualification)

University Education

2005 - 2011 Physics at the Westfälische Wilhelms-Universität Münster with degree "Diplom-Physiker"
Title of diploma thesis: "Präparation und Charakterisierung von randomisierten laseraktiven Partikelsystemen"
2011 - present Dr. rer. nat. in physics at the Leibniz Universität Hannover

Professional Affiliations

2008 - 2011 Research assistant at Westfälische Wilhelms-Universität Münster
2011 - present Research scientist at Laser Zentrum Hannover e. V.

Danksagung

Eine Doktorarbeit fertigzustellen ist ein langes Experiment dessen Ausgang zu Anfang nicht ersichtlich ist. Auf dem Weg zum Abschluss der Promotion hatte ich das Glück von zahlreichen Menschen unterstützt zu werden denen ich an dieser Stelle herzlich meinen Dank aussprechen möchte.

Zuallererst möchte ich meinem Doktorvater Prof. Uwe Morgner für die Betreuung in dieser Zeit und die kontinuierliche Unterstützung bei fachlichen und organisatorischen Herausforderungen danken. Ich konnte bei zahlreichen Seminaren und Workshops meine Expertise stets erweitern und hatte die Gelegenheit viele Kontakte in der Arbeitsgruppe zu knüpfen.

Bei Prof. Detlev Ristau bedanke ich mich für die Übernahme des Zweitgutachtens.

Mein größter Dank gehört sicherlich Katharina Hausmann und Dr. Henrik Tünnermann für ihren essentiellen und weitreichenden Beitrag während der gesamten Zeit. Katharina danke ich für zahlreiche Stunden der experimentellen Unterstützung und viele konstruktive Diskussionen. Henrik danke ich für die Bereitstellung des Simulationsprogramms und für wichtige Ideen bei der Durchführung der numerischen Untersuchungen.

Ich danke meinem Masterstudenten Kai Liu für seine Mitarbeit während der anfänglichen Phase dieser Doktorarbeit.

Meinem Gruppenleiter Dr. Hakan Sayinc und meinem Abteilungsleiter Dr. Jörg Neumann danke ich für viele produktive Diskussionen während der gesamten Zeit und das intensive Korrekturlesen des Manuskripts. Sie haben es mir ermöglicht die Resultate dieser Arbeit auf Fachkonferenzen vorzustellen und meine berufliche Erfahrung bei der Mitarbeit in weiteren Projekten zu erweitern.

Bedanken möchte ich mich ebenfalls bei Andreas Wienke für die ausgezeichnete Büroatmosphäre und für die Unterstützung auch außerhalb der Arbeit.

Großer Dank gebührt auch den restlichen Mitgliedern der Abteilung Laserentwicklung und insbesondere der Gruppe Faseroptik. Ebenfalls möchte ich mich bei der Geschäftsführung des Laser Zentrum Hannover, namentlich Dr. Dietmar Kracht, und weiteren Mitarbeitern, insbesondere Andreas Grunewald, bedanken.

Bei Matthias Pospiech bedanke ich mich für die professionelle L^AT_EX-Vorlage.

Abschließend drücke ich meinen herzlichen Dank Christina aus für ihre Unterstützung und fortwährende Motivation.